2016

# Assessing the Predictions of Biogenic Volatile Organic Compound Emissions from Multiple Chemical Transport Models Within the Greater Metropolitan Region NSW

Jordan N.R. Capnerhurst

# Assessing the Predictions of Biogenic Volatile Organic Compound Emissions from Multiple Chemical Transport Models Within the Greater Metropolitan Region NSW


## Abstract

Within the Greater Metropolitan Region NSW, consideration of the accuracy of predicted biogenic emissions inputted into chemical transport models is important. These biogenic emissions react with anthropogenic compounds producing organic aerosol and ground level ozone, which negatively impact the wider environment. Despite this, there have been few studies in the area regarding these compounds and large uncertainty exists.

To address this issue, the predictions of biogenic emissions from MEGAN and the CSIRO-CTM, within the Greater Metropolitan Region, were assessed using computational and statistical methods. This involved: a model intercomparison between three different model implementations run for February 2011, an assessment of seasonal variability of predicted emissions using a complete 2013 dataset, and a comparison between the outputs of one model using February 2011 and 2013 data.

Predicted emissions from these models revealed that photosynthetically active radiation and temperature explain the majority of the temporal variation in the predicted emissions resulting in a diurnal distribution. However, the majority of spatial variation is explained by leaf area index and broadleaf vegetation cover within each of the models. It was also found that implementations of MEGAN predict higher quantities of emissions than the CSIRO-CTM, and high emissions of isoprene and lower emissions of monoterpenes. Each model also predicts high levels of emissions over national parks. Emissions were found to be seasonally variable with emissions at their highest during summer and lowest during winter. While the spatial distribution remained nearly unchanged throughout the year. The emission predictions for February 2013 were found to be significantly higher than those in February 2011 owing to the increased temperatures predicted for 2013.

This research highlights the importance of using up to date and accurate model inputs and the need for further biogenic flux measurements in the area.



## Degree Type

Thesis

## Degree Name

BEnviSci Hons

## Department

School of Earth & Environmental Science

## Advisor(s)

Jenny Fisher

## Keywords

Atmosphere, air quality, modelling, vegetation


# Assessing the Predictions of Biogenic Volatile Organic Compound Emissions from Multiple Chemical Transport Models Within the Greater Metropolitan Region NSW

JORDAN N. R. CAPNERHURST

A thesis submitted in part fulfilment of the
requirements for the award of the degree of

BACHELOR OF ENVIRONMNETAL SCIENCE (HONOURS)

ENVIRONMNETAL SCIENCE PROGRAM
SCHOOL OF EARTH & ENVIORONMNETAL SCIENCES
FACULTY OF SCIENCE, MEDICINE AND HEALTH
THE UNIVERSITY OF WOLLONGONG

October 2016

*The information in this thesis is entirely the result of investigations conducted by the author, unless otherwise acknowledged, and has not been submitted in part, or otherwise, for any other degree or qualification.*

Jordan N. R. Capnerhurst

25th October, 2016

## Abstract

Within the Greater Metropolitan Region NSW, consideration of the accuracy of predicted biogenic emissions inputted into chemical transport models is important. These biogenic emissions react with anthropogenic compounds producing organic aerosol and ground level ozone, which negatively impact the wider environment. Despite this, there have been few studies in the area regarding these compounds and large uncertainty exists.

To address this issue, the predictions of biogenic emissions from MEGAN and the CSIRO-CTM, within the Greater Metropolitan Region, were assessed using computational and statistical methods. This involved: a model intercomparison between three different model implementations run for February 2011, an assessment of seasonal variability of predicted emissions using a complete 2013 dataset, and a comparison between the outputs of one model using February 2011 and 2013 data.

Predicted emissions from these models revealed that photosynthetically active radiation and temperature explain the majority of the temporal variation in the predicted emissions resulting in a diurnal distribution. However, the majority of spatial variation is explained by leaf area index and broadleaf vegetation cover within each of the models. It was also found that implementations of MEGAN predict higher quantities of emissions than the CSIRO-CTM, and high emissions of isoprene and lower emissions of monoterpenes. Each model also predicts high levels of emissions over national parks. Emissions were found to be seasonally variable with emissions at their highest during summer and lowest during winter. While the spatial distribution remained nearly unchanged throughout the year. The emission predictions for February 2013 were found to be significantly higher than those in February 2011 owing to the increased temperatures predicted for 2013.

This research highlights the importance of using up to date and accurate model inputs and the need for further biogenic flux measurements in the area.

## Acknowledgements

First and foremost, I would like to express my sincere gratitude to my supervisor, Dr. Jenny Fisher, for accompanying me on this thesis writing journey. Your enthusiasm, patience, expertise, and encouragement have been very much appreciated during every stage of this project from the beginning when I didn't know a single thing about atmospheric chemistry to my final submission of this report. I would also like to thank the members of the UOW Centre for Atmospheric Chemistry for being so inviting, accepting, and positive throughout the year especially the numerous PhD. students who helped me get my head around python.

The staff at the NSW OEH Atmospheric science division in Lidcombe also deserve a massive thank you for being encouraging and actively engaging with me and assisting me in solving my research questions. I am also grateful for the time that Yvonne Scorgie has dedicated to helping arrange this project, liaise with other organisations, and being encouraging and helpful throughout. A special mention also needs to be given to Hiep Duc and Toan Trieu for running and rerunning models, arranging large data transfers, and answering my questions throughout the year.

I would also like to thank the external modellers: Jeremy Silver (University of Melbourne) and Kathryn Emmerson (CSIRO) for providing not only model outputs but also helping me to understand them and re-running them when there were issues. It was a pleasure to meet both of you at the CAUL meeting at UOW and I hope this work helps with your research.

Lastly, I would also like to thank my family and friends for their support during this year and all of their help, advice, and most welcome tea.

## Table of Contents

# List of figures

# List of tables

## List of abbreviations

| | |
|---|---|
| AVOC | Anthropogenic volatile organic compound |
| BVOC | Biogenic volatile organic compound |
| CABLE | CSIRO Atmosphere Biosphere Land Exchange model |
| CCAM | CSIRO Conformal Cubic Atmospheric Model |
| CLM | Community Land Model |
| CMAQ | Community Multiscale Air Quality model |
| CSIRO | Commonwealth Scientific and Industrial Research Organisation |
| CTM | Chemical Transport Model |
| ENSO | El Niño–Southern Oscillation |
| EPA | Environmental Protection Authority |
| GMR | Greater metropolitan region |
| GRD | Gridded Data format |
| IOD | Indian Ocean Dipole |
| LAI | Leaf Area Index |
| MEGAN | Models of Emissions of Gasses and Aerosols from Nature |
| MT | Monoterpenes |
| NCO | NETCDF operators |
| NETCDF | Network Common Data Form |
| NMOHC | Non-Methane Organic Hydro Carbon |
| $NO_x$ | nitrogen oxides |
| PAR | Photosynthetically Available Radiation |
| PFT | Plant Functional Type |
| PPFD | Photosynthetic Photon Flux Density |
| $PM_{2.5}$ | particulate matter $\leq$ 2.5 micrometres in diameter |
| SOA | Secondary Organic Aerosols |
| SPS | Sydney Particle Study |
| SQT | Sesquiterpenes |
| VOC | Volatile Organic Compound |
| WRF | Weather Research and Forecasting model |

# 1. Introduction

## 1.1 Background

Atmospheric pollution is a significant environmental concern that has the potential to threaten both human health and environmental sustainability, especially with the onset of anthropogenic climate change and an ever increasing population. Increased public knowledge and the implementation of legislation and standards - by the NSW EPA and Australian Department of Environment, respectively - regarding air quality also contributes to the significance of the issue. Providing information relating to air quality to communities is listed as a priority action in the NSW government strategic plan 'NSW 2021'. Due to these changes, it is becoming increasingly important to gain an understanding of the interactions between the processes taking place on the Earth's surface, anthropogenic activities, and the atmosphere, to prevent further damage and to allow for the creation and employment of solutions into the future. Atmospheric chemical transport models (CTMs) are tools that allow researchers to better understand these complex interactions, and to allow for more informed policy and decision making. These models can be used to better understand and predict the formation, atmospheric concentration, and deposition of tropospheric ozone and aerosols that both have the capacity to impact environmental health and influence global climate patterns. CTMs also have the capability to be used for quantitative earth system studies, and to estimate the past and present impact of climate on air quality (Guenther et al. (2006)).

The emission of hydrocarbons by vegetation and their influence on air quality was first noted by Went in 1960, who linked the oxidation of these hydrocarbons with the "blue haze" often seen over forested areas. From this it was subsequently determined that global vegetation is intrinsically linked to atmospheric chemistry and processes (Kefauver et al. (2014)). These hydrocarbons were later identified and classified as biogenic volatile organic compounds (BVOCs), which were found to account for 85% of total non-methane hydrocarbons in nature (Kefauver et al. (2014)). Despite these large quantities very little research has been undertaken regarding these compounds in an Australian context.

BVOCs are a highly reactive group of chemical species that are prevalent throughout the highly oxidising lower troposphere and atmospheric boundary layer, especially in regions of dense vegetation. Due to their prevalence and high reactivity, they influence important chemical processes at a number of scales, such as the production of secondary organic aerosol (SOA)

and tropospheric ozone, which both have the capacity to negatively impact the human population (Atkinson and Arey (2003); Lathiere et al. (2006)). Because of this significance, BVOCs are an important consideration within atmospheric models due to their potential to impact air quality. Despite their ability to influence SOA and ozone concentrations BVOCs are not directly included in Australian air quality standards (NSW Environmnetal Protection Authority (2015)).

Multiple air quality campaigns have been carried out in the Sydney area, such as the Sydney Particle Studies (SPS) (Cope et al. (2014)), the Metropolitan Air Quality study (MAQS Azzi et al. (2005), and continuous monitoring as part of the Australian air quality monitoring and forecasting system which consists of 42 air quality monitoring stations (Cope et al. (2004); COALA stearing group (2016)). Numerous emission inventories containing antropogenic and biogenic emissions have also been created by the NSW EPA for the region. Despite these studies, and the large quantities emitted worldwide, there is large uncertainty regarding the distribution and quantities of BVOCs emitted within the Greater Metropolitan Region (GMR).

This study will assess and compare the outputs of three different model runs, with different inputs, to determine differences in the ways BVOC emissions are represented and the environmental factors that have the greatest influence within each model configuration. Using the information gained from this comparison, a more in depth analysis of temporal and spatial variability of BVOCs will be performed on a complete years' worth of data from the model used by the NSW OEH. This model is used by the OEH for air quality forecasting and warnings, evaluation purposes, and to allow for the application of pre-emptive emission reduction measures on days when low air quality is predicted (Jiang et al. (2015)).

### 1.2 Project aims and objectives

The aim of this project is to understand, assess and compare methods currently employed to estimate BVOC emissions within the GMR by assessing factors that affect the spatial distribution of emissions, variability between different emission models, and examining spatial and temporal trends in such emissions. The purpose of this research is to assist the NSW OEH to assess their current method of estimating BVOC emissions, to determine whether it is adequate, or whether a better alternative is available.

Aims of this project are:

- To understand and document, for future studies, how each of the three different BVOC models predict emissions, and the required inputs through an analysis of relevant literature.
- To employ computational techniques, and create reusable scripts, to allow for the generation of temporal and spatial representations of BVOC emissions from the raw data outputs of three different atmospheric models operated within the GMR.
- To compare and contrast the spatial and temporal variability and patterns present within the three separate model implementations, during the February 2011 period, to determine the different sensitivities of each model to environmental factors inputted into the model, and how this affects their outputs.
- To apply the understanding and methods from the three model intercomparison mentioned previously to determine seasonal and other temporal influences present within a complete years' worth of data for the year 2013, provided by the OEH.

## 2. Literature review

### 2.1 The importance of biological volatile organic compounds

BVOCs are produced through numerous natural and anthropogenic processes and have the capacity to negatively impact both human health and the environment. The majority of BVOCs originate from terrestrial ecosystems, with ~90% emitted globally from the foliage of plants and trees (Laothawornkitkul et al. (2009)). These terrestrial emissions also represent the overall single largest known reactive hydrocarbon source to the atmosphere (Nelson et al. (2002)). Tropical broadleaf trees within these ecosystems emit BVOCs in particularly high amounts. These higher emission rates are due to the climatic conditions that the plants are exposed to, which are generally conducive to BVOC production, along with their inherent high emission rates (Guenther et al. (2006)). The remaining BVOC flux results primarily from shrubs, due to their widespread distribution, despite the fact individual plants have relatively low emission rates (Guenther et al. (2006)). In contrast, undisturbed, uncut grasses and crops emit less than 3% of BVOCs produced by the equivalent amount of tree foliage. However, when these grasses are cut the quantity of BVOCs emitted increases by ~100 times, although the BVOCs emitted are almost exclusively non-reactive light oxygenated hydrocarbons such as methanol (Nelson et al. (2002)). Only around 5% of these emissions from cut grass and pastures are reactive compounds which significantly affect air quality (Azzi et al. (2005)). Herbaceous vegetation

also has a relatively low contribution to BVOC emission quantities overall due to their low emission rate and restricted distribution (Guenther et al. (2006)).

These differing emission potentials mean that urbanisation and agriculture can have dramatic impacts on BVOC emissions and their spatial distributions (Wiedinmyer et al. (2006)). The specific sources of BVOCs within an individual terrestrial ecosystem can be highly variable, owing to biological processes including stress effects, growth, reproduction, and communication with other plants, mammals, and insects (Kesselmeier and Staudt (1999); Laothawornkitkul et al. (2009)).

The specific biological pathways that result in BVOCs emission differ from plant to plant and BVOC species (Guenther (2013)). Several plant species store BVOCs in their tissues, which isolates them from the atmosphere until the plant is damaged or stressed (Guenther (2013)). Other species release BVOCs into the atmosphere from storage pools, such as glands or resin ducts located on the leaves of the plant, resulting in emission profiles that are relatively continuous and highly temperature dependant (Nelson et al. (2002); Guenther (2013)). The widest variety of BVOC species are released from fruit and flowers, although they are also released in smaller quantities from both above and below ground plant organs, mainly from chloroplasts and stomatal pores (Guenther et al. (1991); Laothawornkitkul et al. (2009)).

Anthropogenic volatile organic compounds (AVOCs) also contribute to the concentration of volatile organic compound (VOC) in the atmosphere as a result of activities such as agriculture, mowing of lawns, energy generation, and transportation (Kesselmeier and Staudt (1999)). Biomass burning, both controlled – as a component of hazard reduction and agriculture – and uncontrolled, have a significant contribution to total VOC emissions (Baker et al. (2016)). Despite these abundant anthropogenic inputs, BVOC emissions are estimated to exceed AVOC emissions by a factor of ~10 (Atkinson and Arey (2003)).

The most common and abundant group of BVOCs are the isoprenoids – isoprene (2-methyl-1,3-butadiene, $C_5H_8$), which by mass constitutes between 30 and 50% of the total emission strength of BVOCs (Arneth et al. (2011)), and monoterpenes (MT), a group of species with the chemical form $C_{10}H_{16}$ which contribute to ~15% of total BVOC emission strength by weight (Arneth et al. (2008); Glasius and Goldstein (2016)). Despite their lower emission rates, sesquiterpenes (SQT) ($C_{15}H_{24}$) have a significant impact on air quality due to their high reactivity (Sakulyanontvittaya et al. (2008); Geron et al. (2016)). Terrestrial ecosystems around the world produce tens of thousands of other species of VOCs which are emitted into the

atmosphere, although they are emitted in such small quantities and have such low atmospheric reactivity that they have a minimal effect on atmospheric chemical processes and composition (Guenther (2013)).

The atmospheric lifetime of BVOCs is comparatively short when compared to other chemical compounds present within the atmosphere (**Table 1 & 2**), generally a few hours or less (Atkinson and Arey (2003)). This short lifetime is the result of the high reactivity and volatility of BVOCs. This reactivity is so significant that it is estimated that isoprene is approximately three times more reactive than weighted average AVOC emitted in motor vehicle exhaust (Nelson et al. (2002)). Due to this high volatility, the major loss pathway of BVOCs within the atmosphere is the formation of SOA following (OH)- initiation (Rattanavaraha et al. (2016)). Interactions and mixing within the atmospheric boundary layer after emissions take place will also influence BVOC concentrations in a region, due to the compounds inherent high volatility (McGrath-Spangler et al. (2015)).

Despite the fact that BVOC emissions have been measured and modelled for many years, it must be noted that the majority of this work has been undertaken in the northern hemisphere using relevant species and conditions which are vastly different to those found within Australia (Nelson et al. (2002)). Within Australia, the majority of detailed studies focus on the GMR due to the high population and quantity of BVOC emitting vegetation in the region, such as eucalyptus, compared to the remainder of the continent.

On a global scale, several estimates of total yearly BVOC emissions have been produced primarily through different implementation of MEGAN ranging from 500Tg C to 1150Tg C (Guenther et al. (1995); Guenther et al. (2006)). Australia has been included in these broad global scale estimates numerous times, such as that of Sindelarova et al. (2014) in which it was estimated that Australia contributes ~70% 556 Tg C /year ($1x10^{12}$g) to the global isoprene budget of 760 Tg C /year. More recently, Chatani et al. (2015) estimated that that the Australian contribution of isoprene and monoterpenes emissions to total yearly BVOC are 535 and 162 Tg C respectively. However, these estimates are highly uncertain as highlighted by Zeng et al. (2015), who found differences of ~10-20% between inventory estimates of isoprene and a factor of six difference between estimates of monoterpenes. This same level of uncertainty is, however, not present in estimates of anthropogenic sources, which are relatively well known and documented within inventories in Australia.

Isoprene, MT, and SQTs influence atmospheric photochemical production processes that lead to the formation of tropospheric ozone (**Figure 1**), and secondary organic aerosol (SOA, **Figure 2**), in a myriad of ways. A more in-depth explanation of these reactions can be found in **Appendix 16**. Both tropospheric ozone and SOA impact air quality and climate, resulting in impacts on both human health and the broader environment. In order to regulate and account for the concentration of these compounds in the atmosphere, to prevent negative outcomes it is important to understand the processes and precursor species, such as BVOCs, that contribute to their formation.

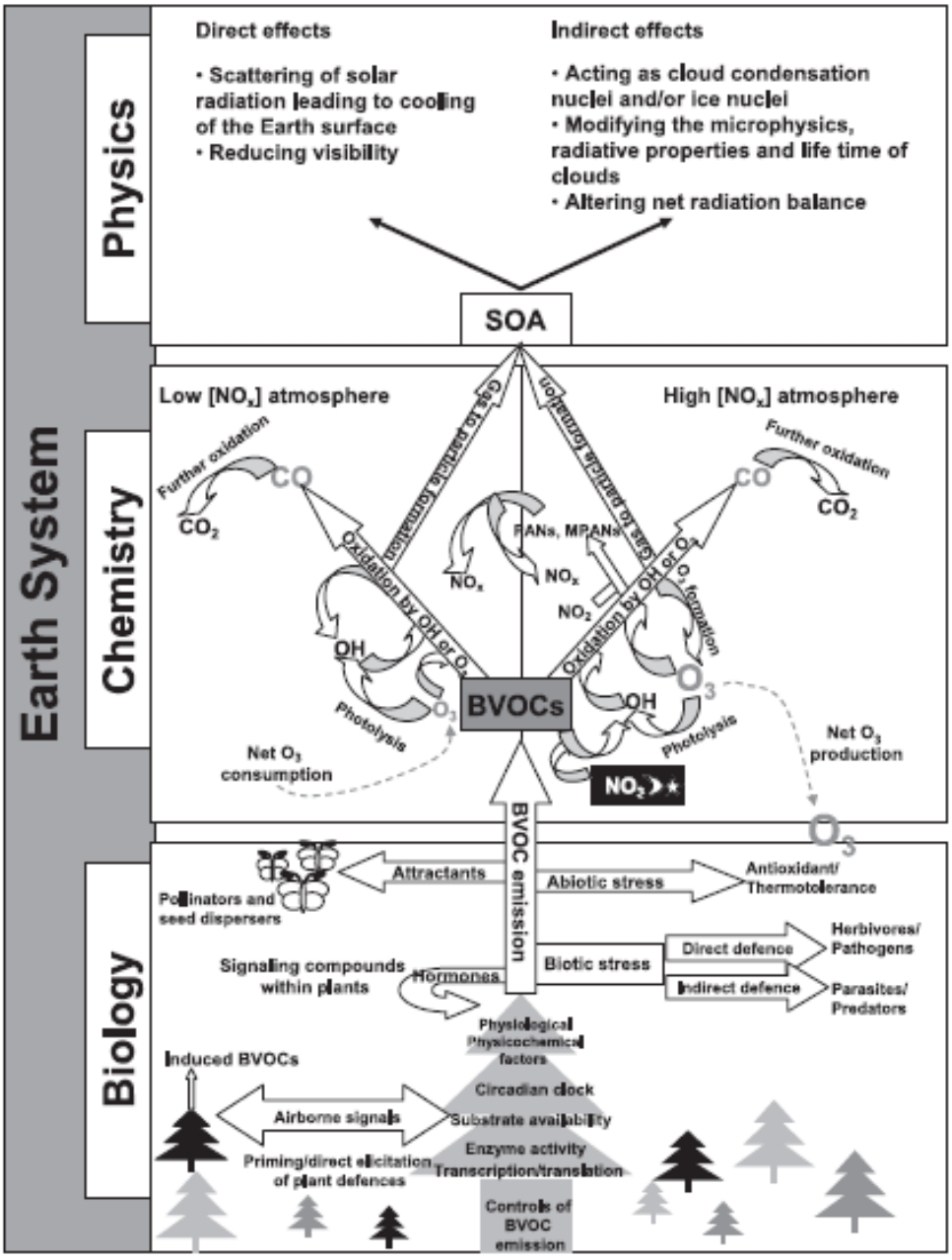


*Figure 1: Schematic diagram showing the formation of SOA from the oxidisation of biogenic and anthropogenic VOCs. (Cope et al. (2014a))*

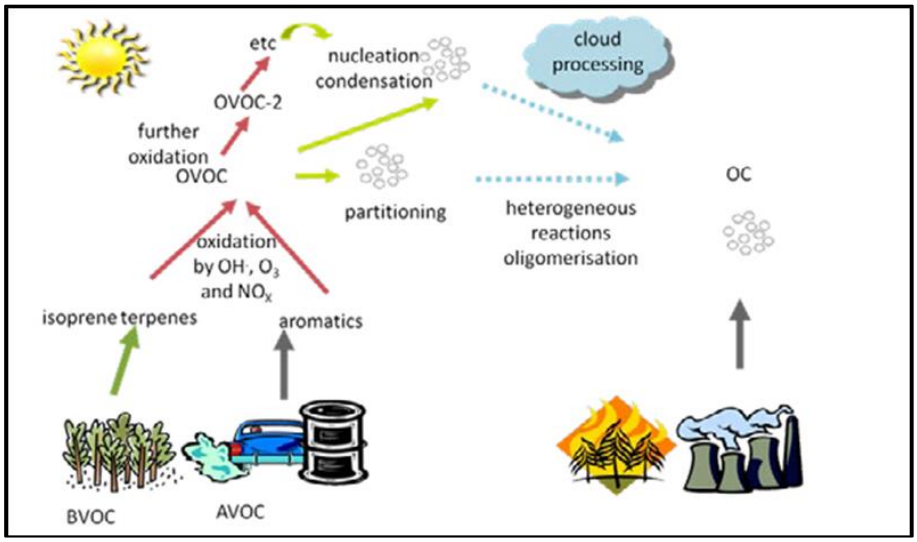


*Figure 2: Reaction pathways of BVOCs leading to the formation of tropospheric ozone. (Laothawornkitkul et al.) (2009)*

| Biogenic VOC | Lifetime[a] for reaction with | | |
|---|---|---|---|
| | OH[b] | $O_3$[c] | $NO_3$[d] |
| Isoprene | 1.4 h | 1.3 day | 1.6 h |
| *Monoterpenes* | | | |
| Camphene | 2.6 h | 18 day | 1.7 h |
| 2-Carene | 1.7 h | 1.7 h | 4 min |
| 3-Carene | 1.6 h | 11 h | 7 min |
| Limonene | 49 min | 2.0 h | 5 min |
| Myrcene | 39 min | 50 min | 6 min |
| *cis*-/*trans*-Ocimene | 33 min | 44 min | 3 min |
| α-Phellandrene | 27 min | 8 min | 0.9 min |
| β-Phellandrene | 50 min | 8.4 h | 8 min |
| α-Pinene | 2.6 h | 4.6 h | 11 min |
| β-Pinene | 1.8 h | 1.1 day | 27 min |
| Sabinene | 1.2 h | 4.8 h | 7 min |
| α-Terpinene | 23 min | 1 min | 0.5 min |
| γ-Terpinene | 47 min | 2.8 h | 2 min |
| Terpinolene | 37 min | 13 min | 0.7 min |
| *Sesquiterpenes* | | | |
| β-Caryophyllene | 42 min | 2 min | 3 min |
| α-Cedrene | 2.1 h | 14 h | 8 min |
| α-Copaene | 1.5 h | 2.5 h | 4 min |
| α-Humulene | 28 min | 2 min | 2 min |
| Longifolene | 2.9 h | > 33 day | 1.6 h |

*Table 1: Calculated atmospheric lifetime of BVOCs. (Atkinson and Arey (2003))*

| Name | Chemical lifetimes[a] Day | Night | Example | Atmospheric concentrations |
|---|---|---|---|---|
| Isoprene | 3 hrs | 1.5 hrs | isoprene | ppt to several ppb |
| Monoterpenes | 2–3 hrs | 5–30 min | α-pinene; β-pinene, sabinene | ppt to several ppb |
| | 40–80 min | 5–20 min | limonene, t-β-ocimene, myrcene | |
| | 15–20 min | <1 min | terpinolene, α-phellandrene | |
| | <5 min | <2 min | α-terpinene | |
| Sesquiterpenes | <4 min | <2 min | β-caryophyllene | not detectable due to high reactivity |
| ORVOC | <1 day | | 2-methyl-3-buten-2-ol | 1–3 ppb |
| OVOC | >1 day | | methanol, acetone | 2–30 ppb |

[a] Lifetimes are estimated in relation to $[NO_3] = 10$ ppt, $[O_3] = 20$ ppb for night; and to $[OH] = 10^6$ molecules/$cm^3$, $[O_3] = 20$ ppb for daylight conditions.

*Table 2: Comparison of BVOC lifetimes and atmospheric concentrations in parts per thousand (PPT) and parts per billion (PPB). (Kesselmeier and Staudt (1999))*

### 2.1.1 BVOC contribution to tropospheric ozone

Ozone has the capacity to significantly impact both the environment and humans in a multitude of different ways. Because of these potential impacts it is important to understand BVOC emissions, as these can act as precursors to ozone formation within urban environments.

BVOCs in the atmosphere can influence concentrations of ozone in many ways depending on the concentrations of $NO_x$ (nitrogen oxides) present, which are predominantly the result of anthropogenic activities such as fossil fuel combustion, and the characteristics of the local environment (Lathiere et al. (2006)). The reaction series that produces ozone from BVOCs can be summarised as $NO_x$+ BVOC+ sunlight → $O_3$ (NSW Office of Environment and Heritage (2010)). When in the presence of sufficient $NO_x$, reactions between BVOCs and NOx generally produce ozone. However, under certain conditions, their reaction can instead cause ozone destruction (Lathiere et al. (2006)).

Several estimates of the contribution of BVOCs to ozone production in the troposphere have been made. Early modelling studies found that globally, BVOCs contribute about 40% of photochemical ozone production, resulting in a 17% increase of the tropospheric ozone column compared to a column without BVOCs present (Houweling et al. (1998)). More recently, Zare et al. (2014) estimated that BVOCs contribute about 22% of global photochemical ozone produced in the atmosphere. Zare et al. (2014) also emphasised that different regions of the world have differing contributions of BVOCs to photochemical ozone. For example, in South America, BVOCs contribute up to 42% of photochemical ozone. No estimates of this type exist for Australia, although similar contributions would be expected as those of South America due to similarly low anthropogenic emissions and high BVOC emissions.

Increased concentrations of ozone have been linked to crop damage, resulting in an estimated global economic loss of $11 billion dollars per year (Pugh et al. (2013)). Within an Australian context it is estimated that increased ozone concentrations have the capacity to cause economic losses between $12.5 and 50 million USD per year due to crop losses. This is due to the fact that ozone present in the troposphere strongly oxidises living tissues. Ozone also negatively impacts human health by causing damage to the cardio-pulmonary system (Pugh et al. (2013)).

Interactions between ozone and BVOCs are two way, complex, and involve numerous feedbacks (Pyle et al. (2005)). As ozone is a greenhouse gas it also absorbs infrared radiation emitted by the earth's surface, which contributes to atmospheric warming and radiative climate

forcing. Formation of ozone is intensified when there are greater amounts of solar radiation passing through the atmosphere. For example, minimal ozone is produced at night however lower concentrations of OH are also present which means that any remnant ozone can oxidise BVOCs. Along with ozone the presence of BVOCs may also result in the production of SOA that also has the capacity to negatively impact humans and the environment.

### 2.1.2 BVOC contribution to secondary organic aerosol

BVOCs, especially MT and SQTs, within the atmosphere can contribute to the formation of SOA through several chemical pathways. The most significant process resulting in the production of SOA is the precipitation and condensation of gaseous species (van Donkelaar et al. (2007)). Isoprene also produces SOA, albeit in smaller quantities than MT and SQT. The most common reactions resulting in SOA are BVOCs reacting with OH, $O_3$, and $NO_3$ radicals to produce compounds that are less volatile, which in turn condense into SOA (Smolander et al. (2014)). These SOA contribute to as much as 50-85% of global total organic aerosols (Glasius and Goldstein (2016)).

Like ozone, the increased presence of SOA in an urban environment due to BVOCs can negatively impact human health in various ways, including cardio-pulmonary related issues that contribute to more than a million deaths annually (Pugh et al. (2013)). Work by Cope et al. (2004), Broome et al. (2015) and NSW Office of Environment and Heritage (2014) has shown that a 1ppb increase in ozone concentration in the GMR on a given day causes a 0.27% increase in all-age respiratory mortality for that period.

The aerosols that policy makers and researchers are most interested in are those with an aerodynamic diameter of less than 2.5 μm ($PM_{2.5}$), as these have the greatest impact on human health, radiative climate forcing, and atmospheric visibility (Sakulyanontvittaya et al. (2008)). SOA can make up between 13-30% of total $PM_{2.5}$ aerosol which result from the presence of BVOCs, and so their consideration is important to prevent widespread health issues (Kleindienst et al. (2010); Sakulyanontvittaya et al. (2008))**.**

Climatic forcing is also a result of increased concentrations of SOA due to radiative forcing, scattering and absorption of incoming solar radiation, and changes in albedo (**Figure 3 and 4**) (Laothawornkitkul et al. (2009); Wiedinmyer et al. (2006)) . Increased concentrations of SOA can also result in decreased visibility within the atmosphere, which can negatively influence

human activities, such as air travel (**Figure 4**). Within the atmosphere SOA influence cloud formation, as they act as nuclei for water droplets to condense onto (Jacob (1999)). These changes to cloud formation cause increased albedo and subsequently supress precipitation (McGrath-Spangler et al. (2015)). Because of the potential for BVOCs to contribute to the compounds discussed in the previous sections it is important to understand the factors that contribute to their emission so that they can be appropriately managed and mitigated.

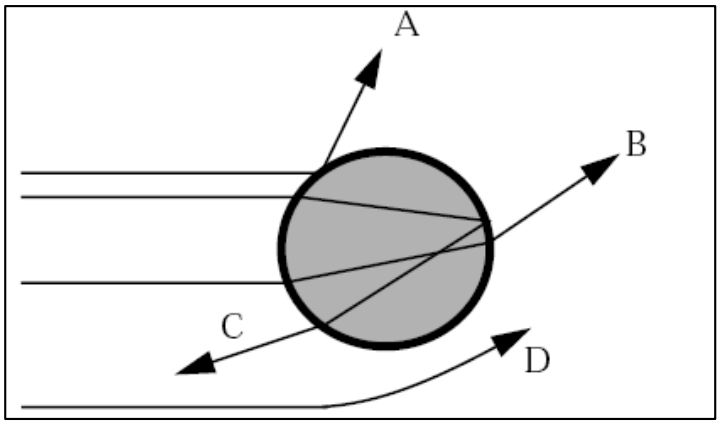


*Figure 3: Scattering of radiation due to SOA and associated processes: Reflection (A), refraction (B), reflection(C) and diffraction (D). (Jacob (1999))*

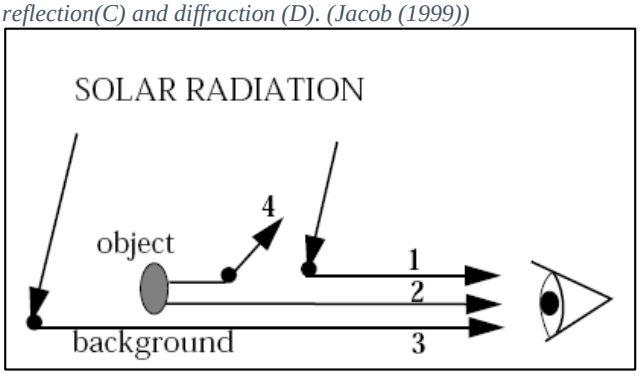


*Figure 4:Reduction of visibility as a result of SOA. Visibility of an object is determined by its contrast with the background (2 vs 3). Contrast is reduced by SOA scattering (1 and 4). (Jacob (1999))*

### 2.1.3 Factors influencing BVOC emissions

The dominant factors that influence BVOC emissions are relatively well known and are simple to measure. These include various environmental and plant specific factors, which include but are not limited to ambient temperature (**Figure 5**), photon flux density of solar radiation (**Figure 5**), foliar area, water stress, phenological events, vegetation productivity, vegetation cover, and vegetation type (Lathiere et al. (2006)). The most difficult of these factors to quantify is the vegetation cover of an area.

A common method of quantifying this vegetation cover is the prescription of a leaf area index (LAI). LAI is a dimensionless variable that is defined as the total one-sided area of photosynthetic tissue per unit ground surface area (Jonckheere et al. (2004)). Generally the vertical distribution of LAI is assumed to follow a triangular distribution, with peak LAI occurring at 3/3rds of the plant height, and dropping to zero at 1/3 of the canopy height (Nelson et al. (2002)). The LAI of vegetation will differ depending on seasonality, species composition, developmental stage, and prevailing site conditions, and as such is used to quantify the amount and age of foliage at a given location (Jonckheere et al. (2004); Guenther et al. (2012)). LAI values generally range between 2 (for annual crops), and 17 (for old growth forests) (Jonckheere et al. (2004)).

Due to these influences, emission rates are sensitive to climate and land cover type/use, and generally show strong diurnal and seasonal variability (Millet et al. (2016)) (**Figure 6**). However, the emission rates of individual BVOC species are affected by these factors to different degrees (Guenther (1993)). Monoterpenes are mainly influenced by leaf temperature, whereas isoprene emissions are influenced to a high degree by both leaf temperature and photosynthetically active radiation (PAR) (Guenther (1993)). PAR is the spectral range which photosynthetic organisms are able to use to produce energy (Jacob (1999)). Changes in these variables over time result in differing seasonal and diurnal emission profiles. For example, isoprene emissions at night will be far lower than monoterpene emissions, due to the strong influence that PAR has on isoprene emissions. This is despite the fact that isoprene emission rates are much higher during the day (**Figure 5**). Isoprene emissions start rapidly in the morning and build with the increase in photosynthetic photon flux density (PPFD a mole of PAR photons) until a saturation point at a given PPFD level (**Figure 4 Jacob (1999))**. Emissions of BVOCs have also been found to vary in the long term - for example, emission of isoprene is highly dependent on the temperature the plant has experienced recently (Nelson et al. (2002)). Despite these relationships, there are no consistent taxonomic relationships between vegetation and BVOC emissions even within the same genus (Pacifico et al. (2009)), making precise estimates of emissions for modelling difficult.

Because of the relationship between emissions and environmental variables discussed previously it is expected that anthropogenic influences, such as climate change, and urban greening will impact BVOC emissions in the future.

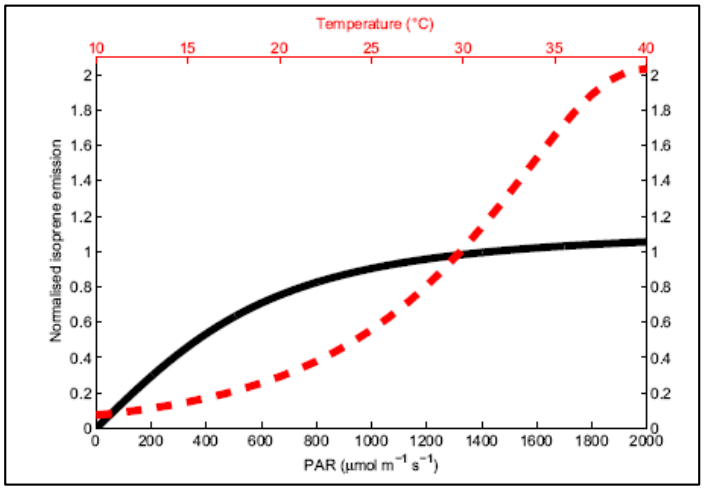


*Figure 5: Response of isoprene emission flux to photosynthetically available radiation (PAR) (solid line) and temperature (dashed line). Isoprene is normalised to standard conditions. Pugh et al. (2013)*

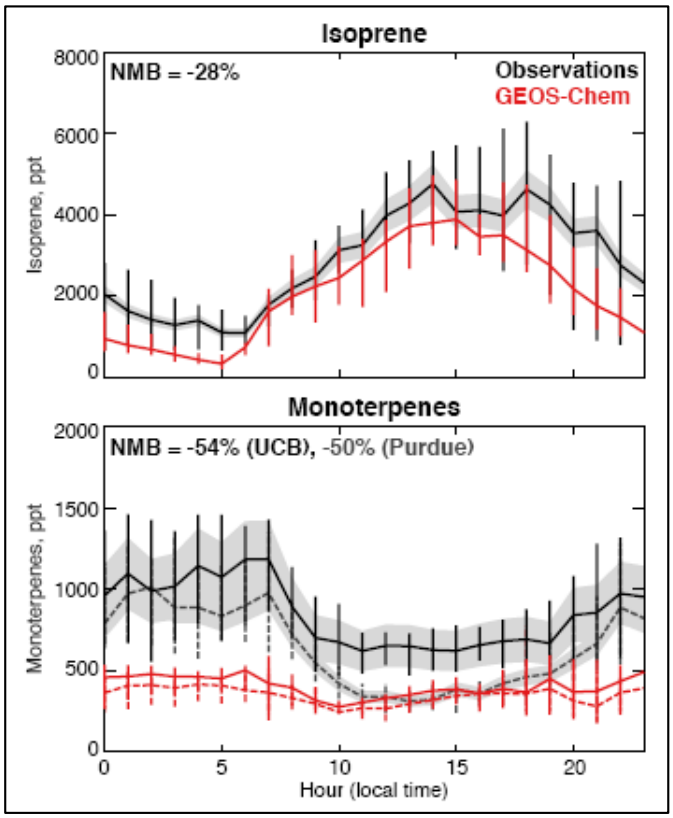


*Figure 6: time series of observed (black) and modelled (red) BVOC mixing ratios displaying different diurnal patterns of isoprene (top) and monoterpenes (bottom). Fisher et al. (2016)*

### 2.1.4 Projections of future BVOC emissions

Because of the impact that anthropogenic processes such as global warming and urbanisation are having on the environment it is important to assess how these impacts will influence emissions into the future.

BVOC emissions display an inverse relationship with atmospheric $CO_2$ concentrations (Unger (2013)) and a positive relationship with ambient temperature, so the effect that anthropogenic climate change will have on future emission rates of BVOCs as temperatures and $CO_2$ concentrations both rise is unknown. Pacifico et al. (2009) estimated that by 2100, 21$^{st}$ century climate change will result in an increase in isoprene emissions between 25 and 75% of present day emissions. Whereas Unger (2013) and Lin. et al. (2016) estimated that increased concentrations of $CO_2$ within the atmosphere will maintain current BVOC concentrations despite increasing temperatures and vegetation productivity. Another anthropogenic process that is expected to have an influence on BVOC emissions is increasing rates of urbanisation, resulting in areas that were previously forests being transformed into urban areas where there is comparatively little vegetation to emit BVOCs (Lathiere et al. (2006)). This increased urbanisation can lead to increased BVOC emissions in some circumstances, as has already been observed in the mega city Beijing, China (Ghirardo et al. (2015)). Increases in the number of trees due to urban greening also significantly change the chemistry of the regional atmosphere, as tropospheric ozone causes vegetation to release stress-induced BVOCs. These stress-induced BVOCs have a significant effect on SOA formation, causing much larger quantities to be formed. As such, urban planning is important to prevent unwanted increases in BVOC emissions as a consequence of urban greening (Ghirardo et al. (2015)).

### 2.1.5 BVOCs in Australia and the GMR

Due to Australia's unique ecology and climate, BVOC emissions are an important consideration for the future. It has been estimated - through various modelling and remote sensing studies - that biogenic emissions in southeast Australia may be amongst the highest in the world, due to the dominance of densely forested parimarily eucalypt ecosystems with high BVOC emission factors (**Figure 7**) (He et al. (2000) COALA stearing group (2016)).

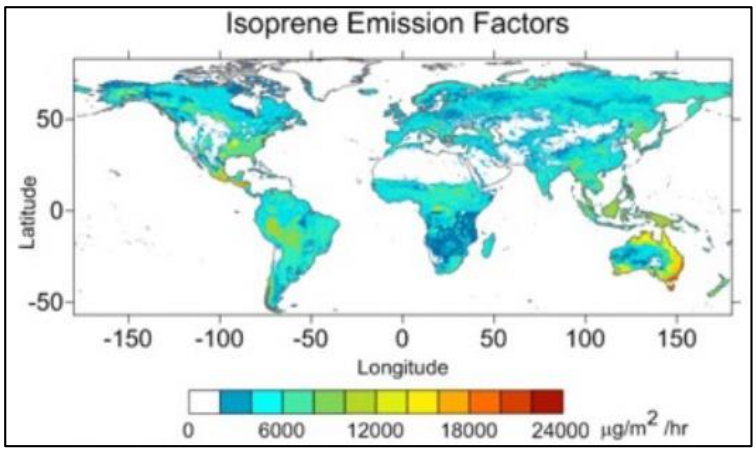


*Figure 7: Global Isoprene emission factors used within MEGAN. (Guenther et al. (2012))*

Despite this, relatively little is known regarding the exact quantity of emissions, and their spatial and temporal distribution on the Australian continent (Emmerson et al. (2016)). This uncertainty is apparent as modelled BVOC emission inventories in southeastern Australia have differences of a factor of 2-3 for isoprene, and 5-10 for monoterpenes (Zeng et al. (2015); Emmerson et al. (2016)). Field estimates were also undertaken by Emmerson et al. (2016) and compared to the forementioned model runs. This comparison suggested that in South East Australia, monoterpene emissions are underestimated, and isoprene emissions are overestimated (COALA stearing group (2016)). These large uncertainties are in stark contrast to AVOC emissions, which are reasonably well known. This, coupled with the fact that continental Australia occupies 22% of the land area in the southern hemisphere (Emmerson et al. (2016)), means that correctly representing Australian BVOCs within CTMs is important to understand and predict atmospheric chemical processes on local to hemispheric scales.

Australia is also a region of interest for studying BVOC emissions due its relatively clustered population distribution and large amounts of undisturbed terrestrial vegetation (COALA stearing group (2016)). This allows for the study of BVOC emissions in an environmnet that is relatively free of anthropgenic influence, and over numerous spatial gradiants - such as the transition between natural and builtup environmnets.

Another factor that makes the GMR, and more specifically Sydney, unique is the seperation of urban environmnets with surrounds of dense vegetation. Because of this surrounding vegetation, it is likely that BVOCs are transported over urban areas of Sydney by meterological processes such as wind and sea breeze circulations (Millet et al. (2016)). Once these BVOCs are present over urban centers they have the capacity to have a noticeable impact on air quality, and possible health implications, through both natural processes and anthropogenic

interactions. The interactions and processes that influence these events are complex and difficult to quantity using ground based measurements and monitoring, due to their large scale and high reactivity. Hence, to further understand these complex processes and attempt to mitigate possible environmnetal damage, CTMs are employed as part of a wider air quality monitoring system.

## 2.2 Chemical transport models (CTMs)

The accurate forecasting of air quality and subsequent impacts at various scales require the use of CTMs. CTMS allow for estimates of various parameters on a large scale that would be expensive and impractical to measure using field based techniques and ground monitoring.

For regional scale models simulating emission, chemical processes, atmospheric transport, and deposition an Eulerian (box) modelling framework is used (**Figure 8**) (Jacob (1999)). An Eulerian model allows for the modelling of multiple complex interactions, by simulating species concentrations through solving mass balance equations in an array of fixed computational cells (Jacob (1999)). CTMs are generally coupled to a high resolution meteorological model which provide predictions of factors such as precipitation, humidity, and ambient temperature (Hess et al. (2004)). Differences in vegetation type, and resulting emission rate, are also accounted for within CTMs through the prescription of plant functional types (PFT). PFTs are classes of vegetation that share similar responses to environmental factors that are assigned to a grid cell in space. This allows for the determination of the BVOC emission capacity of a specific area.

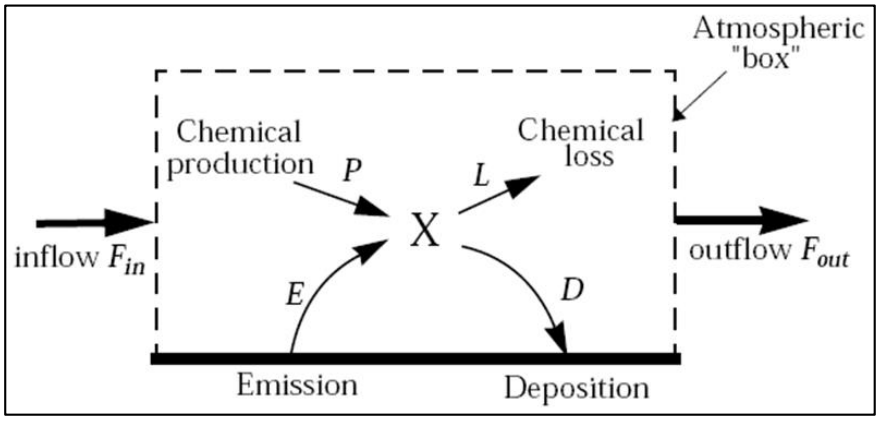


*Figure 8: One box in a Eulerian model, which couples together many boxes together in a 3D framework to represent the atmospheric concentration of species x in this example. (Jacob (1999))*

The means that a CTM is coupled to the external meteorological model can be manipulated so that either one way interactions can occur (offline coupling), or 2-way interactions can be

allowed (online coupling), depending on the model specifications and application (Grell et al. (2004)). An offline modelling approach involves meteorological data being saved at specific time intervals and used to drive a CTM at a later time, with only meteorology influencing chemistry (Grell et al. (2005)). The separation of chemistry and meteorology within an offline model can lead to a loss of information about atmospheric processes that occur in a time scale much smaller than the output of the meteorological model (Kirstine and Galbally (2004)). In contract, an online model provides a simulation that is closer to what actually happens in the atmosphere. As well as allowing interactions between meteorology and chemistry it also allows for the chemistry to interact with the meteorology. An example of chemistry influencing meteorology are the interactions between aerosol and cloud condensation nuclei which result in precipitation. This precipitation would subsequently effect atmospheric BVOC concentrations (Grell et al. (2005)).

CTMs consist of many different inline models and components, all of which are integrated to determine concentrations of chemical species within the atmosphere. To create and validate these models field campaigns, remote sensing, and laboratory based work must be undertaken to determine various factors, including the atmospheric interactions of specific chemical species, and plant specific emission factors (Pacifico et al. (2009)). An emission factor is the quantity of emissions that the designated area will theoretically emit under standard conditions defined by the model. A good example of the emission factor prescription process can be found in Nelson et al. (2002). Deviations from these standard conditions are generally accounted for with a scaling parameter. Field campaigns, remote sensing, and models produce data of different temporal and spatial scales and as such are applicable to different applications (**Figure 9**). For example, isoprene emissions can be remotely sensed on a continental scale using formaldehyde columns ($CH_2O$ a reaction product of isoprene) (Abbot et al. (2003)).

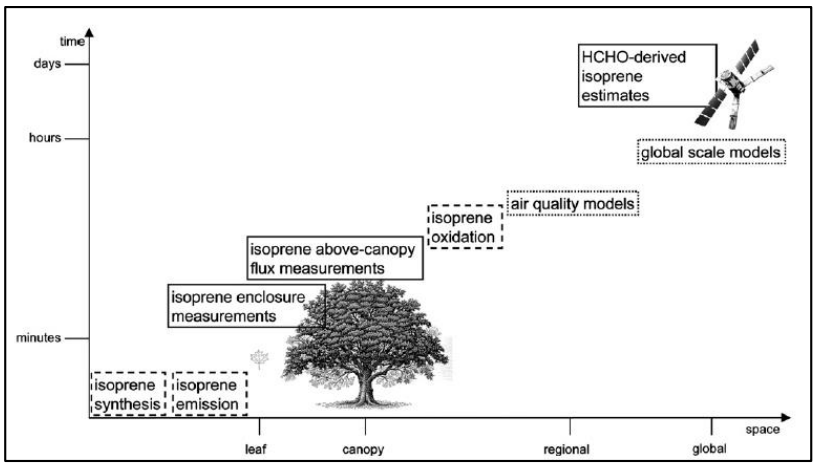


*Figure 9: temporal and spatial scales of processes, observations and intended model applications related to isoprene emissions and impacts. (Pacifico et al. (2009))*

One component that is required to effectively run a CTM is the BVOC emissions module (Cope et al. (2009)). Several different models are available to calculate emissions from terrestrial ecosystems, including the Model of Emissions of Gasses and Aerosols from Nature (MEGAN) (Guenther et al. (2012), and the inline BVOC module used in the CSIRO CTM (Nelson et al. (2002); Cope et al. (2009)). These models allow for small scale measurements - such as the emission rate of a specific species of plant - to be extrapolated and combined with other processes to create a holistic representation of the spatial and temporal distribution of BVOC emissions on a local to regional scale (Ito et al. (2009)). Once the emissions of BVOCs are calculated by either the CSIRO CTM inline biogenic model or a biogenic specific model, such as MEGAN, the data can be combined with other emissions such as AVOCs and used within an overall CTM to calculate total VOC concentration. This final concentration is a function of the mixing depth of the boundary layer, horizontal advection, emission rate from the underlying vegetation, and rate of removal (Emmerson et al. (2016)). Once concentration has been calculated, this information can be used to determine and predict overall air quality within a region - including ozone and/or SOA events that have the capacity to harm living organisms and negatively impact on human health. Within this study the outputs of three model implementations will be assessed including MEGAN, CSIRO CTM, and CSIRO CTM coupled to MEGAN. These different implementations will be further explained in subsequent sections 2.4.1 – 2.4.3.

### 2.2.1 The CSIRO CTM BVOC emission module

The CSIRO CTM has been developed over 15 years to address regional air quality issues within the Australian continent (Cope et al. (2009)). Typically, the CSIRO CTM is used to model photochemical smog production at a local to regional scale, and can be run both online and offline (**Figure 10**). The model encompasses a three- dimensional Eulerian modelling framework which accounts for the emission, chemical processes, transport, and wet and dry deposition of a gas phase or an aerosol-gas mix (**Figure 12**) (Cope et al. (2009)). The CTM uses meteorology from the CSIRO Conformal Cubic Atmospheric Model (CCAM) which provides predictions of factors that influence BVOC emissions including: wind velocity, water vapour mixing temperature, rainfall, and radiation (McGregor and Dix (2008)). CCAM is also capable of modelling large scale climate drivers such as the Indian Ocean Dipole (IOD) and El Niño–Southern Oscillation (ENSO) through the modelling of sea surface temperatures (Watterson et al. (2008)). CCAM is a model with variable resolution over the study domain,

allowing for both global and continental circulations to be accounted for, and enhanced resolution over a selected smaller region (**Figure 11** Trieu et al. (2015)).

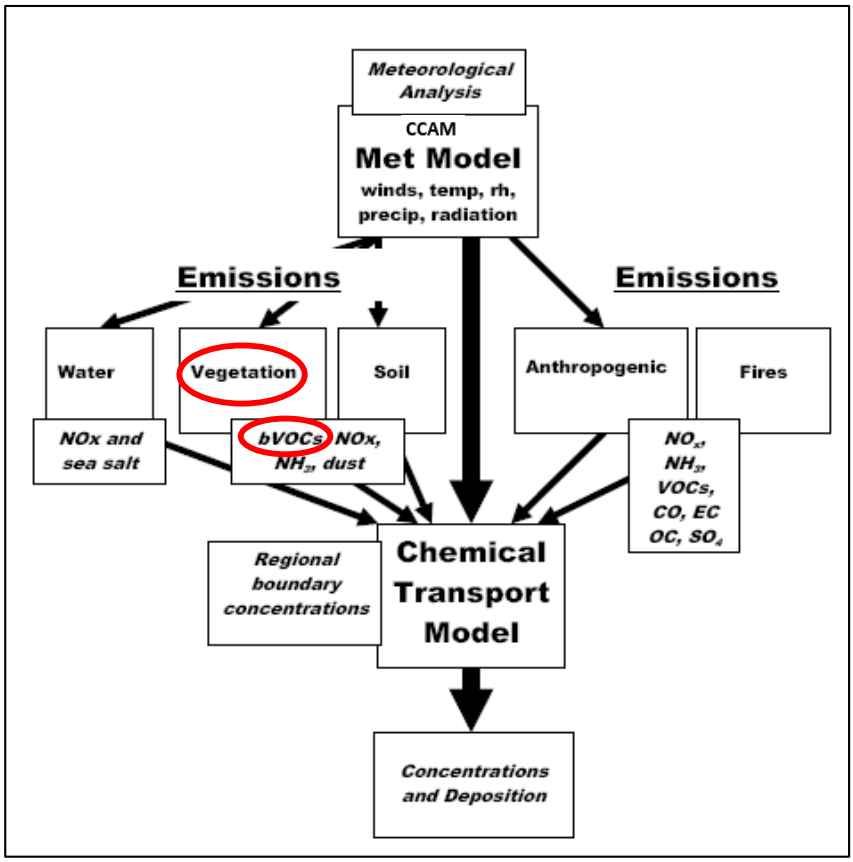


*Figure 10: Schematic of CSIRO CTM and how the biogenic module (Red circles) is used in the overall model (Cope et al. (2014))*

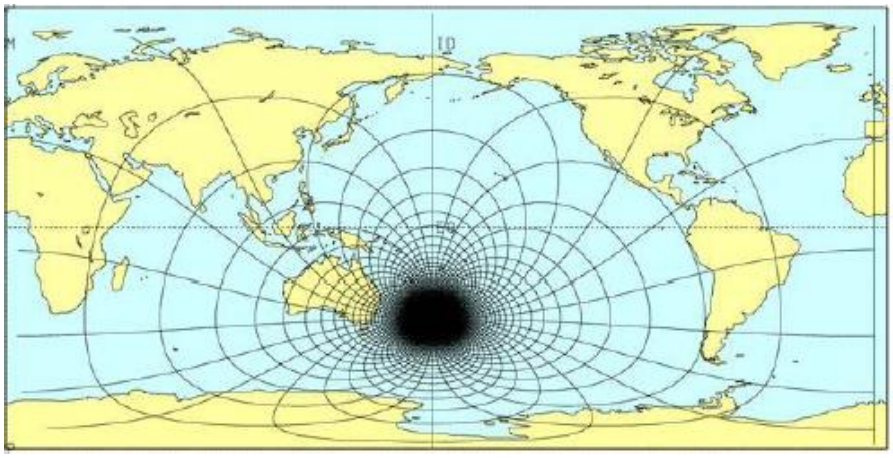

*Figure 11: Example of CCAM variable resolution capacity with 8km grid over New Zealand. (Katzfey (2015)*

The CSIRO Atmosphere Biosphere Land Exchange model (CABLE) is used within CCAM to provide information relating to land cover and surface characteristics, such as leaf area index (LAI, derived from MODIS data) and surface roughness (Kowalczyk et al. (2006)).

Within CCAM, global background concentrations that are transported into the Australian region by advection are taken into account using a nested grid approach. This approaches uses numerous distinct study domains with varying sizes and resolutions depending on the application of the model (Cope et al. (2009)). As part of this approach each nest has a higher resolution but consequently covers less area. The domains used to model emissions in the CSIRO CTM for the data contained in this report are regional domains which are focused on the Sydney Greater Metropolitan Region **(GMR, figure 13).** The CTM includes inline algorithms for modelling BVOCs from forest canopies, cut and uncut pastures, and grasses. The following sections will provide the details and inputs of the canopy emission model, but not the pasture and grasses model as this information is not assessed in this report as it was not available.

The governing equation of the CSIRO CTM Biogenic canopy model is Emissions (*E*) of substance, *i* from source *j* (kg/year) is:

$$E_{i,j} = \sum_{k=1}^{8760} \left(A_j \times B_{m,j} \times EFi_j \times f\left(LAI_j, PAR_j, T_j\right) \times 10^{-9}\right) \qquad (\mathbf{1})$$

Where:

$A_j$ ($m^2$): is the area of vegetation type j

$B_{m,j}$ (g leaf): is the leaf biomass of vegetation type j

$EF_{I,j}$ : is the emission factor for substance i from vegetation type j under ideal conditions (µg /g leaf biomass/ hour)

$f\ (LAI_j, PAR_j, T_j)$*:* Equations which account for LAI, PAR and temperature

*i*: Substances (either VOC or speciated VOC)

*j*: Vegetation type (Either tree canopy or pasture and grasses)

*k* (h/yr): time interval

$10^{-9}$ (kg/µg): conversion factor

8760: Hours in a year

For a given BVOC from a particular canopy source, the total emission will depend on the quantity of vegetation present in the study area ($A \times B_m$), the rate BVOCs are emitted from the vegetation under ideal conditions (*EF*), and a scaling parametrisation that accounts for

deviations from ideal conditions, as defined within the emissions factor. Factors accounted for within this scaling parameter are temperature, radiation, and time of day *f*(*LAI, PAR, T*) (NSW Environmnetal Protection Authority (2012)). The scaling factors included in **Equation 1** to correct for changes in **:** PAR, LAI, and temperature are defined within the 'Chemical Transport Model Technical Description' (Cope et al. (2009)). The emission factors included within **Equation 1** are also defined and expanded upon within this technical description.

### 2.2.2 MEGAN 2.1

MEGAN is a widely used empirical BVOC modelling framework that is capable of estimating BVOC fluxes between terrestrial ecosystems and the atmosphere, through the use of simple mechanistic algorithms that account for the major known processes that control BVOC emissions (Guenther et al. (2012)). The framework can be run online or offline and was developed to allow for the calculation of BVOC emissions over much of the earth's surface in numerous different biomes (Guenther et al. (2012)).

To facilitate these calculations, MEGAN uses meteorological parameters such as solar radiation and temperature to predict emissions of ~150 chemical species, using either emission factor maps based on global observations (10 chemical species **Equation 3**), or plant functional types to predict the remaining 140 chemical species (**Figure 12**, **Table 3 & Equation 2** Guenther et al. (2012)). For example, isoprene has one emission factor map as it is only 1 compound, so emissions can be estimated directly by the chemical model (**Figure 12)**. In contrast, MEGAN calculates emissions for 34 species of monoterpenes, so some will use emission factor maps and the others will use PFTs. This study uses both methods to calculate emissions within MEGAN. The emissions of these compounds are then converted into common reaction schemes that are generally used in CTMs.

The equation MEGAN uses to calculate emission rate, $E$ (μg compound/ $m^2$ /hour) for compound class $i$ from PFT $j$ is:

$$Ei = \sum_{j=1}^{nPFT} ( EF_{ij} \times \gamma_{ij} \times X_j) \qquad (2)$$

Where:

$EF_{i,j}$ ($mgm^{-2}\ h^{-1}$) is an emissions factor of species $i$ for vegetation type $j$ with fractional box grid coverage $x_j$ which represents emissions at standard conditions

$\gamma i$ (normalised ratio) is an emission activity factor that accounts for changes in emissions due to deviations from standard conditions. This includes: response to light, temperature, leaf age, soil moisture, CO2, and LAI.

Thus emissions over an area of a given compound class will depend on the PFT coverage ($nPFT\Sigma_{j=1}$), the emission factor and coverage of the present PFTs ($EF_xX$) and an activity factor that accounts for deviations from ideal conditions (Guenther et al. (2006); Guenther et al. (2012)) Emmerson et al. (2016).

To calculate emission rate, $E$ of species $k$ in a given grid cell, $xy$ using global emission factor maps and canopy characteristics MEGAN uses:

$$Ek = EF_{k,xy} \sum_{j=1}^{nPFT} (\gamma_{kj} \times X_j) \qquad (\mathbf{3})$$

Where:

$EF_i$, ($mgm^{-2}$ $h^{-1}$) is an emissions factor of species $i$ from the specific emissions factor map fractional box grid coverage $x_j$ which represents emissions at standard conditions

In this equation, MEGAN uses PFTs to define environmental and canopy characteristics and to define the fractional grid box areal coverage, but the results are not sensitive to the PFT emission rate (Guenther et al. (2006); Guenther et al. (2012)) Emmerson et al. (2016).

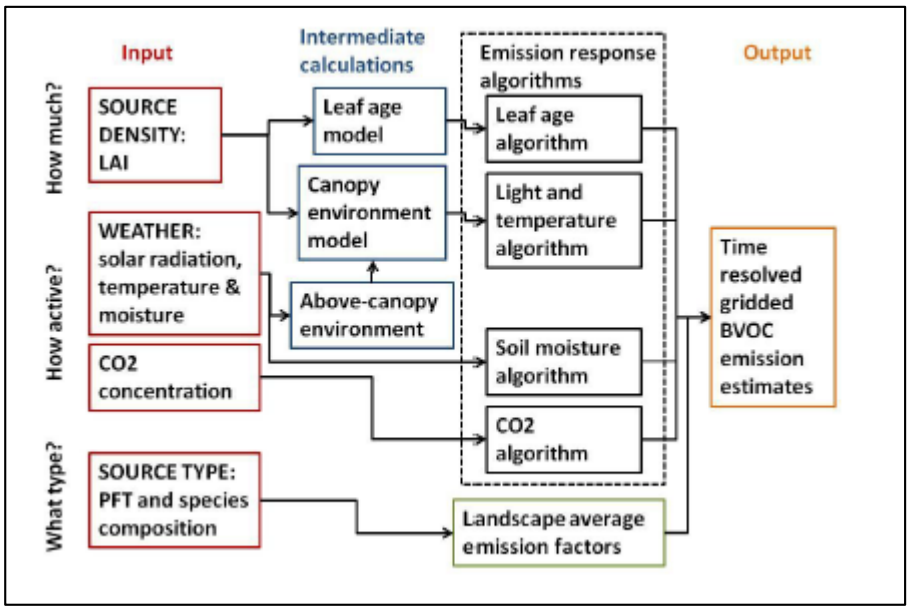


*Figure 12: Schematic of MEGAN driving variables and model components. (Guenther et al. (2012)).*

| Compound Class | Compound names |
|---|---|
| isoprene | isoprene |
| myrcene | myrcene |
| sabinene | sabinene |
| limonene | limonene |
| 3-carene | 3-carene |
| *t*-$\beta$-ocimene | *t*-$\beta$-ocimene |
| $\alpha$-pinene | $\alpha$-pinene |
| $\beta$-pinene | $\beta$-pinene |
| $\beta$-caryophyllene | $\beta$-caryophyllene |
| $\alpha$-farnesene | $\alpha$-farnesene |
| 232-MBO | 232-MBO |
| methanol | methanol |
| acetone | acetone |
| CO | CO |
| Other Monoterpenes (34 compounds) | aromatic monoterpenes (dimethyl styrene, meta-cymenene, p-cymene, and o-cymene), monoterpenes ($\alpha$-phellandrene, $\alpha$-thujene, $\alpha$-terpinene, $\gamma$-terpinene, terpinolene, $\beta$-phellandrene, camphene, bornene, $\alpha$-fenchene, allo-ocimene, cis-$\beta$-ocimene, verbenene and tricyclene), oxygenated monoterpenes (camphor, fenchone, piperitone, myrtenal, $\alpha$-thujone, $\beta$-thujone, 1,8-cineole, borneol, linalool, 4-terpineol, $\alpha$-terpineol, cis-linalool oxide, trans-linaool oxide and bornyl acetate) and monoterpenoid-related compounds ($\beta$-ionone, ipsenol and estragole). |
| Other Sesquiterpenes category (30 compounds) | sesquiterpenes ($\alpha$-bergamotene, $\beta$-bisabolene, $\beta$-farnesene, $\alpha$-humulene, acoradiene, aromadendrene, $\beta$-bergamotene, $\alpha$-bisabolene, $\beta$-bourbonene, $\delta$-cadinene, $\delta$-cadinene, $\alpha$-cedrene, $\alpha$-copaene, $\alpha$-cubebene, $\beta$-cubebene, $\beta$-elemene, germacrene B, germacrene D, $\beta$-gurjunene, $\gamma$-humulene, isolongifolene, longifolene, longipinene, $\alpha$-muurolene, $\gamma$-muurolene, $\beta$-selinene, and $\delta$-selinene), oxygenated sesquiterpenes (cis-nerolidol, trans-nerolidol and cedrol). |
| Bidirectional VOC (5 compounds) | ethanol, acetaldehyde, formaldehyde, acetic acid, formic acid |
| Stress VOC (15 compounds) | ethene, dimethyl-nonatriene (DMNT), 3-hexenal, 2-hexenal, 3-hexenol, 3-hexenyl acetate, hydrogen cyanide, hexanal, 1-hexenol, methyl jasmonate, methyl salicylate, toluene, indole, trimethyl-tridecatetraene (TMTT), jasmone |
| Other VOC (49 compounds) | leaf surface compounds (homosalate, 2-ethylhexyl salicylate, geranyl acetone, oxopentanal, and methyl heptenone), organic halides (methyl bromide, methyl chloride and methyl iodide), sulfur compounds (diallyl disulfide, methyl propenyl disulfide, propenylpropyldisulfide, carbon disulfide, carbonyl sulfide, hydrogen sulfide, methyl mercapten, dimethyl sulfide and dimethyl disulfide), alkanes (methane, ethane, propane, pentane, hexane, heptane), alkenes (butene, propene, 1-dodecene, 1-tetradecene), benzenoids (benzaldehyde, methyl benzoate, 2-phenylacetaldehyde, eugenol, anisole, benzyl acetate, benzyl alcohol, and naphthalene), oxygenated VOC (pentanal, hexanal, heptanal, octanal, nonanal, decanal, octanol, octenol, heptanone, 2-butanone, pyruvic acid, 331-methylbutenol, 321-methylbutenol, neryl acetone, $\alpha$-terpinyl acetate, phenylacetaldehyde and nonenal) |

*Table 3: MEGAN compound classes and individual compounds. (Guenther et al. (2012))*

### 2.2.3 Coupling of MEGAN 2.1 to CSIRO CTM

The offline version of MEGAN 2.1 is designed to be used with the Weather Research and Forecasting (WRF) modelling system, as described by Guenther et al. (2012). This code was extracted from the WRF system and coupled to the CSIRO CTM, as was used in Emmerson et al. (2016). The implementation of this coupling means that some inputs required for modelling will be different to those within the standard CSIRO-CTM.

The inputs that are required to be different for this coupling are: underlying vegetation maps and PAR, with other variables required provided by CCAM as per the original CTM (Emmerson et al. (2016)). This implementation predicts emissions using equations **2** and **3**, as discussed in the previous section depending on the compound being predicted.

# 3. Regional setting and method development

## 3.1 Regional setting: The Greater Metropolitan Region

The GMR is the largest metropolitan area in NSW Australia, with a population of 4.6 million people, 64 local government areas, and over 60% of the state's total population (**Appendix 18**) (NSW Office of Environment and Heritage (2014); Broome et al. (2015)). Sydney is the largest city within the GMR located in the temperate climatic zone on the east coast of Australia, at latitude 33.8$^{o}$S (**Figure 13, Figure 14**) and as such experiences four distinct seasons including cool to cold winters, and warm to hot summers (Hart et al. (2006)). Sydney is located within the Sydney sedimentary basin (**Appendix 4)**, which creates a relatively isolated air shed, meaning that only rarely are ozone and aerosols transported from industrial areas to the north and south of Sydney (Hart et al. (2006)). The major urban areas within the Sydney region are bounded by elevated terrain to the north, south, and west, along with the Tasman sea to the east (Jiang et al. (2016)).

Exceedances of ozone national concentration standards, specifically in the central and western parts of the region, are most commonly associated with a sea breeze that transports emissions from the CBD and eastern suburbs (Hart et al. (2006)). Despite the fact that ozone and $PM_{2.5}$ levels in the Sydney metropolitan region are relatively low when compared to other industrialised countries, and exceedances occur infrequently, it is estimated that 430 premature deaths and hospital emissions occurred in 2007 due to $PM_{2.5}$ (Broome et al. (2015)). These exceedances within the GMR are associated with high temperatures and regional bushfire events, and hence generally only occur intermittently during warmer summer months (Trieu et al. (2015)).

Significant clearing of vegetation has occurred in the highly urbanised parts of the region such as Sydney (Nelson et al. (2002)). Despite this, the Sydney area is bounded by multiple reserves and four large national parks including The Royal National Park, Ku-Ring-Gai Chase National Park, Nattai National Park, and Blue Mountains National park in which the vegetation remains mostly intact (**Figure 14)**. Numerous pockets of parkland and remnant bush also contribute to the diverse and widespread vegetation cover of the region (Nelson et al. (2002); Azzi et al. (2005)). These areas are of particular interest as they likely produce large quantities of BVOCs that have the capacity to negatively influence air quality in the region.


*Figure 13: Regional setting: Sydney Metropolitan Region (Blue square)*

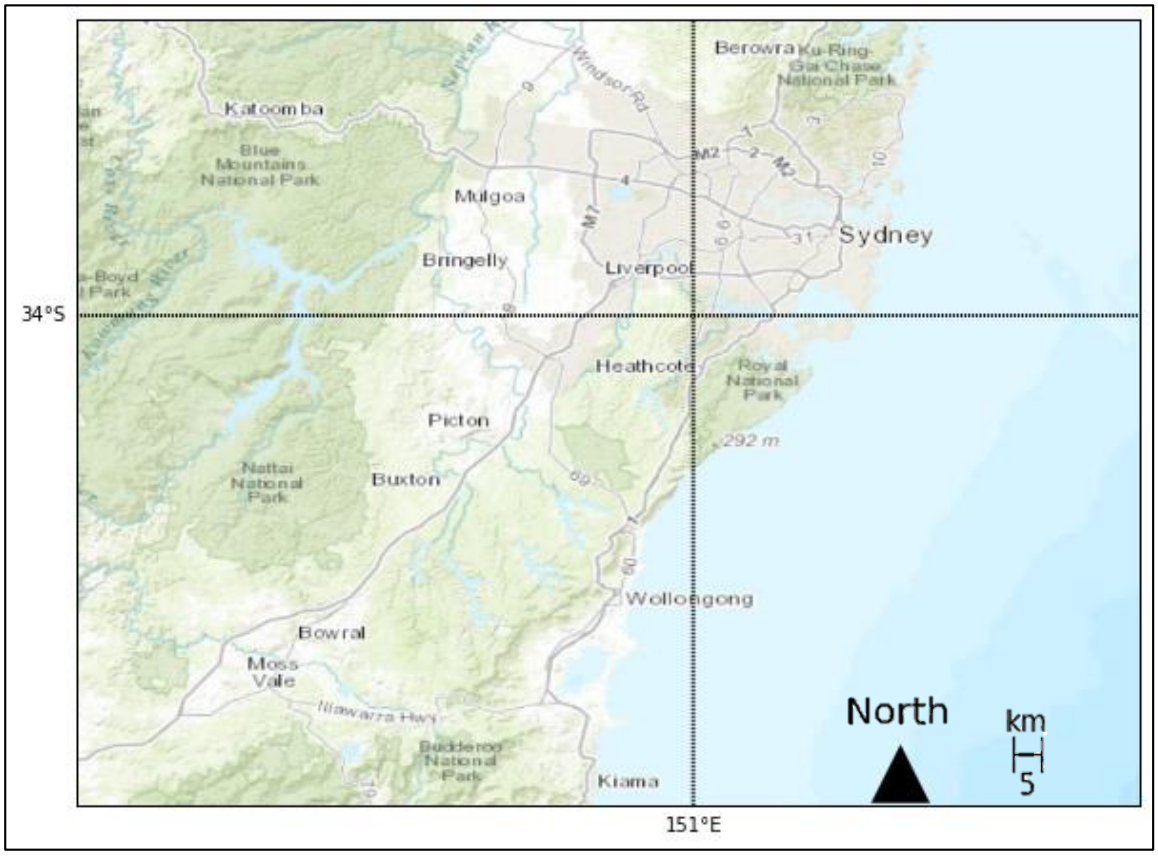


*Figure 14: Regional map of Sydney region showing high levels of vegetation surrounding urban areas (Domain 3)*

## 3.2 Model intercomparison datasets

February 2011 was chosen for the intercomparison component of this study as data was available for all three models implementations, which allowed for a straightforward comparison. February is also near the expected peak of annual BVOC emissions in the Southern Hemisphere, due to generally high temperatures and long daylight periods. This month also coincided with the SPS1 campaign involving field measurements and the implementation of the CSIRO CTM (Cope et al. (2014)). Unfortunately, this study focused on BVOC reaction products, mainly SOA, and as such emissions could not be directly compared. All three model runs used the CB05 chemical mechanism.

Data files containing modelled daily outputs were acquired from the NSW OEH, CSIRO, and The University of Melbourne. The three datasets obtained for February 2011 were produced respectively by an online implementation of the CSIRO CTM Biogenic module (CSIRO-CTM-Original), an offline implementation of MEGAN 2.1 (MEGAN-Offline), and an online implementation of MEGAN 2.1 coupled to the CSIRO CTM Biogenic module (CSIRO-CTM-MEGAN). Each model dataset consisted of 28 days of hourly data, resulting in 648 individual data frames. The most notable difference between the inputs of the three models is that the land cover/ PFTs used within the MEGAN-Offline implementation is a vegetation climatology (**Table 4**) which assumes that the distribution of vegetation is based mostly on meteorology. The meteorology used to create such a dataset is a yearly average and as such may not accurately reflect the inter-annual variability in nature. The MEGAN-offline model implementation also uses offline meteorology, which means that the meteorology is determined before BVOC emissions are predicted, thus meteorology can influence emissions but not vice versa (**Table 3)**. As is the case for the vegetation, this meteorology is based on a yearly average and also may not accurately reflect inter-annual variations. Each model differed in the way that they outputted emissions, with MEGAN-Offline and CSIRO-CTM-MEGAN both outputting monoterpenes and isoprene as separate variables in opposed to CSIRO-CTM-Original which outputted both chemical species as one variable that could not be differentiated.

| Model name | Time period | Description | D1 Resolution (Km) | D2 Resolution (Km) | D3 Resolution (Km) | Meteorology source | Land cover/ PFTs | LAI | Speciated BVOC Emissions |
|---|---|---|---|---|---|---|---|---|---|
| CSIRO-CTM-Original | 2011 Feb-Mar | 2.2.1 | 9 | 9 | 3 | CCAM | CABLE 2011 | MODIS Feb[1] | No |
| MEGAN-Offline | 2011 Feb-Mar | 2.2.2 | 25 | 5 | 1 (regrid to 3) | CMAQ (Offline) | CLM4 2003 | CLM4-SP 2001 v4 | Yes |
| CSIRO-CTM-MEGAN | 2011 Feb-Mar | 2.2.3 | - | 3 | 3 | CCAM | IGBP 2003 | MODIS FEB 2011 | Yes |

*Table 4: Sources of 2011 model inputs and resolution at given domain*

[1] Year Unknown

Anthropogenic activities and fires also produce BVOCs and as such are included in overall BVOC inventories however, this data is not included in the information assessed during this study. Methane and other light oxygenated hydrocarbons have also not been considered within these model runs and have been reviewed in detail elsewhere. The three domains used within the three different model runs overlap to a large degree, and consist of different resolutions depending on the domain and model being run (**Figure 15, Table 5**). The domain used within the 2011 period was chosen to be domain three as it allowed for plotting of emissions at a higher resolution of 3x3 $km^2$ that was consistent across all three model runs. Despite the fact that domain three covers the smallest area, the higher resolution allowed for a better comparison of the spatial distribution of predicted emissions, and analysis of minute differences and similarities that would not be discernible at lower resolutions.


*Figure 15: Map of Sydney GMR and domains used D1: Purple D2: Blue D3: Black (UTM)*

| Domain # | Lower left corner latitude: | Lower left corner longitude: | Upper right corner latitude: | Upper right corner Longitude | Area $km^2$ | Resolution |
|---|---|---|---|---|---|---|
| D1 | 36.7246° S | 147.804° E | 31.4146° S | 153.114° E | 279 070 | 9x9 $km^2$ |
| D2 | 34.836° S | 150.079° E | 33.066° S | 151.849° E | 31 717 | 3x3 $km^2$ |
| D3 | 34.717° S | 150.100° E | 33.565° S | 151.651° E | 18 176 | 3x3 $km^2$ |

*Table 5: Dimensions of domains used*

## 3.3 Annual analysis of CSIRO CTM dataset

The year 2013 was chosen for the annual analysis of emissions as it is currently the most recent data that is available to the OEH. The predictions used for the 2013 analysis were produced using the CSIRO-CTM-Original model, as it is the model that the OEH currently employs for air quality modelling activities within the GMR. This dataset consisted of 365 days of hourly data, resulting in 8760 individual data frames. The largest domain (domain 1, **Table 6**) was used for this component of the study as it allowed for large scale seasonal changes to be observed across a much wider area. Domain three data was not available for this time period, so domain 1 data over the domain 3 area was used for a comparison between the 2011 and 2013 CSIRO-CTM-Original model runs. This required the 2011 data to be regridded to 9x9 $km^2$ for the sake of consistency. The LAI data used within the 2013 run is the same dataset that is used within the 2011 modelling run, albeit at a different resolution. The 2013 datasets also employed the CB05 chemical mechanism.

| Model name | Time period | Description | D1 Resolution (Km) | D2 Resolution (Km) | D3 Resolution (Km) | Meteorology source | Land cover/ PFTs | LAI | Speciated BVOC Emissions |
|---|---|---|---|---|---|---|---|---|---|
| CSIRO-CTM-Original | 2013 Jan-Dec | 2.4.1 | 9 | - | - | CCAM | CABLE 2013 | MODIS Jan-Dec [2] | No |

*Table 6: Sources of 2013 model input and resolution at given domain*

## 3.4 Development of emission maps and time series for the GMR

The outputted emission files obtained from external organisations were in Network Common Data Form (NETCDF) format, containing a single 24-hour period each. These files were concatenated along a record dimension to create a monthly file for analysis using the Unix based toolkit NETCDF Operators v4.6.0 (NCO) (see **Appendix 1** for commands used). Python 2.7 Anaconda was used to regrid all of the MEGAN-Offline data set using a linear interpolator, as it was originally outputted at a 1x1 $km^2$ resolution (**Appendices 6 & 8)**. Efficient data management and organisation were important considerations during this project as around 500 individual files, ranging between 100mb and 300mb constituting around 11 thousand frames, were required for the entire project.

An initial assessment of the data was undertaken using the Unix based visual browsers Ncview v2.1.1 and ncdump, however these packages do not produce figures that are of adequate quality for published reports (**Appendix 1**). The emission data contained within the monthly files was then imported into a Python 2.7 Anaconda distribution in array format **(Appendix 17)**. The majority of the data had at least four dimensions (day, hour, latitude, longitude) in their associated arrays and were manipulated over space or time to produce relevant plots. Once the

[2] Year unknown

data was imported into Python 2.7, new scripts were written specifically for this study that involved multiple operations applied over different dimensions including averaging, reshaping, slicing, calculating standard deviations, calculating correlation coefficients, addition, and mapping (**Appendices 2 & 3** for modules used and sample scripts). Different scripts (some up to 600 lines long for the annual analysis) were written to analyse the output data from each model, as each data set was arranged differently. Great care was taken to ensure that the resulting script library was well documented, easy to understand and easy to execute so it can be used in subsequent activities by OEH staff if required.

These manipulated arrays were then mapped in raster format and plotted as time series using self-written scripts containing numerous other modules over the study area. Different scripts were written for each model dataset due to differences in the data and array structure. The units of emissions used within the data were standardised to kg/km$^2$/hour, and time zones of these plots converted from UTC to Sydney local time using various operations in python 2.7. Along with this, the data points that are located above the ocean were masked as null using python 2.7 scripts as to not skew the analysis. The provided data files also include other variables of interest, such as LAI and temperature, and these were also mapped and plotted using a similar process to the emissions data. Various other model inputs were obtained in gridded data format (GRD) and were converted to NETCDF using the "multidimensional toolbox" contained within ARCGIS v10.3.1. The way that these arrays were organised required manipulation using numerous commands to make the data organisation consistent, and to allow for comparisons. Remotely sensed imagery and topographic maps were obtained within Python and integrated into the plotted datasets using an API, although this meant that Python encountered issues when attempting to plot place labels on the resulting maps, and as such these details are not present within these maps. The data was kept in its 3x3 km$^2$ resolution for mapping, as smoothing using an interpolator would have resulted in a loss of spatial information. Once these plots were produced careful attention was needed to preserve the resolution of the plots. This is best viewed in digital form as this allows for zooming to view fine details such as place labels.

Numerous difficulties and delays were encountered during this process due to issues and inconsistencies within the data files that were obtained from the respective external organisations. These issues included units being inconsistent with their accompanying description, models being run incorrectly using the wrong inputs, and numerous variables lacking a description or being incorrectly labelled. In some cases, these issues required the model to be re-run by the external organisation, resulting in further delays in file availability.

Unfortunately, some variables such as PAR and rainfall, that would have been highly valuable for analysis, were not included within their relevant model outputs and as a result could not be analysed.

Through exploring and plotting the data, these issues were found and consequently resolved by the external modellers. This will result in a simpler analysis of this data in future studies, and overall air quality modelling exercises being more accurate and closer to what actually occurs in nature.

## 4. February 2011 model intercomparison results and discussion

### 4.1 Monthly mean spatial distribution of emissions

**Figure 16** shows the combined monthly mean emissions of isoprene and monoterpenes for February 2011 across domain 3, as simulated by each of the three models. It is expected that BVOC emissions will be amongst their highest yearly levels during this period because it is summer, and as such both temperature and PAR will be amongst their highest yearly levels. The figure shows that the spatial distribution of modelled BVOC emissions throughout domain 3 differ between the CSIRO-CTM-Original and both MEGAN-Offline and CSIRO-CTM-MEGAN runs with the CSIRO-CTM-Original run predicting significantly lower emissions through the majority of the domain. This is contrasting to both MEGAN-Offline and CSIRO-CTM-MEGAN predictions, which were for the most part similar in both the quantities of BVOCs emitted and their spatial distribution. The predictions of the CSIRO-CTM-Original are also more uniform across the entire domain, compared to both MEGAN-Offline and CSIRO-CTM-MEGAN runs in which various emission hot spots occur.

Another difference between the CSIRO-CTM-Original and both MEGAN outputs is the prominent area of zero emissions in the shape of a backwards ‘c’ - south of Blue Mountains National Park - present in both MEGAN outputs, but not the CSIRO-CTM-Original run. This area is set as null data within the MEGAN PFT and emission factor inputs, as it is the area of Warragamba dam, and as such is expected to produce zero emissions due to the large expanse of water where there are very few, if any, BVOC emitting plants. The CSIRO-CTM-Original does not capture this region of zero emissions despite being at the same resolution as the other two outputs.

To better compare the spatial relationships between the models, the normalised monthly mean distribution of total biogenic emissions for February 2011 is shown in **Figure 17**. These and

all other normalised values used within this report were obtained by dividing all of the original values by the overall maximum value of the specific dataset. This figure shows that all three model runs predict higher BVOC emissions in the north east part of the domain, even though this difference is much smaller in the CSIRO-CTM-Original run compared to both MEGAN runs. A consistency throughout the model outputs is the prediction of significantly lower emissions in the immediate Sydney, Wollongong, Kiama, and Moss Vale areas. These zones of lower emissions are expected, as these areas are urbanised and hence contain significantly less vegetation to contribute to emissions. Another notable consistency across all three model outputs is the prediction of BVOC hotspots over the five national parks in the region (**Figure 15**), although this is not as pronounced within the CSIRO-CTM-Original dataset. These hotspots are expected due to the large quantities of undisturbed vegetation in these areas that most likely emit significant quantities of BVOCs. As a result, BVOCs emitted from the national parks have the potential to significantly influence urban air quality under certain meteorological conditions. These conditions would involve wind patterns that transport the BVOCs, that are emitted in national parks - or any other highly emitting area - over urban areas. Once these BVOCs are in the proximity of urban areas it is likely that they will react with anthropogenic compounds such as $NO_x$ resulting in ozone and or SOA.

Despite the similarities between both MEGAN-Offline and CSIRO-CTM-MEGAN, runs there are numerous differences in the spatial distribution of predicted emissions that are introduced by coupling the MEGAN code to the CSIRO CTM. The main difference between the datasets is that CSIRO-CTM-MEGAN predicts that the areas of highest emissions are clustered in the northwest corner of the domain, north of Katoomba, with very few other areas of high emissions. In contrast, Offline-MEGAN predicts an area of high emissions in the northwest corner of the domain, albeit not as high or large as CSIRO-CTM-MEGAN, along with several other hotspots of high emissions including small areas to the north and south of Sydney, and to the south of Wollongong. These differences could be due to a variety of reasons that will be discussed in subsequent sections 4.2-4.5. Unfortunately, no field studies have assessed the spatial distribution of emissions in the region. Modelling undertaken as part of the NSW EPA 2008 emission inventory, which employed a similar version of CSIRO-CTM-Original provided the only source of comparison for the same domain (**Appendix 11**).

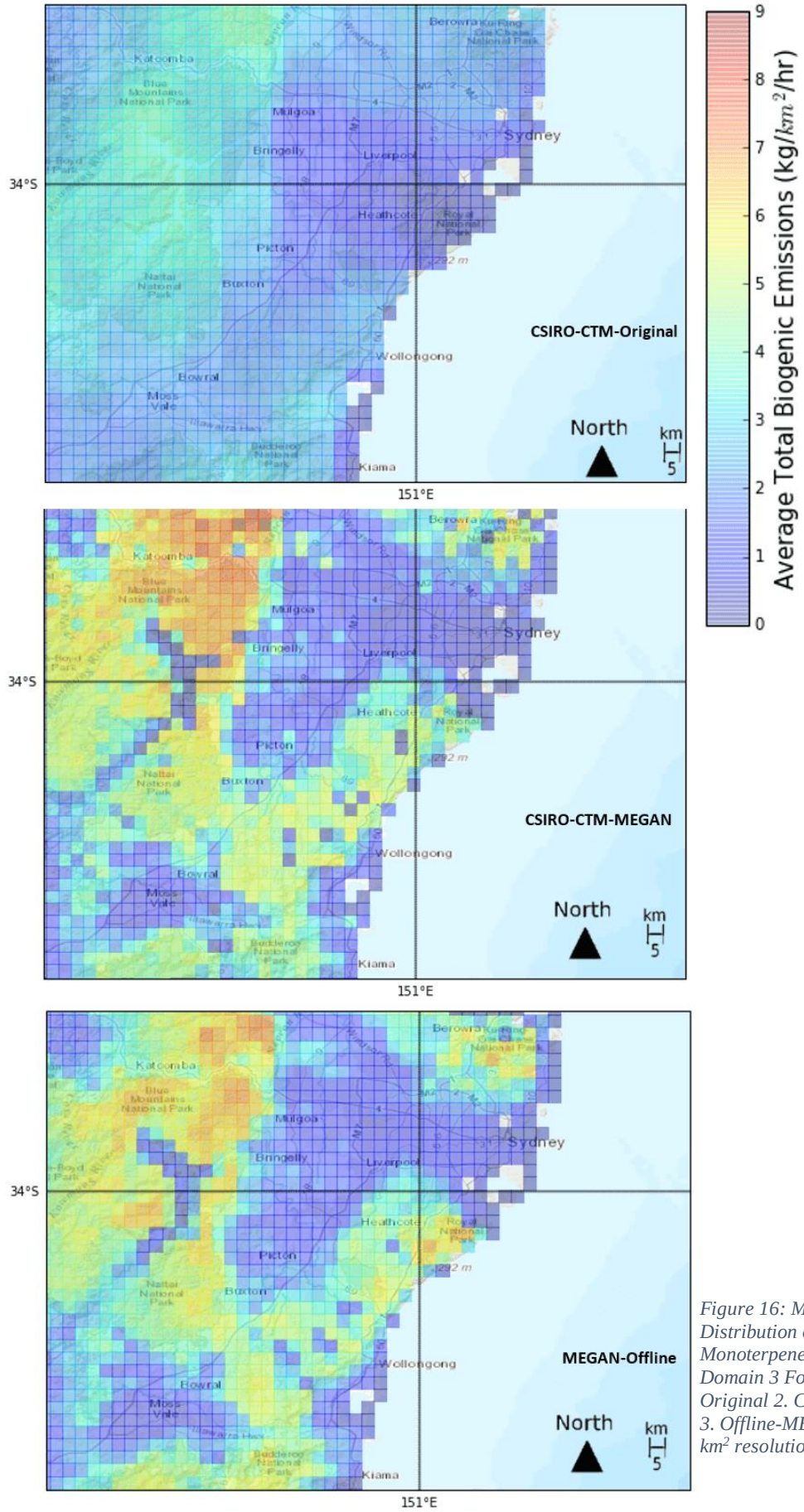


*Figure 16: Monthly Average Distribution of Isoprene and Monoterpenes February 2011 Domain 3 For 1. CSIRO- CTM-Original 2. CSIRO- CTM- MEGAN 3. Offline-MEGAN Domain 3 (3x3 km$^2$ resolution)*

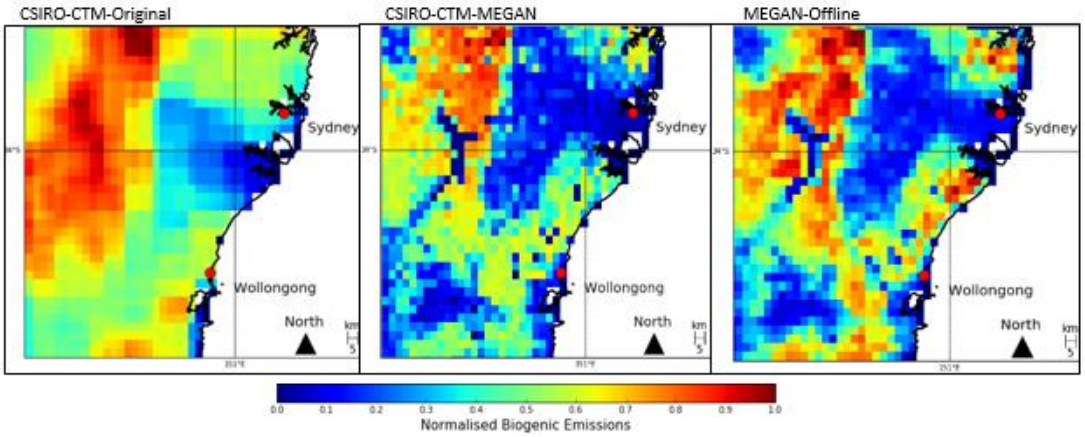


*Figure 17: Normalised Average Distribution of Isoprene and Monoterpenes February 2011 Domain 3 For 1. CSIRO- CTM-Original 2. CSIRO- CTM- MEGAN 3. Offline-MEGAN Domain 3 (3x3 km$^2$ resolution)*

The monthly average spatial distribution of separated isoprene and monoterpene emissions - as simulated by MEGAN-Offline and CSIRO-CTM-MEGAN - is shown in **Figure 18 (**speciated emissions were not available for the CSIRO-CTM-Original model run). In both models isoprene is the dominant BVOC emission over the entire domain, with average emissions being ~15x higher than those of monoterpenes. Despite this difference, the spatial distribution of both compounds is relatively similar.

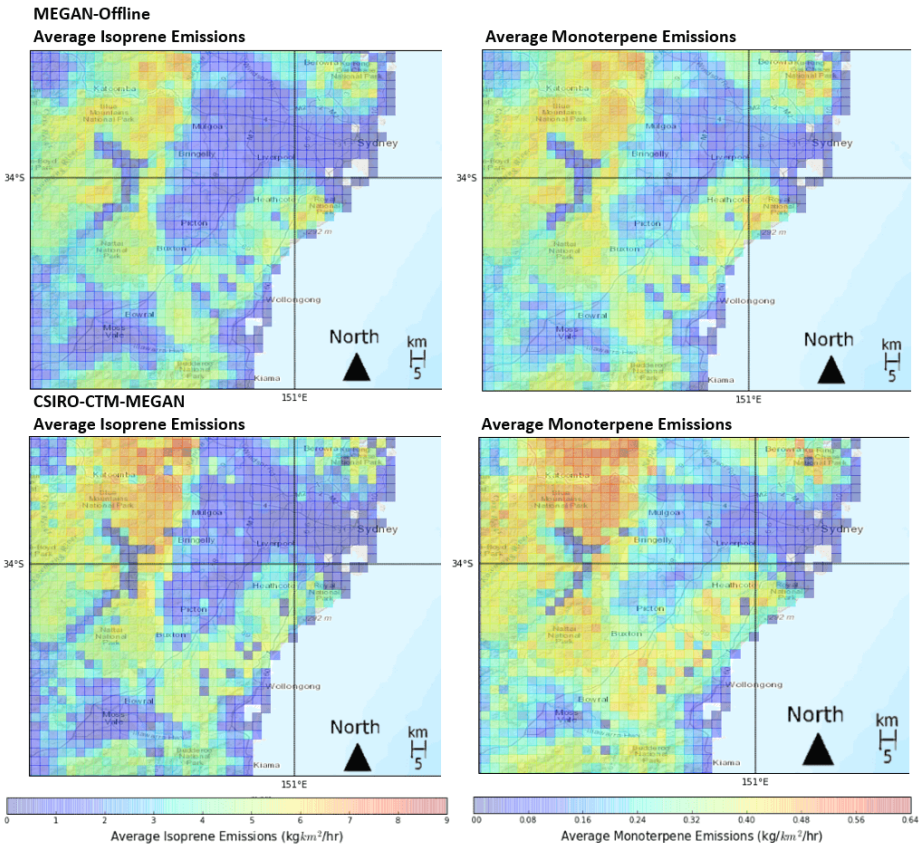


*Figure 18: Monthly average distribution of spectated BVOC emissions for 1. MEGAN-Offline 2. CSIRO-CTM-MEGAN Domain 3 (3x3 km$^2$ resolution)*

## 4.2 Factors influencing spatial distribution of BVOC emissions

### 4.2.1 Leaf area index

LAI is a variable that varies seasonally, and as such, single LAI maps have been produced for the month of February for each model run as shown in **Figure 19**. The LAI datasets used within each model are obtained from significantly different sources for different years **(see section 3.3**). The MEGAN-Offline dataset was regridded from 1x1 $km^2$ to 3x3 $km^2$ which may explain the seemingly higher level of variability from grid to grid.

One of the most notable observations that can be drawn from this dataset is that the distribution and magnitude of LAI used within the CSIRO-CTM-Original run is significantly different to that used in the other two models which means that it was likely recorded in a different year to the other datasets (it is unknown when this dataset was recorded). The spatial variability of the LAI used in the CSIRO-CTM-Original contributes significantly to the spatial distribution of emissions with large values in the western and south eastern part of the domain. The LAI dataset used however does not explain the consistently lower overall emissions predicted by the CSIRO-CTM-Original model relative to the other two models.

In contrast, both CSIRO-CTM-MEGAN and Offline-MEGAN LAI datasets exhibit greater spatial variability than CSIRO-CTM-Original. The two datasets are similar despite the fact that both were created using different processes. The data provided by CSIRO-CTM-MEGAN was remotely sensed from satellite data, and MEGAN-Offline data was predicted using an earth systems land model (CLM4-SP). Both MEGAN LAI inputs capture a similar distribution of vegetation, including an area of higher emissions to the south west of Wollongong, although this area is larger in the CSIRO-CTM-MEGAN run. This area of higher LAI does not correspond with significantly higher predictions of BVOC emissions within either model run, most likely because of the low average temperatures in the area (**Figure 27)**. This area of higher LAI is not captured by the CSIRO-CTM-Original which has very little spatial variability present in the area. The most notable difference between the MEGAN runs is that CSIRO-CTM-MEGAN predicts consistently higher LAI in the area between the hotspot in the northwest corner of the domain and the urban areas along the coast. This difference also does not create any significant differences in predicted BVOC emissions within the models, due to temperature influences. The distribution of LAI within either model does not explain the

distribution of BVOC emission hotspots within the domain, for example, the area of highest emissions in the north west corner of the domain.

**Figure 20** shows the normalised LAI used within all three simulations. These normalised maps show significantly larger LAI values surrounding urban areas, albeit these areas are significantly smaller in the MEGAN-Offline dataset. These predictions of LAI values are reasonable, as vegetation in urban areas is generally sparse and not given the opportunity to reach heights that it would in a non-urban area, due to safety concerns and aesthetic reasons. These lower LAI contribute to lower emission predictions in these urban areas from all 3 models.

The prescribed LAI values within each dataset explain a significant proportion of spatial variability of BVOC emissions within each of the models, $R^2$ = 0.84, 0.70. 0.74 (**Table 7**). However, it is expected that the LAI dataset provided with CSIRO-CTM-MEGAN will be the most realistic, as it is the only dataset that is based on real-time observations during the study period.

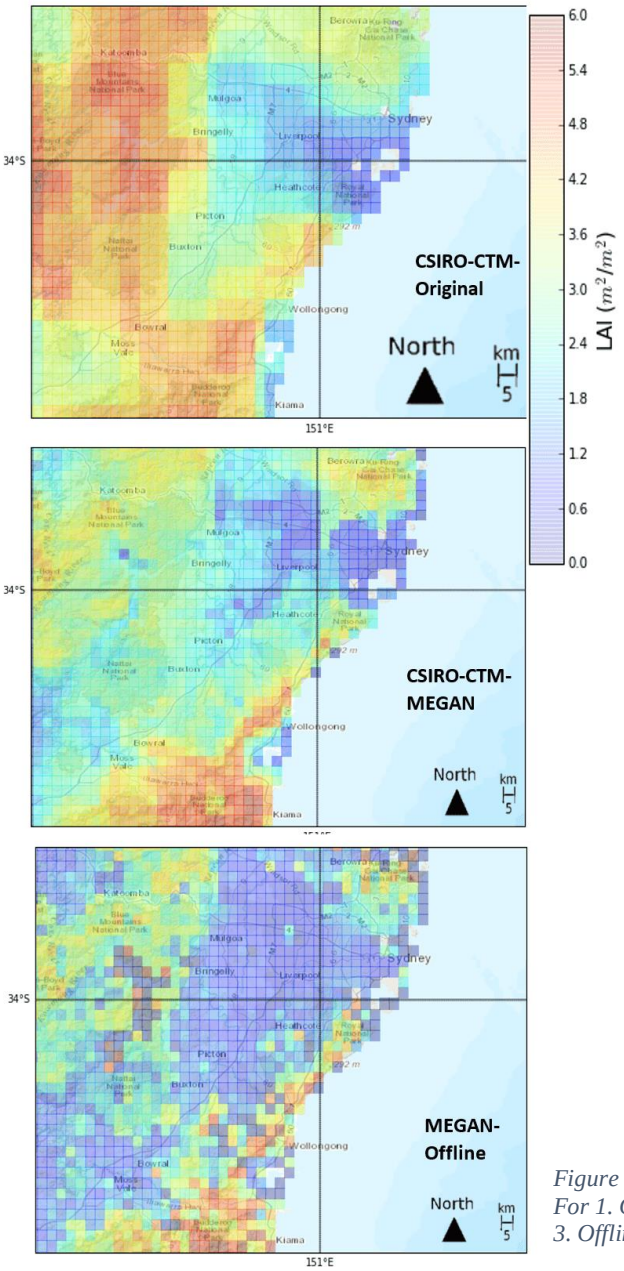


*Figure 19: Leaf area index February 2011 Domain 3 For 1. CSIRO-CTM-Original 2. CSIRO-CTM-MEGAN 3. Offline-MEGAN Domain 3 (3x3 km2 resolution)*

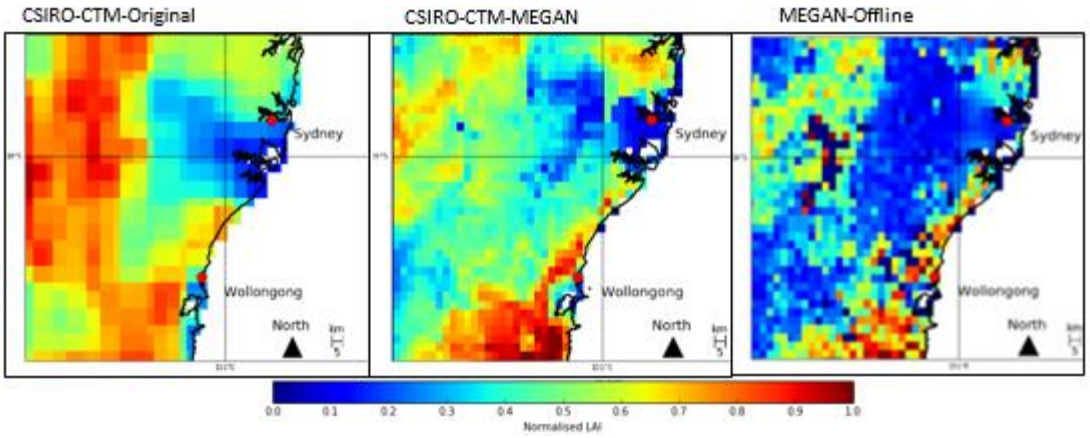


*Figure 20: Normalised Leaf area index February 2011 Domain 3 For 1. CSIRO-CTM-Original 2. CSIRO-CTM-MEGAN 3. Offline-MEGAN Domain 3 (3x3 km$^2$ resolution)*

### 4.2.2 Plant functional type and land use

**Figure 21** shows the spatial distribution of the PFTs used within the Offline-MEGAN model run**.** The Offline-MEGAN PFT values are relatively well distributed over the domain, unlike both the CSIRO-CTM-original and CSIRO-CTM-MEGAN, which both display large blocky clusters (**Figures 22 & 23**). There are 16 PFTs used within MEGAN, however only a few are present within the domain being studied. The data used within MEGAN-Offline is also gradated over space as opposed to the other datasets, in which differences in cover are only separated by well-defined lines. Despite this high level of detail, it cannot be overlooked that these distributions are based on a vegetation climatology (**Table 6)**, and are predicted for 2001, and as such most likely do not reflect the actual distribution.

**Figure 21** shows that within domain 3 there is a large extent of broadleaf tree cover, both in the northwest corner of the domain and the area to the south of Sydney. There is, however, a lack of such vegetation in the immediate vicinity of Sydney. These areas of high broadleaf tree coverage correspond to areas of high emissions of BVOCs ($R^2$=0.81). This relationship is expected as broadleaf vegetation is one of the largest sources of BVOCs in the environment (Guenther et al. (2006)). Although the distribution of broadleaf tree cover explains the fundamental distribution of BVOC emissions, it does not give details such as the distribution of hotspots as in **Figure 16**.

**Figure 21** also displays the distribution of herbaceous vegetation cover within the modelled domain. The distribution of herbaceous vegetation is almost inverse to that of broadleaf vegetation with high percentage cover in the Sydney area, Wollongong, an area to the west of Wollongong, and in the north-western corner of the domain ($R^2$=0.26). These areas correspond with lower levels of emissions, as small pockets of herbaceous vegetation emit low quantities of BVOCs (Guenther et al. (2006)).

The spatial distribution of needle leaf tree cover is also shown in **Figure 21**. There is very little needle leaf tree coverage in the region, regardless this vegetation type contributes very little to the spatial variability of total BVOC emissions ($R^2$=0.15).

The spatial distribution of shrub cover is also shown in **Figure 21**. The spatial distribution of shrub cover is very similar to that of herbaceous vegetation, albeit with lower percentage coverage. Much like herbaceous vegetation, shrubs are assigned a relatively low emissions rate

within the model, which explains why their spatial distribution is similar to that of areas of low BVOC emissions ($R^2$=0.20).

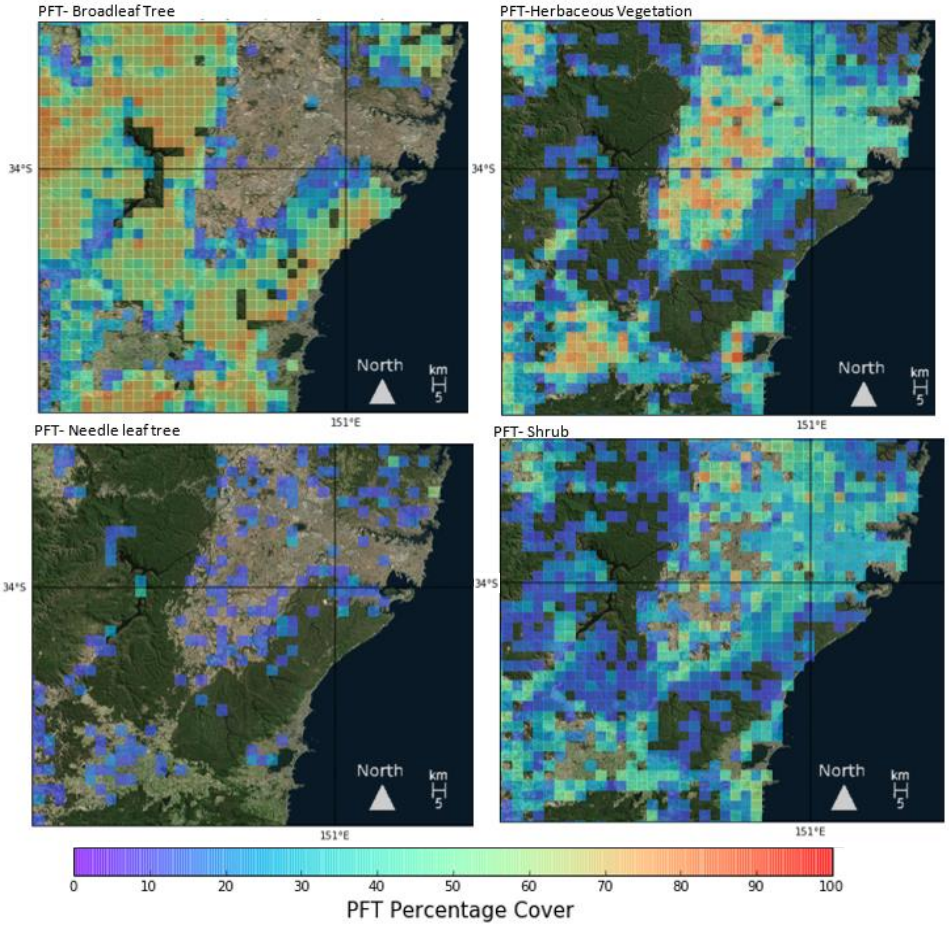


*Figure 21: Percentage land cover of plant functional types used within Offline-MEGAN model run. 1. Broadleaf tree 2. Herbaceous Veg 3. Needle leaf tree 4. Shrub Domain 3 (3x3 km$^2$ resolution)*

The spatial distributions of the PFTs used within CSIRO-CTM-MEGAN are shown in **Figure 22**. The PFTs in this dataset are classified similarly to those used within the MEGAN-Offline, with the exception of the PFTs needle leaf tree present in MEGAN-Offline, and cool grass which is present in CSIRO-CTM-MEGAN. This dataset was specifically created for the study undertaken by Emmerson et al. (2016) from high resolution data obtained as part of the International Geosphere Biosphere Project, although this dataset is based on the predicted 2003 distribution.

Both the percentage cover and distribution of broadleaf trees ($R^2$=0.60) are greater than that of MEGAN-Offline throughout the entire domain. It would be expected that this would produce higher quantities of BVOCs throughout the domain due to inherently high emission factors. However, this influence is outweighed by temperature (**Figure 27**), as MEGAN-Offline predicts higher emissions throughout the majority of the domain (**Figures 16 and 17**). The distribution and percentage cover of herbaceous vegetation ($R^2$=0.35) and shrubs ($R^2$=0.41) is

reduced compared to those used in MEGAN-Offline. It would be expected that this would have a minimal influence on emissions thought the domain, as herbaceous vegetation and shrubs have relatively low emission factors to begin with. As was the case with needle leaf trees, cool grass has a relatively low influence on the spatial distribution of biogenic emissions ($R^2$=0.20).

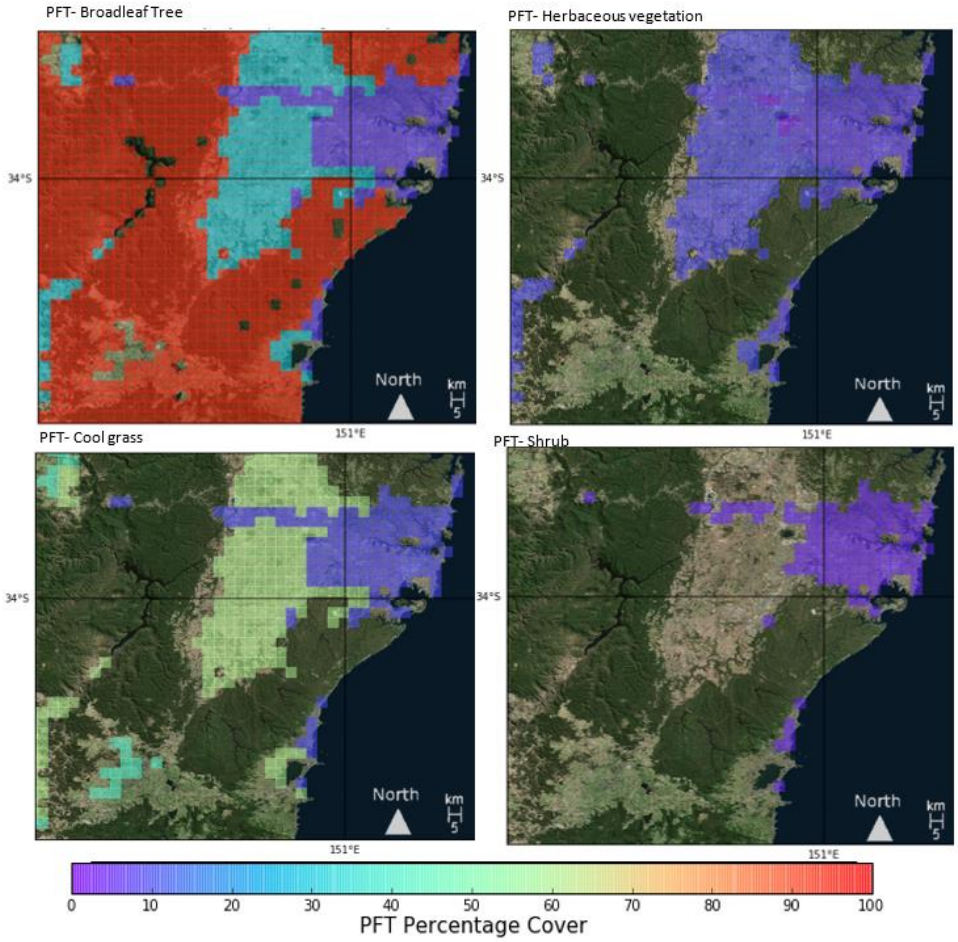


*Figure 22: Percentage land cover of plant functional types used within CSIRO- CTM- MEGAN model run. 1. Broadleaf tree 2. Herbaceous vegetation 3. Cool grass 4. Shrub Domain 3 (3x3 km$^2$ resolution)*

In contrast to the high resolution PFT maps provided by Offline-MEGAN, and CSIRO-CTM-MEGAN the CSIRO-CTM-Original implements a blocky overview of broad land cover types within the region obtained from CABLE, as in **Figure 23**. Unlike both MEGAN implementations, the CSIRO-CTM-Original model does not use PFT data and instead classifies areas as 1 of 32 pre-defined land cover types. These classifications also include canopy height, plant height data, and other variables - such as albedo - that correspond to specific land cover types as can be found in Hurley (2008). The land cover types within the dataset are prescribed somewhat inaccurately, and it is unknown what period they represent. For example, a very small area of the Wollongong region is classified as urban, with the remainder of the region, including Port Kembla (a largely industrialised area), classified as either ocean or tall mid dense forest. Larger bodies of water such as Warragamba dam are also not included within this

dataset, despite being the same resolution as the other models which have these features present. It is expected that these land cover types will influence the spatial distribution of emissions to some extent, although this information could not be found in the literature. Despite this, it can be reasoned to an extent that areas classified as "urban" will emit lower levels of emissions than vegetated areas, especially the various types of forests that cover the majority of the domain.

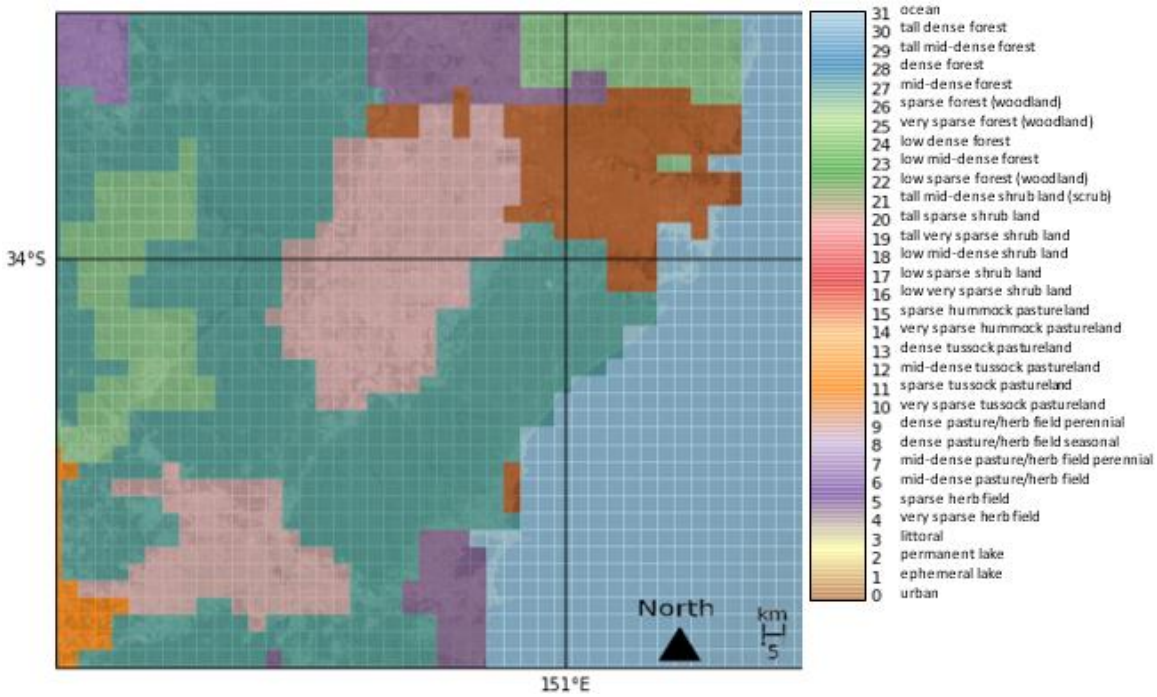


*Figure 23: Land cover types used within CSIRO- CTM- Original Domain 3 (3x3 km$^2$ resolution)*

### 4.2.3 Ambient temperature

The monthly mean predicted ambient temperature distribution used as part of the meteorological input for each model is shown in **Figure 24**. The temperature predictions used within all three models are very consistent in both the prediction of hotspots and colder temperatures, which is expected as the meteorology is being predicted for the same time period, albeit using different offline and online meteorological models (**Table 6**). A discrepancy between the predictions that is not expected is the higher temperatures predicted by CSIRO-CTM-Original than CSIRO-CTM MEGAN, as both use the same meteorological model CCAM. The differences between the predictions could be the result of a number of issues including but not limited to: different model parameter setup, the way that meteorology is manipulated in order to be used in MEGAN, and differences in the allowed model spin up time.

Despite these differences, the values predicted within all three models also roughly fall into the range of average measured temperatures during the time period (22.5$^o$C-25.5$^o$C) (**Appendix**

**12**) Australian Bureau of Meteorology (2016)). Another consistency between all three temperature distributions is the prediction of high average temperatures in the immediate area of Sydney and its suburbs due to a heat island effect. Despite these urban areas having the highest average temperatures within the domain, the BVOC emission rates in these areas are amongst the lowest in the domain. This is due to the assigned PFTs and land use classifications of these areas not being as conducive to BVOC production as other high emitting areas, such as that in the north western corner of the domain despite the fact that the temperatures in this area are lower on average. Another consistency between the meteorological inputs of the three model runs is the prediction of lower temperatures over the Moss Vale area which corresponds to lower levels of predicted emissions, as the area is urban and not conducive to biogenic emission production even if higher temperatures were present. The spatial distribution of average temperature only partially contributes to the spatial distribution of BVOC emissions ($R^2$= 0.35, 0.38, 0.38 **Table 7**). However, temperature does explain a significant proportion of the temporal variability of emissions (**sections 6.4- 6.5**).

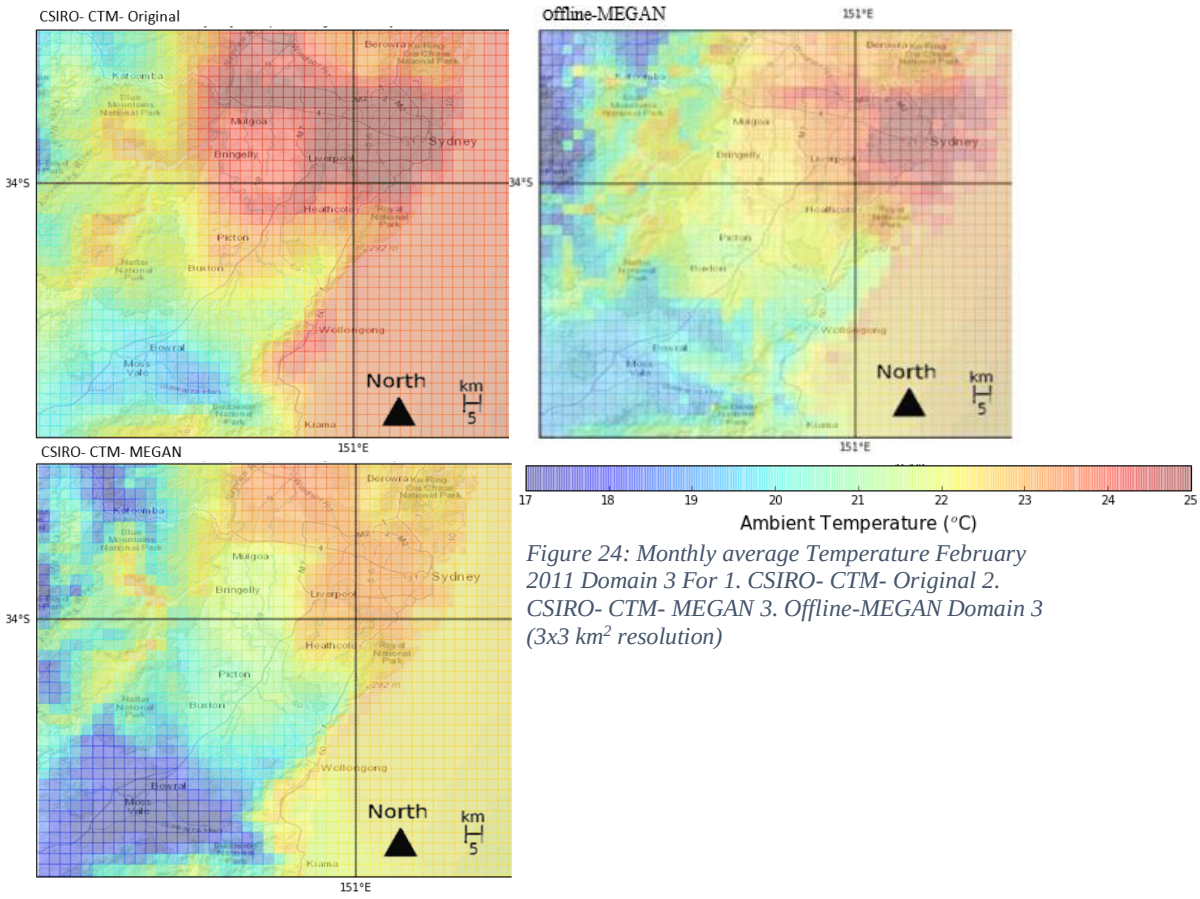


*Figure 24: Monthly average Temperature February 2011 Domain 3 For 1. CSIRO- CTM- Original 2. CSIRO- CTM- MEGAN 3. Offline-MEGAN Domain 3 (3x3 km$^2$ resolution)*

### 4.2.4 Spatial correlation between BVOC emissions and other variables

**Table 7** contains the squared Pearson correlation coefficients that were calculated for environmental factors included within the model files that were expected to have an influence on the average spatial distribution of BVOC emissions. These values were computed using the grid box- to - grid box variability of monthly means excluding ocean boxes. This information reveals that different variables affect the spatial distribution of BVOC emissions predicted by each model to different extents. LAI is the largest contributing factor to the spatial distribution of emissions in all models except for CSIRO-CTM-MEGAN. The largest contributing variable to the distribution of emissions predicted by CSIRO-CTM-MEGAN is the PFT broadleaf vegetation which is also the 2$^{nd}$ highest contributor to the distribution of emissions in MEGAN-Offline. This was anticipated in both models due to the high emission factor of broadleaf vegetation. Another interesting relationship is the relatively low influence that temperature and PAR has on the spatial distribution of emissions across all three models. The influence that these have on emissions will be assessed in subsequent sections. The fact that needle leaf trees explains 40% of variation within MEGAN-Offline is unexpected, however, it does stand to reason as these species are amongst the lowest emitters of BVOCs and as such their presence is anti-correlated with emissions. The PFT shrub was found to have a high influence on emissions within MEGAN-Offline, much higher than within CSIRO-CTM-MEGAN. This is a result of differences in the ways that PFTs were originally prescribed and mapped. Along with the fore mentioned PFTs, all others have a relatively low influence on the spatial distribution of emissions. Several of the variables discussed within this section are co-variable, and as such it cannot be definitively held that a certain variable accounts for a quantitative amount of variability. For example, areas not covered by broadleaf vegetation are not necessarily entirely lacking in vegetation, but may be covered in other vegetation types. There will also be reasonably strong correlation between LAI and broadleaf vegetation.

| | LAI | Temperature | PAR | Broadleaf veg. | Herbaceous veg. | Shrub | Needle leaf | Cool grass |
|---|---|---|---|---|---|---|---|---|
| CSIRO-CTM-Original | .84 | .35 | | | | | | |
| CSIRO-CTM-MEGAN | .70 | .38 | | .81 | .26 | .20 | | .20 |
| MEGAN-Offline | .74 | .38 | .40 | .60 | .35 | .41 | .15 | |

*Table 7: Spatial correlation ($R^2$) between BVOC emissions and environmental factors*

## 4.3 Temporal distribution of emissions

**Figure 25** shows the predicted monthly average time series of isoprene and monoterpenes for February 2011 as simulated by each of the models. This was calculated by averaging emissions over the entire domain, with the shading representing the spatial standard deviation. An obvious and continuous diurnal pattern can be observed within this time series with emissions reaching their highest in midday and dropping to negligible quantities at night. Because of this diurnal pattern it is expected that BVOCs will primarily impact on air quality in the afternoon as BVOCs react with anthropogenic emissions that are remaining after the morning peak in traffic. On the majority of days both MEGAN model runs predict significantly higher quantities of BVOCs than the CSIRO-CTM-Original. Despite this, it is evident that the CSIRO-CTM-Original predicts slightly higher BVOC emissions at night (**Appendix 7**). Throughout the majority of the time period CSIRO-CTM-MEGAN predicts the highest BVOC emissions, with only four days where the MEGAN-Offline run predicts higher emissions.

The predictions of the CSIRO-CTM-Original are also the most uniform and have a smaller range during the time period (generally ranging between 2 and 6 kg/hour) compared to both other MEGAN runs. The variability of both MEGAN runs is significantly larger, with the largest range of predictions produced by the CSIRO-CTM-MEGAN run being ~22 kg/hour and the MEGAN-Offline run being ~20 kg/hour.

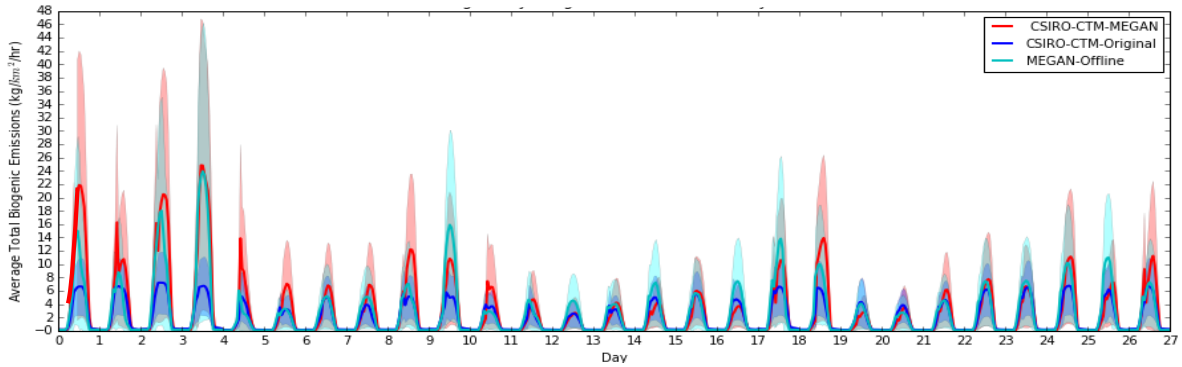


*Figure 25: Monthly Average Temporal Distribution of Total Biogenic emissions and standard deviations from model runs in Domain 3 February 2011 (kg/km2/hour)*

The daily average diurnal time series of isoprene and monoterpenes summed over the full domain from the three models is shown in **Figure 26**. The shading in this figure is the variability over different days in the simulation. Over February the two MEGAN runs are very similar in their predictions although the range of predictions produced by CSIRO-CTM-MEGAN are slightly larger. The predictions from the CSIRO-CTM-Original are on average significantly lower during daylight hours, with less day to day variability, but are slightly

higher than the other two models at night time. The basic shape and magnitude of these predictions is consistent with the data from the 2008 emissions inventory undertaken by the NSW EPA (**Appendix 10**), although these values were also obtained from a version of the CSIRO-CTM model and may not necessarily accurately represent what is occurring in nature.

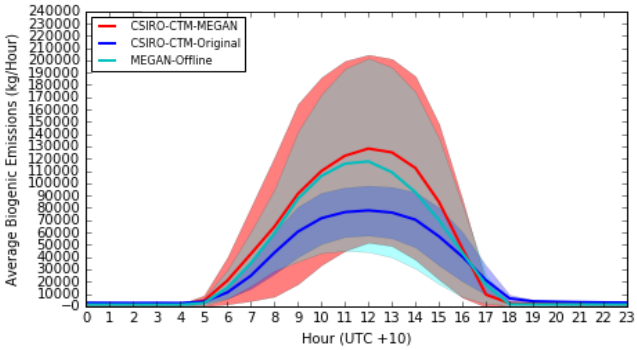


*Figure 26: Daily average diurnal distribution and standard deviations of Total Biogenic emissions from model runs in domain 3 February 2011 (Kg/Hour)*

**Figure 27** displays the time series of average speciated emissions from the two MEGAN model runs that this data was available for. The average quantities of isoprene and monoterpenes emissions tended to be significantly different within each model throughout the time period. This large disparity between monoterpene and isoprene emissions is also present in numerous other field and modelling studies undertaken in the region. Field measurements obtained by Emmerson et al. (2016) were compared to the CSIRO-CTM-MEGAN model output. This comparison suggests that the model overestimated isoprene emissions by a factor of up to 6 and underestimated monoterpene emissions by a factor of 4 (**Figures 28 & 29)**. Winters et al. (2009) also encountered a similarly large discrepancy when comparing measured emission fluxes with values found within the literature. Müller et al. (2008) also found that MEGAN overestimates isoprene by comparing modelled and remotely sensed data. This discrepancy is also present within the data obtained as part of the NSW EPA 2008 emissions inventory (**Appendix 9**). The reason for this discrepancy is cited as the prescription of emission factors based on enclosure measurements of year old saplings to the eucalyptus PFT within MEGAN. This skews predicted emissions as numerous enclosure studies suggests that young saplings produce lower quantities of monoterpenes and higher quantities of isoprene (Street et al. (1997); Winters et al. (2009)). The same PFT issue is also present in the PFT data used within MEGAN-Offline resulting in a similar discrepancy. The emission factor prescribed to eucalyptus species is especially important as a large proportion of the study region is dominated by broadleaf vegetation, of which the majority is various species of eucalyptus (**Figures 21 & 22** Guenther et al. (2012)). It was also found by Sindelarova et al. (2014) that if low soil moisture conditions were accounted for within MEGAN predictions of isoprene emissions

were 50% lower and subsequently closer to observations. Despite these problems there is no single increase/decrease factor that would correct emission rates for all seasons (Emmerson et al. (2016)) .

Another obvious difference between the two species is their diurnal patterns and the way that their emissions vary at night. While concentrations of isoprene are significantly higher during daylight hours they drop to zero at night. Conversely, while monoterpene emissions are lower during the day they continue to be emitted in very small quantities at night. This pattern of speciated emissions is due to the way that monoterpenes are not as dependant on PAR as isoprene (Guenther (1993)), and this is consistent with other studies such as that undertaken by Acton et al. (2015) and Emmerson et al. (2016) (**Figures 28 & 29**). This difference in night time chemistry cannot be fully appreciated within these emission plots as reactions that take place at night result in dramatically different distributions of these species as can be seen in a plot of modelled concentrations. An example of this can be found in a study undertaken by Millet et al. (2016) who found that isoprene concentrations in an area peak at night.

Speciated emissions were unavailable for the CSIRO-CTM-Original model run. However, a rough comparison between **Figures 25 & 28** shows that predicted emissions have a higher correspondence than CSIRO-CTM-MEGAN and MEGAN-Offline to observed emission

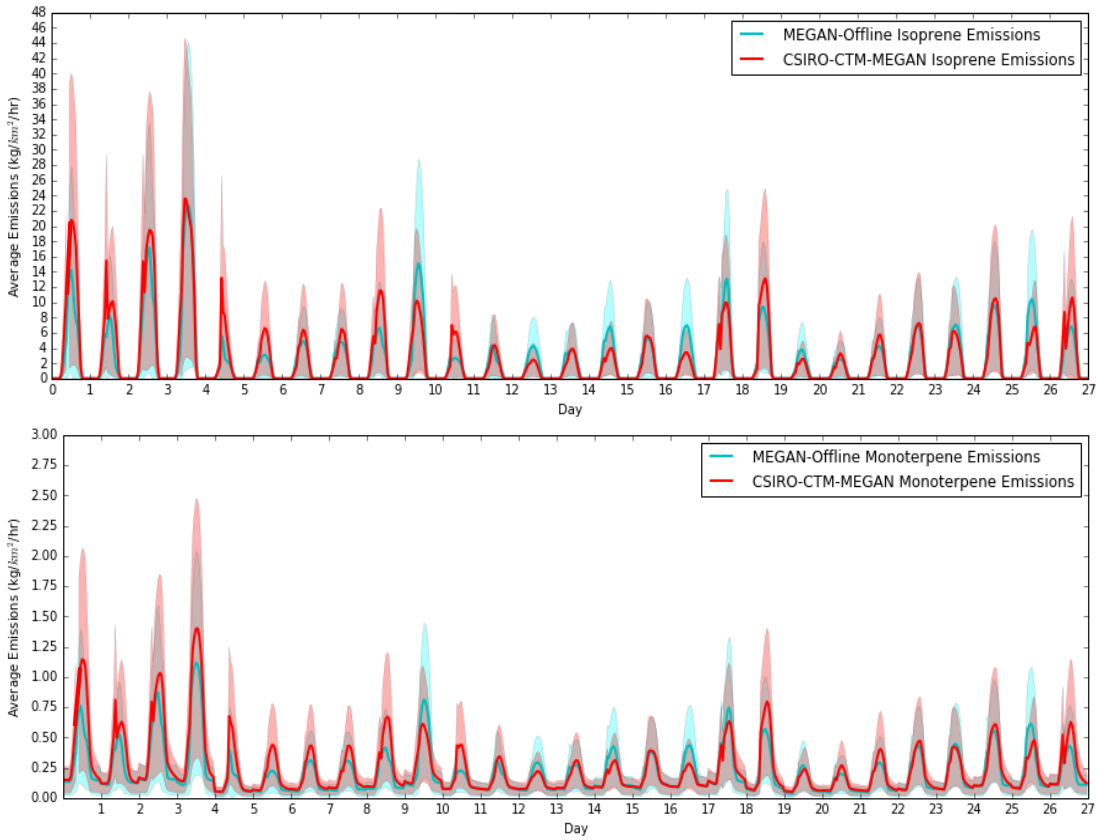


*Figure 27: Average temporal distribution of speciated emissions from MEGAN-Offline and CSIRO-CTM-MEGAN*

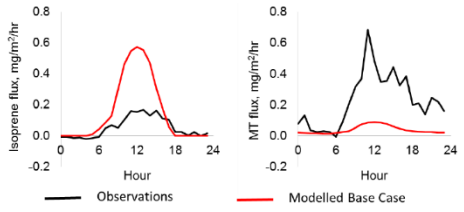


*Figure 28: Mean Diurnal cycles of isoprene and monoterpene (MT) emission fluxes from measurements and CSIRO-CTM-MEGAN at Tumbarumba NSW (An area rich in eucalyptus) Emmerson et al. (2016)*

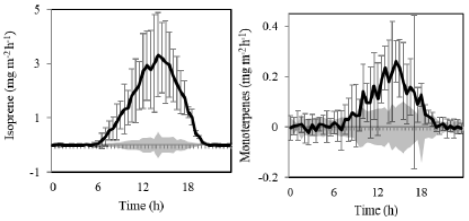


*Figure 29: Mean diurnal fluxes of isoprene and monoterpene with standard deviation measured in a forest in northern Italy Acton et al. (2015)*

## 4.4 Factors influencing temporal variability

### 4.4.1 Ambient temperature

The time series of the average ambient temperature predictions used within each of the three model runs is shown in **Figure 30**. It was found that the general temperature trends predicted by each of the models followed similar patterns despite the fact that numerous variations were present, with the largest being ~8$^{o}$C on day 0. This is likely a model spin up related issue as each of the meteorological models attempts to stabilise. It is unknown which models this effects, or to what extent, as spin up information did not accompany the data files obtained from the relevant external organisations. Both CSIRO-CTM-Original and CSIRO-CTM-MEGAN generally predicted higher temperatures than MEGAN-Offline during the entire period, which explains the higher BVOC emission predictions of CSIRO-CTM-MEGAN, but not the significantly lower predictions from the CSIRO-CTM-Original. Some of the temperature differences during the time period are unexpectedly large for, example there is a ~6$^{o}$C difference between MEGAN-Offline and CSIRO-CTM-Original on day 3. CSIRO-CTM-MEGAN also predicts higher temperatures for days 5-11. These temperature differences have a large effect on the temporal variability of emissions throughout the domain with emissions having a high correlation with temperature (**Table 8**). For example, during the increased temperatures predicted by CSIRO-CTM-MEGAN on day zero the predicted emissions are also significantly higher (**Figure 25**).

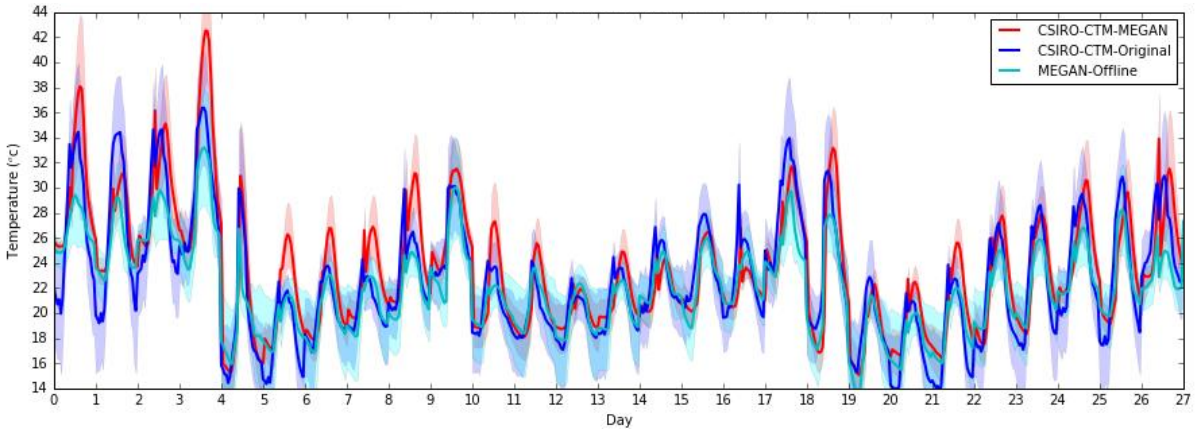


*Figure 30: Monthly Average ambient temperature predictions and standard devastations used in model runs Domain 3 February 2011 (°c)*

### 4.4.2 Temporal correlation between emissions and other variables

**Figures 31 and 32** show a spatial representation of the temporal correlation between BVOC emissions and temperature and LAI. These figures were created by calculating the hourly correlation between emissions and the relevant environmental factor for each cell individually, and then plotting these values spatially. A comparison with **Figure 16** reveals that the temporal correlation between temperature and BVOCs is highest, where emissions are highest consistently across all 3 models. This high level of correlation is reflected in the overall correlation between emissions and temperature within each of the models ($R^2$=0.77, 0.72, 0.98), as shown in **Table 8**. This information also shows that the emissions predicted by MEGAN-Offline are more strongly correlated with temperature than the other two models.

Conversely, the temporal correlation between LAI and BVOC is not consistent amongst the models. LAI and temperature values recorded within each model are also not necessarily independent from each other.

The LAI correlation maps from the CSIRO-CTM-Original and CSIRO-CTM-MEGAN display the same fundamental distribution as the emissions themselves with large patches of low correlation surrounding urban areas and slightly lower quantities over the remainder of the domain. The correlation map from MEGAN-Offline displays consistently low correlation across the entire domain with smaller hotspots in highly vegetated areas such as national parks. This reduced influence of LAI on emissions in urban areas is the result of the prescribed PFT and land type within MEGAN-Offline as these areas are not conducive to BVOC production. Along with this, the fact that MEGAN-Offline employs an LAI dataset based on meteorology

likely contributes to the low correlation between LAI and emissions. This low influence across all three models is also reflected in the overall correlation between emissions and LAI (0.49, 0.44, 0.35) as shown in **Table 8**. PAR explains the largest amount of temporal variability ($R^2$=0.99) in the MEGAN-Offline run. As PAR is expected to have a large influence on isoprene emissions Oderbolz et al. (2013) it is unfortunate that PAR data over the time period was only available for the MEGAN-Offline run for which the correlation is high.

| | Temperature | PAR | LAI |
|---|---|---|---|
| | | | |
| CSIRO-CTM-Original | .77 | | 0.49 |
| CSIRO-CTM-MEGAN | .72 | | 0.44 |
| MEGAN-Offline | .98 | .99 | 0.35 |

*Table 8: Temporal correlation ($R^2$) between BVOC emissions and environmental factors*

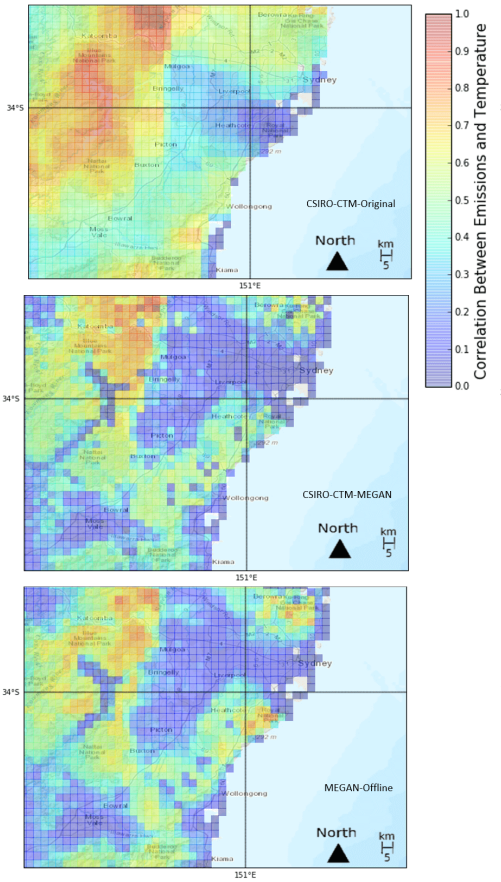


*Figure 32: Temporal correlation between BVOC emissions and ambient temperature Domain 3 (3x3 km2 resolution)*

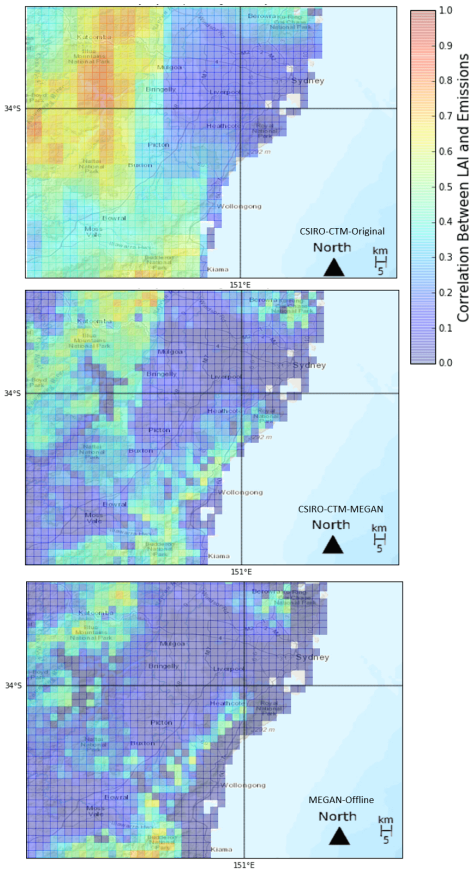


*Figure 31: Temporal correlation between BVOC emissions and LAI Domain 3 (3x3 km$^2$ resolution)*

### 4.5 Summary of spatial and temporal factors influencing BVOC variability

It was observed in previous sections 4.2.4 and 4.4.2 that various environmental factors influence the spatial and temporal variability of BVOC emissions in a variety of ways within each of the three models. The factors that were found to explain the highest amount of spatial variability of emissions during the study period (**Figure 16**) were LAI ($R^2$=0.84, 0.70, 0.74) and the PFT 'broadleaf vegetation' ($R^2$=0.81, 0.60). Temperature and PAR (where available) explained the largest amount of temporal variability within each of the models (**Figure 25** $R^2$=077, 0.72, 0.98) and ($R^2$=0.99). These findings highlight the importance of accurate and up to date model inputs to allow for emission predictions that are spatially correct, and to capture temporal variability of BVOC emissions in nature due to land use changes, and changes in the distribution of vegetation. It is more likely that the spatial distribution of the predictions from the three models are inaccurate as the data was not acquired for the specific time period being studied. In contrast, the variables that contribute to the temporal variability of emissions are obtained for the specific time period from meteorological models that are commonly used, and have been validated and as such there is a smaller chance that these variables are inaccurate.

# 5. Seasonal variability in CSIRO-CTM-Original 2013 January- December results and discussion

## 5.1 Average monthly distribution of BVOCs

**Figure 33** shows the average monthly distribution of emissions over domain 1 as predicted by the CSIRO-CTM-Original model for the year 2013. The quantity of BVOCs emitted varies significantly from month to month, with the highest emissions occurring in summer and lowest in winter. This relationship is expected due to the positive influence that temperature and PAR have on the temporal distribution of BVOC emissions, as discussed in pervious sections (Guenther (2013)). This seasonal cycle is likely a factor that significantly contributes to increased ozone exceedances during summer within the GMR as BVOCs are transported over urban areas where they react with anthropogenic compounds. Globally, relatively few studies assessing the seasonal variability of BVOCs have been undertaken with the majority being

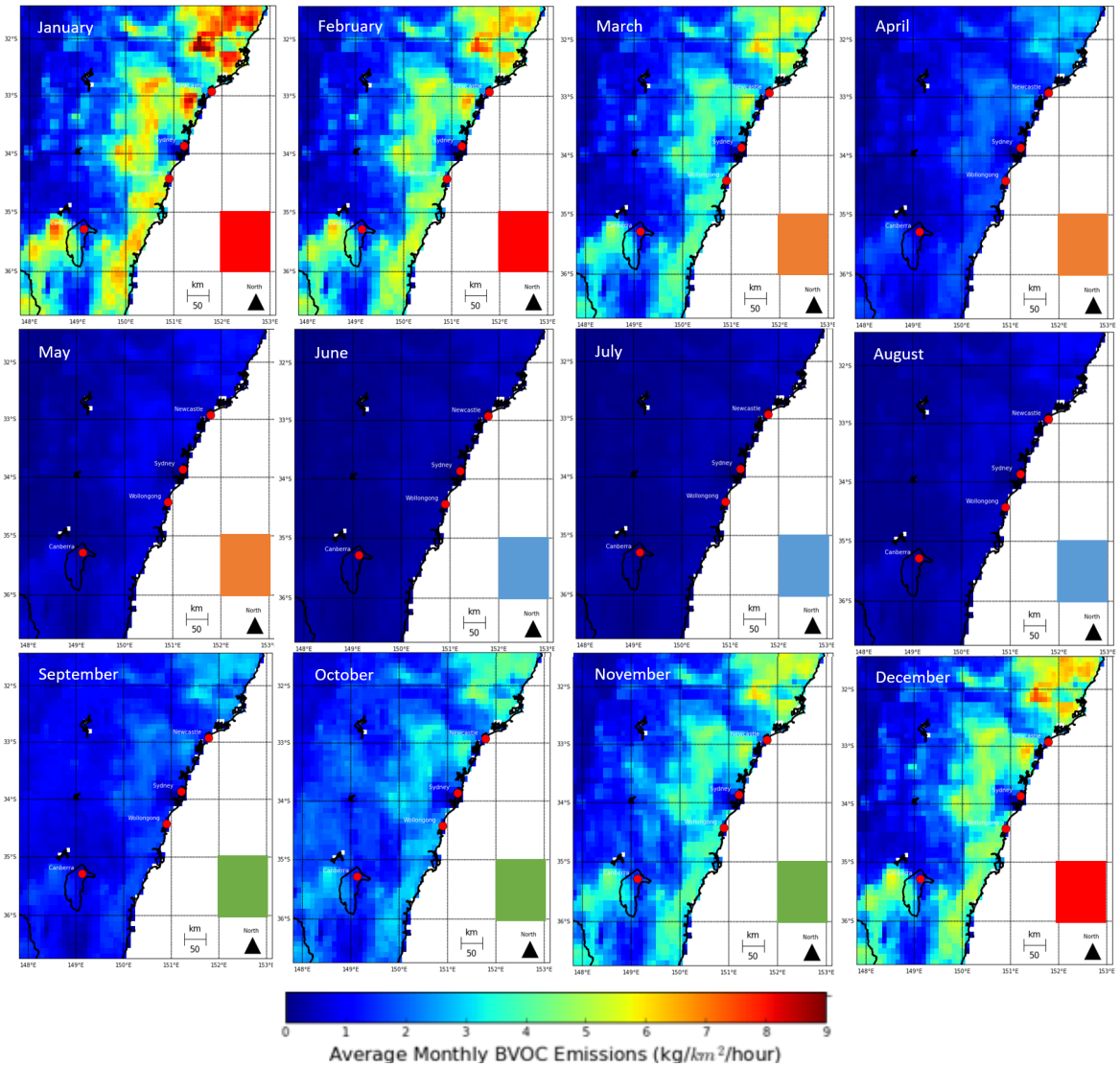


*Figure 33: Monthly average distribution of BVOC emissions 2013 Domain 1 (9x9 km2 resolution) Note: Seasons are represented with different colours within this section Red= summer, orange= autumn, blue= winter and green= spring*

undertaken in Europe and south-eastern USA. These include field and modelling studies undertaken by Abbot et al. (2003), Palmer et al. (2006), Steinbrecher et al. (2009), Oderbolz et al. (2013) and Baudic et al. (2016), who also observed that emissions are at their highest during summer, and lowest during winter.

These studies conclude that emissions are lower in winter due to lower average temperatures, and PAR. They also found that the leaves of deciduous trees in the region significantly contribute to isoprene emissions. These deciduous plants are however, unlikely the reason for reduced emissions during winter in the GMR, as the majority of native Australian vegetation (including eucalyptus) are evergreen, and as such retain their leaves year-round (White et al. (2000)).

The normalised plots in **Figure 34** show that despite these seasonal changes in quantities, the spatial distribution of BVOCs remains largely the same despite a significant increase in emissions to the west occurring in the middle of spring. This may be due to a larger distribution of deciduous vegetation in this area, which undergo a growing period in spring resulting in increased BVOC emissions. The basic distribution of emissions over the area includes numerous hotspots, the majority of which are located over national parks along the coast with the exception of the area to the north east of Newcastle, as in **Figure 34.**

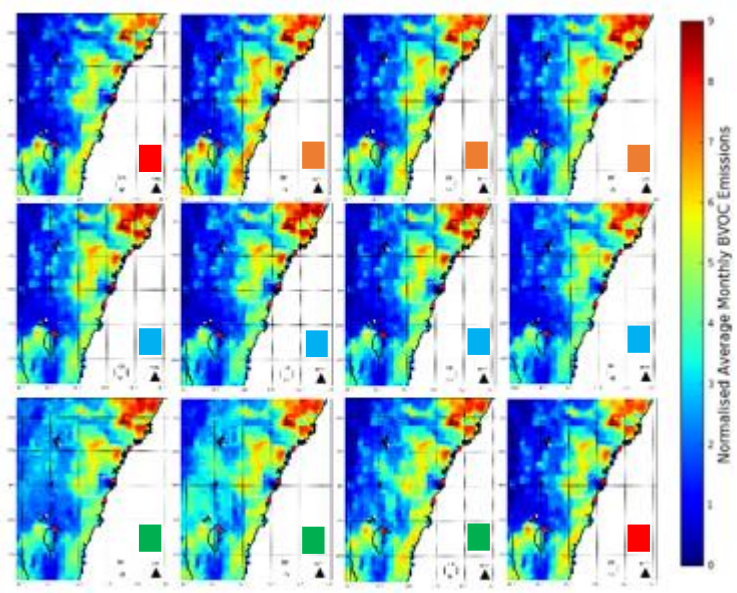


*Figure 34: Normalised average distribution of BVOC emissions 2013 Domain 1 (9x9 km$^2$ resolution)*

## 5.2 Factors influencing spatial distribution of BVOC emissions

### 5.2.1 Leaf area index

The spatial distribution of monthly LAI used within the 2013 CSIRO-CTM-original model run is shown in **Figure 35**. Towards the end of autumn, the spatial distribution and quantity of LAI across the domain grows, especially in inland areas, until summer when it declines again. The distribution of LAI occurs in numerous hotspots throughout the domain with the majority occurring along the coast, or over national parks. The distribution of LAI is very similar to the distribution of normalised emissions (**Figure 34**) due to high seasonal $R^2$ correlation values, ranging between 0.91 and 0.98 (**Table 9)**. Because of this high correlation it is integral that monthly LAI values are accurate, as these explain a large proportion of the spatial distribution of monthly emission estimates. Measured LAI of vegetation varies significantly depending on the precipitation that the vegetation has experienced prior to measurement ((Jones (1968); Tesemma et al. (2014)). Because of this relationship, LAI is influenced by large scale climatic patterns such as ENSO and IOD, which influence the Australian climate - especially rainfall - in a variety of ways over time (Verdon et al. (2004); Murphy and Timbal (2008)). It is difficult to tell if this pattern of LAI accurately reflects the LAI over the modelled period, as no rainfall data was included with the model outputs and it is unknown what year the data was acquired. However, average seasonal rainfall data acquired from BOM (**Figure 36**) shows that rainfall in the domain 1 region is on average slightly lower during winter and spring than in summer and spring. In light of this seasonal pattern, the LAI dataset used within the model was likely acquired during a climatic anomaly when rainfall was higher than average during winter and spring. Because of this, it is unlikely that this LAI dataset will accurately represent the spatial distribution of vegetation for the majority of years. As stated in the previous section, the majority of native vegetation present within the GMR is evergreen and thus will retain its leaves year round. Because of this, the LAI across the region is not expected to significantly drop during autumn as it would in other regions of the world. However, the expansion of LAI to the west probably contributes to the increased emissions observed in **Figure 34**.

### 5.2.2 Ambient temperature

The average ambient temperature used within the 2013 model run is shown in **Figure 37**. The temperature over the entire domain varies significantly from season to season, with the highest temperatures (~35$^o$c) occurring in January and the lowest (~4$^o$c) occurring in June. This seasonal variation explains a significant amount of the seasonal variability of BVOC emission

as seen in **Figure 34**. Despite this pattern, very little spatial variability exists within the datasets, with temperatures remaining homogenous over the majority of the domain (including the ocean) for each season.

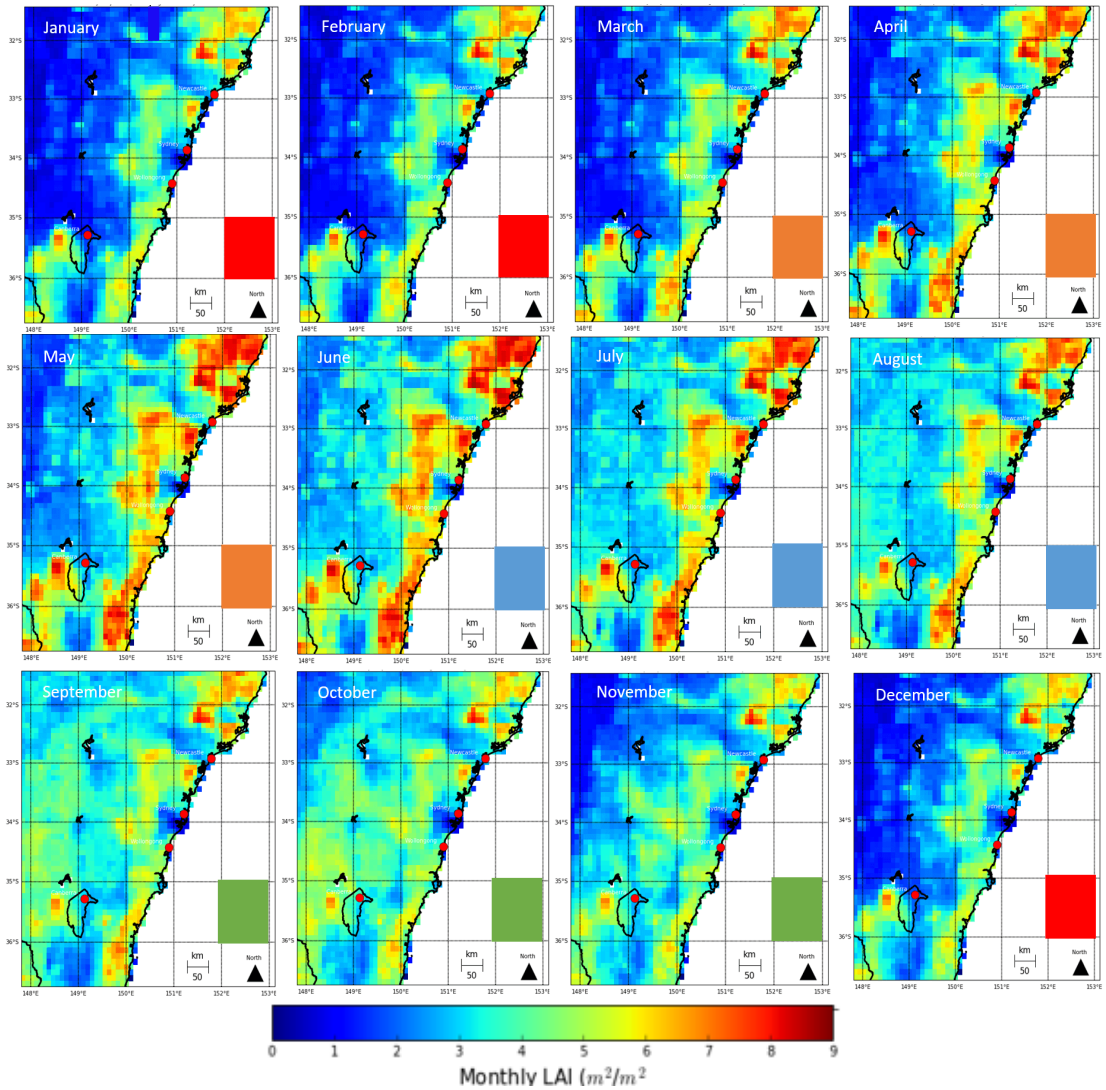


*Figure 35: Monthly distribution of LAI used within CSIRO-CTM-Original 2013 model run Domain 1 (9x9 km$^2$ resolution))*

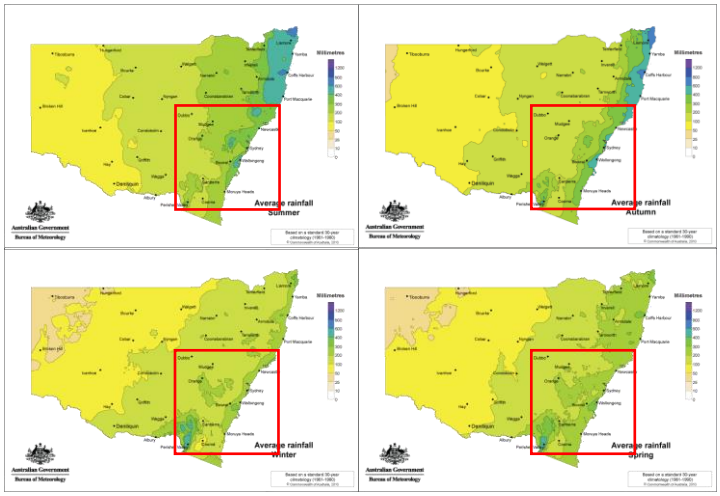


*Figure 36: Average Seasonal Rainfall Data based on 1961-1990 Note: Domain 1 is represented as a red square*

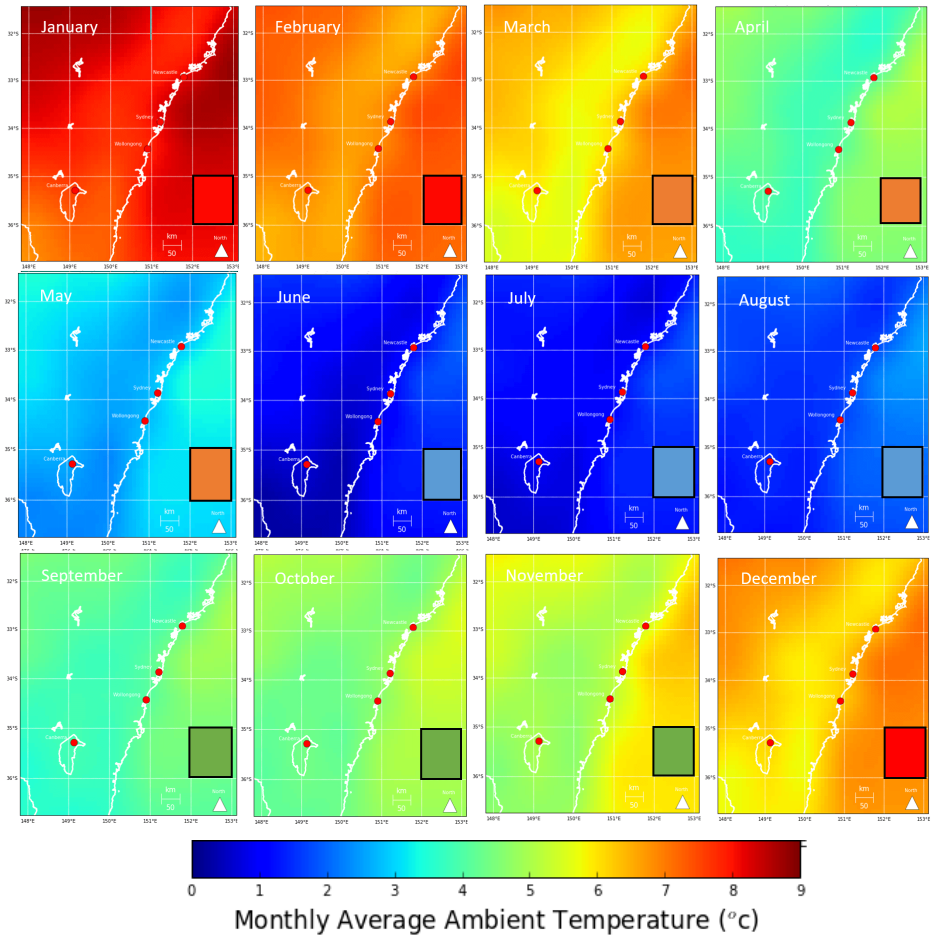


*Figure 37: Average Ambient Temperature 2013 Domain1 (9x9 km$^2$ resolution)*

### 5.2.3 Spatial correlation between BVOC emissions and other variables

**Table 9** presents the spatial correlation between average seasonal emissions and a number of environmental variables. LAI contributes significantly to the average spatial distribution of emissions. This relationship is relatively consistent between each season with the lowest correlation occurring in winter ($R^2$=0.91), and the highest in summer ($R^2$=0.98). The correlation between the spatial distribution of emissions and temperature is also moderately high throughout the domain with the lowest correlation occurring in winter ($R^2$=0.52), and the highest in autumn ($R^2$=0.71). This result is consistent with the results of the previous model intercomparison, however, the two CSIRO-CTM-Original model runs employ the same LAI dataset so it is unlikely that they accurately represent what is happening in nature in both instances.

| | LAI | Temperature |
|---|---|---|
| Summer | 0.98 | 0.69 |
| Autumn | 0.97 | 0.71 |
| Winter | 0.91 | 0.52 |
| Spring | 0.93 | 0.67 |

*Table 9: Spatial correlation between emissions and environmental factors averaged over 3 months*

## 5.3 Temporal distribution of emissions and temperature

**Figure 38** shows the 12 hourly time series of both average BVOC emissions (multiplied by 3 to better show variability) and temperature as predicted by the 2013 CSIRO-CTM-Model run. It is clear that a sinusoidal, seasonal pattern exists, involving emissions beginning to drop in autumn until they are at their lowest in winter. In spring, emissions begin to rise until their maximum in summer. This pattern is expected due to the large influence that temperature and PAR have on the temporal distribution of emissions, and is consistent with the spatial variability of emissions (**Figure 33**), and the results of the model intercomparison. BVOC emissions follow the same diurnal pattern as the modelled 2011 data, with emissions reaching their peak at mid-day and dropping off at night. Emissions are also consistent throughout summer and towards the end of spring. Apart from these two periods emissions are relatively inconsistent and fluctuate at irregular intervals. This is due to a thresholding effect present within the model, so that once temperatures surpass a certain temperature emissions stabalise. When temperatures drop significantly so do emissions due to their temperature dependence. This even occurs in summer during periods of very low temperature - for example, the large drop in temperature at the beginning of February. During warmer periods the range of emissions (represented by light shading) increases significantly, and vice versa. This seasonal pattern means that the largest quantiles of BVOCs being emitted in summer also coincides with the period that ozone maxima generally occur in the GMR. Because of this it is probable that emitted BVOCs contribute to these maxima to at least some extent.

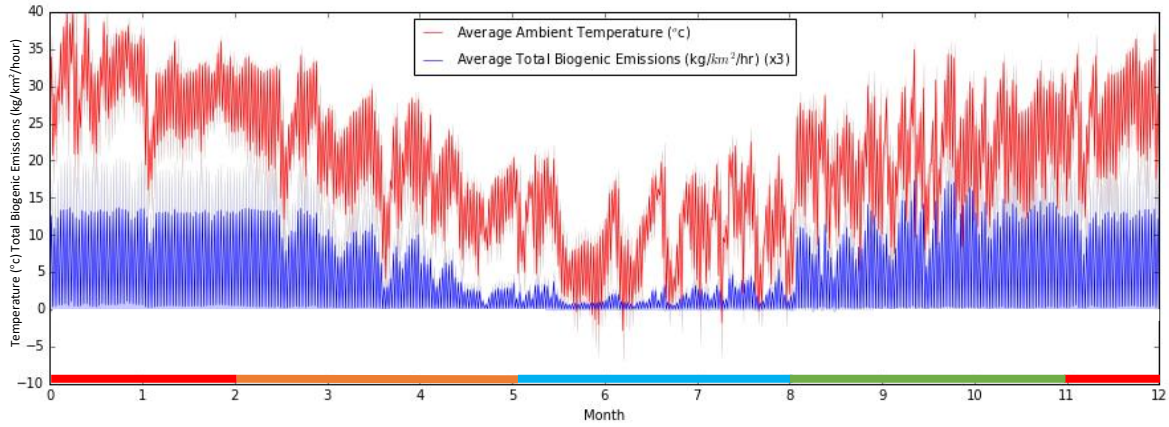


*Figure 38: 2013 12 Hourly average Temperature and emission time series including standard deviations over grid boxes*

**Figure 39** shows the monthly total emissions predicted by CSIRO-CTM-Original for the 2013-time period. This pattern is of similar shape and magnitude to the data obtained during the NSW EPA 2008 emissions inventory which employed a slightly modified version of the CSIRO-CTM-Original model (**Appendix 9**).

From these values it was calculated that the total emissions over the year were 0.281549 Tg (1.595444 Tg C). This value is very small when compared to Australia- wide BVOC emission estimates that are in the range of hundreds of teragrams. One reason for this smaller predicted value is the reduced area of measured emissions in this study. Another reason for this smaller value may be because most global scale BVOC emission estimates are generally created using an implementation of MEGAN which predicts significantly higher quantities of emissions, as was found in the model intercomparison**.**

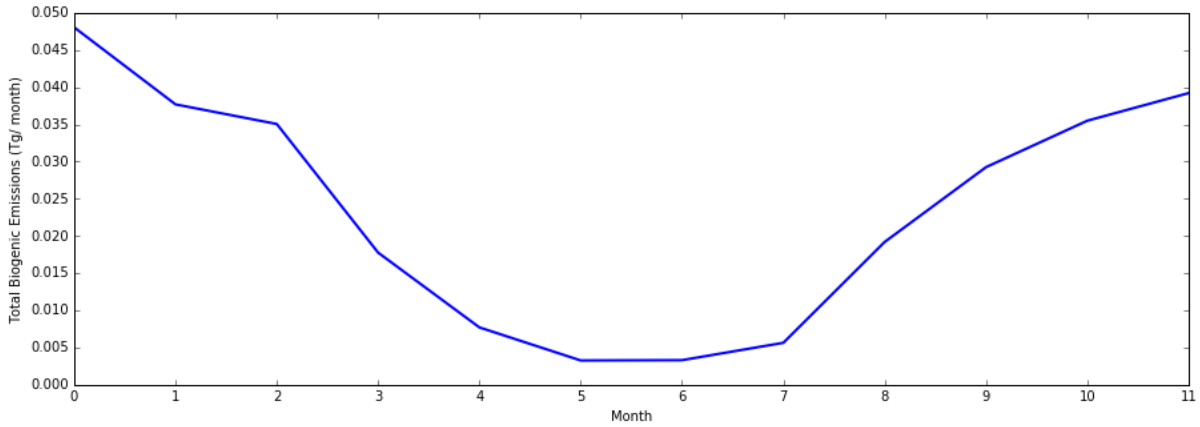


*Figure 39: 2013 Monthly total emissions time series*

### 5.3.1 Temporal correlation between BVOC emissions and other variables

**Figures 40 and 41** show the seasonal gridded temporal correlation between temperature and LAI. These plots were calculated using the same technique as described in section 4.4.2. From summer until winter the correlation between emissions and temperature maintain a very similar spatial distribution until just before spring when the spatial distribution shrinks slightly before growing significantly, especially to the west. Like the 2011 data, the temporal correlation between temperature and emissions is the highest where emissions greatest in hotspots located mainly along the coast. This pattern is reflected to an extent in **table 10,** which shows that temporal correlation between emissions and temperature is lowest in winter and highest in autumn. The correlation between LAI and emissions has a considerably different spatial distribution and seasonal pattern. The highest correlation occurs in hotspots along the coast where emissions are highest, much like the distribution of emissions and temperature discussed previously. Correlation between emissions and LAI that cover the widest area is observed during spring and winter, and is lowest in summer, despite the more pronounced hotspots present during this period. **Table 10** shows that despite these larger distributions occuring during winter and spring the largest average correlation occurs in autumn.

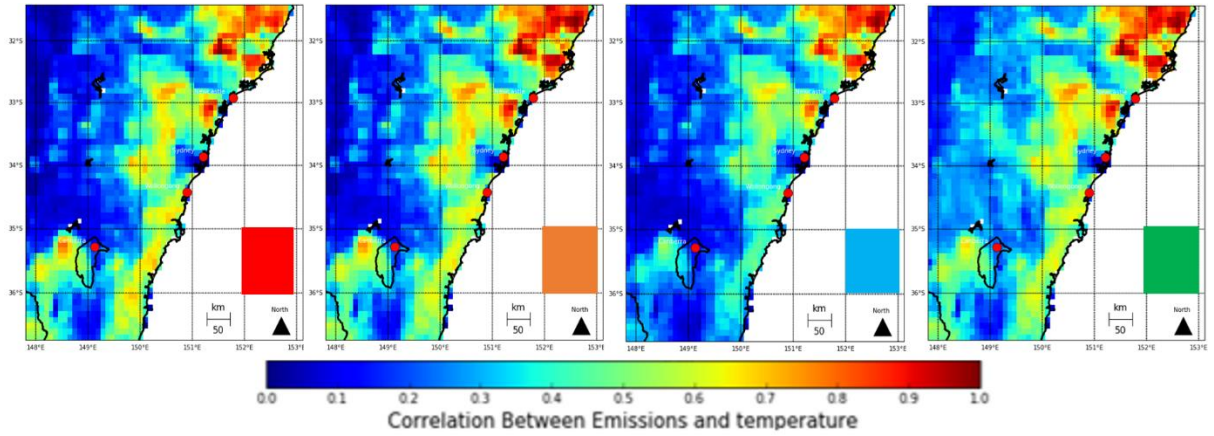


*Figure 40: seasonal temporal correlation between emissions and temperature 2013Domain 1 (9x9km$^2$ resolution)*

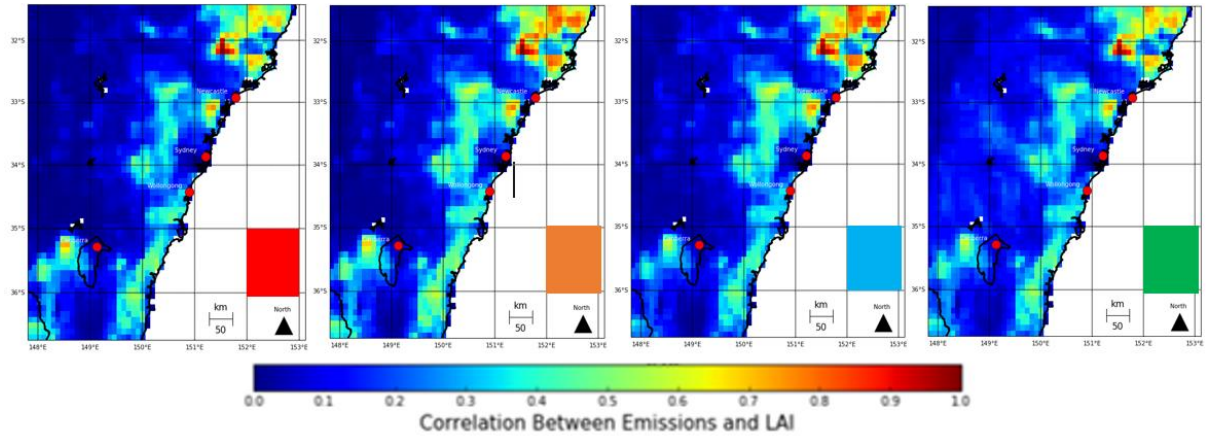


*Figure 41: seasonal temporal correlation between emissions and LAI 2013 Domain 1 (9x9 km$^2$ resolution)*

| | Temperature | LAI |
|---|---|---|
| Summer | 0.77 | 0.41 |
| Autumn | 0.81 | 0.61 |
| Winter | 0.69 | 0.52 |
| Spring | 0.74 | 0.56 |

*Table 10: Temporal correlation between emissions and environmental factors*

# 6. Comparison between February 2011 and February 2013 CSIRO-CTM-Original results and discussion

## 6.1 Spatial distribution of BVOC emissions

**Figure 42** shows the spatial distribution of emissions predicted by the CSIRO-CTM-Original model run from 2011 (regridded to 9x9 $km^2$), and the 2013 dataset used in the previous section. The biggest discrepancy between the two sets of data is that emissions throughout the domain, excluding urban areas, are higher in 2013. While the greatest consistency is the prediction of high emissions over national parks (**Figure 15)** to the west and south of the domain. The 2013 model run predicted that areas fringing larger urban regions emitted greater quantities of BVOCs, although this could also be a resolution impact. It is unfortunate that 3x3 $km^2$ data was not available for 2013 as it would have allowed smaller scale differences (such as those observed in the model intercomparison) to be detected. Despite this, these datasets demonstrate that emissions will be always be lower in urban areas regardless of temperature.

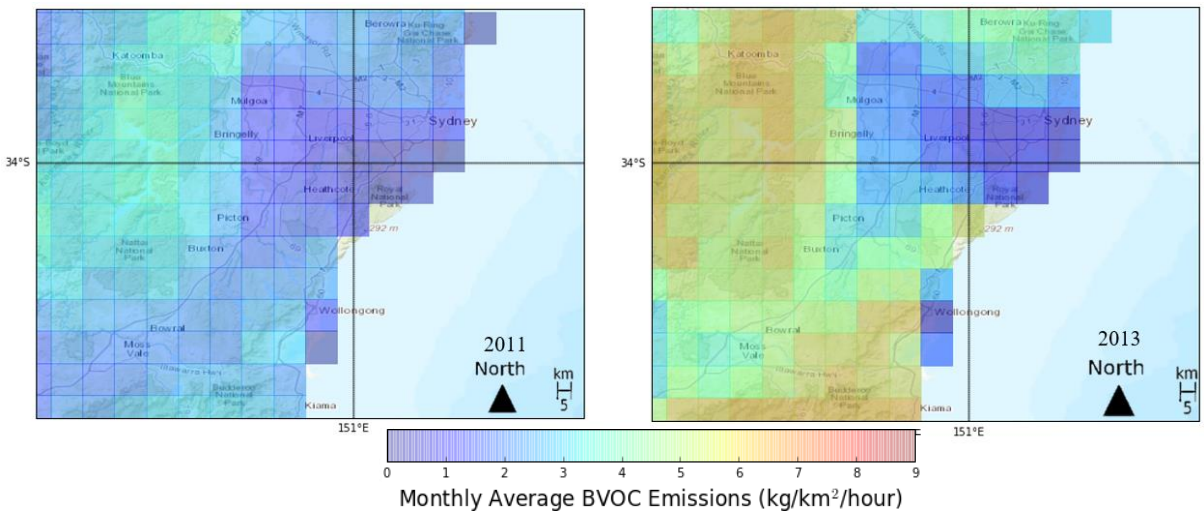


*Figure 42: Average Spatial Distribution of Emissions February: 2011 (left), 2013 (right) (9x9 $km^2$ resolution)*

## 6.2 Ambient temperature

**Figure 43** shows the annual temperature over the domain during 2011 and 2013. Predicted temperatures throughout the domain are significantly higher during February 2013, which is the major contributing factor to the higher predicted emissions in **Figure 33,** as the LAI dataset used in both is the same dataset. The spatial distribution of average temperature is significantly different between the two time periods, with 2011 displaying a far more detailed distribution.

This is compared to the 2013 distribution which is far more homogenous with only minor west to east variation in temperature across the domain.

During 2011, observations obtained by BOM showed that a large portion of the domain experienced temperatures that were on average 1.5ºC higher than average (Australian Bureau of Meteorology (2012)). Conversely, observations recorded in 2013 by BOM showed that a large portion of the domain experienced temperatures 1ºC cooler than average (Australian Bureau of Meteorology (2014). When these deviations are combined with overall average temperature data (**Appendix 12** Australian Bureau of Meteorology (2016)), it can be roughly estimated that in 2011 temperatures are expected to range between 22.5-25.5ºC on average and range between 20-23ºC in 2013.

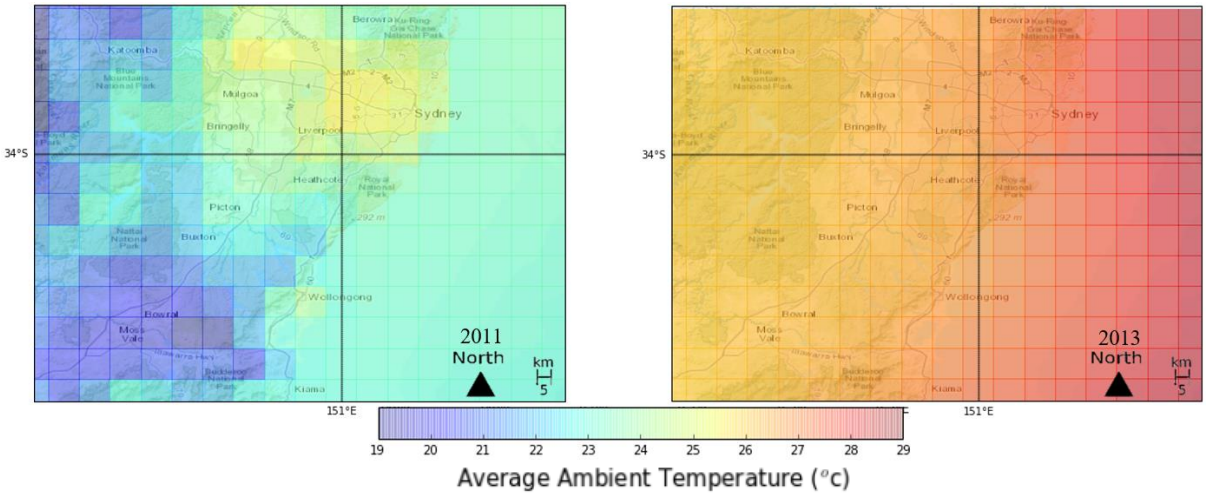


*Figure 43: Average Spatial Temperature Distribution February: 2011 (left), 2013 (right) (9x9 km$^2$ resolution)*

When these approximations are compared with the temperature data used within both model runs it becomes obvious that there is a significant discrepancy between observed temperatures and modelled temperatures during February 2013. This discrepancy results in significantly higher emissions being predicted for the February 2013 period. Conversely, the predicted temperatures for the February 2011 period are much closer to the observed values. This inaccurate temperature prediction during February 2013 is likely an error in the running of CCAM or the use of incorrect inputs into the model. Despite the fact that the 2013 meteorological predictions may not accurately reflect what is happening in nature they demonstrate the influence that temperature has on the variability of emissions and what may be expected into the future due to anthropogenic warming.

### 6.3 Spatial correlation between BVOC emissions and other variables

**Table 11** shows the spatial correlation between biogenic emissions and environmental influences. The correlation between LAI and emissions is consistent across the two model runs.

An unexpected difference is present between the correlation between emissions and temperature of the two model runs with 2013 having an $R^2$ value 0.22 higher than that of the 2011 model run. This value is, however, plausible as the distribution of temperature is far more uniform across the entire domain compared to 2011 as in **Figure 43**.

| | LAI | Temperature |
|---|---|---|
| Feb 2011 | 0.84 | 0.35 |
| Feb 2013 | 0.86 | 0.57 |

*Table 11: Spatial correlation between emissions and environmental factors February 2011 and 2013*

## 6.4 Temporal distribution of emissions

**Figure 44** shows the temporal distribution of emissions predicted from both the 2011 and 2013 model runs. Both model runs produce predictions of similar magnitude and diurnal pattern, although the range of emissions produced by the 2013 model is larger on the majority of days, extending both higher and lower. This large range of emissions is consistent with the differences in spatial distribution shown in **Figure 41**. **Figure 45** shows the daily average diurnal distribution of emissions for February 2011 and 2013. The 2013 model run predicts both a larger quantity and range of emissions than the 2011 run. The diurnal pattern displayed by each model differs slightly from those in **Figure 26**, as these show a distribution that is significantly flatter on top. This flat top distribution is generally indicative of BVOC emission predictions in an Eulerian box that contains a reasonable amount of water (Emmerson (2016) personal communication). It is possible that these model runs do contain at least a few boxes with water present due to the larger 9x9 $km^2$ grid cells, some of which contain water and land, resulting in boxes with water being introduced to the resulting emission plots.

Despite the significantly higher temperatures predicted for 2013 the resulting emission profiles still display lower values and variability of those produced by MEGAN-Offline and CSIRO-CTM-MEGAN (**Figures 25 & 26**).

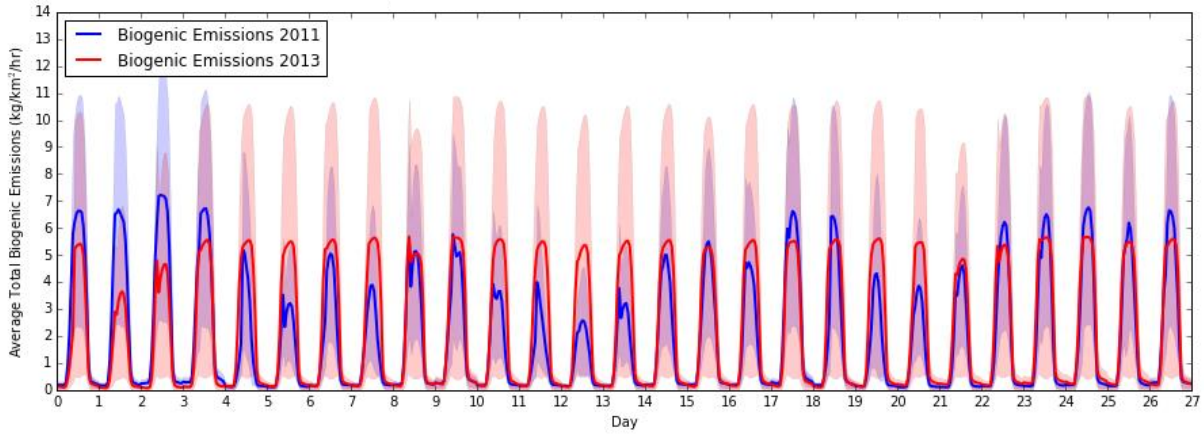


*Figure 44: Temporal distribution of emissions February 2011 and 2013*

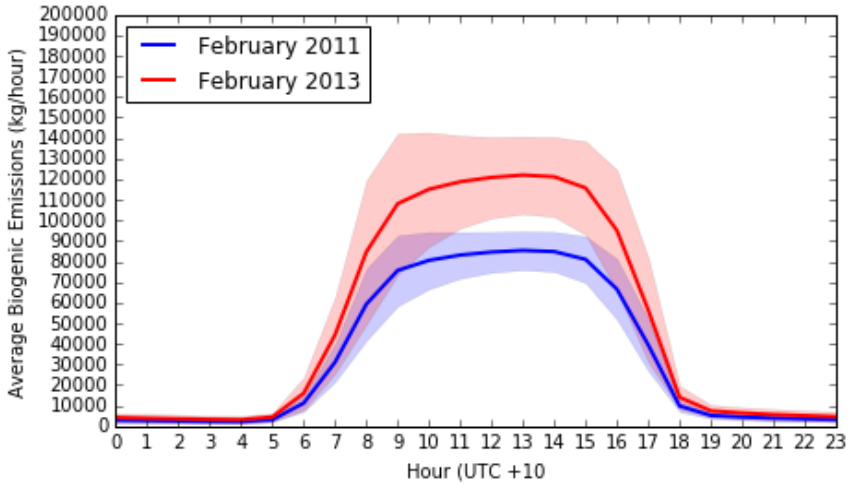


*Figure 45: Daily average Diurnal distribution and standard deviations of total Biogenic emissions from Domain 3 2011 and 2011*

## 6.5 Temporal correlation between emissions and other variables

The temporal correlation between biogenic emissions and environmental influences is shown in **Table 12**. Both temperature and LAI have a very similar influence of across the 2 model runs. This is expected as both datasets have been produced by the same model implementation with only the inputted meteorology differing.

**Figures 46 and 47 both** display a spatial representation of the temporal correlation between emissions and environmental factors. The spatial distribution of temporal correlation between temperature and emissions is very similar between the two model runs (**Figure 46)**. The only minor differences are an area of higher correlation to the west of the Sydney area in the 2011 model run, and the greater area of low correlation surrounding the Sydney area in the 2013 model run. It is likely that these differences are the result of resolution differences between the two model runs or errors in the way CCAM was run for 2013.

The spatial distribution of temporal correlation between LAI is significantly different between the two models, with the correlation in 2013 being significantly lower across the majority of the domain despite having the same basic distribution. As above, resolution differences likely contribute to this discrepancy. Despite the fact that these two datasets are supposed to be predicted using the same model implementation (CSIRO-CTM-Original) small differences were likely introduced during model set up for example differences in model spin up times. These differences in model set up likely result in differences in overall emissions between the two periods in **Figure 42**.

| | Temperature | LAI |
|---|---|---|
| Feb 2011 | 0.77 | 0.49 |
| Feb 2013 | 0.76 | 0.41 |

*Table 12: Comparison between temporal distribution of emissions*

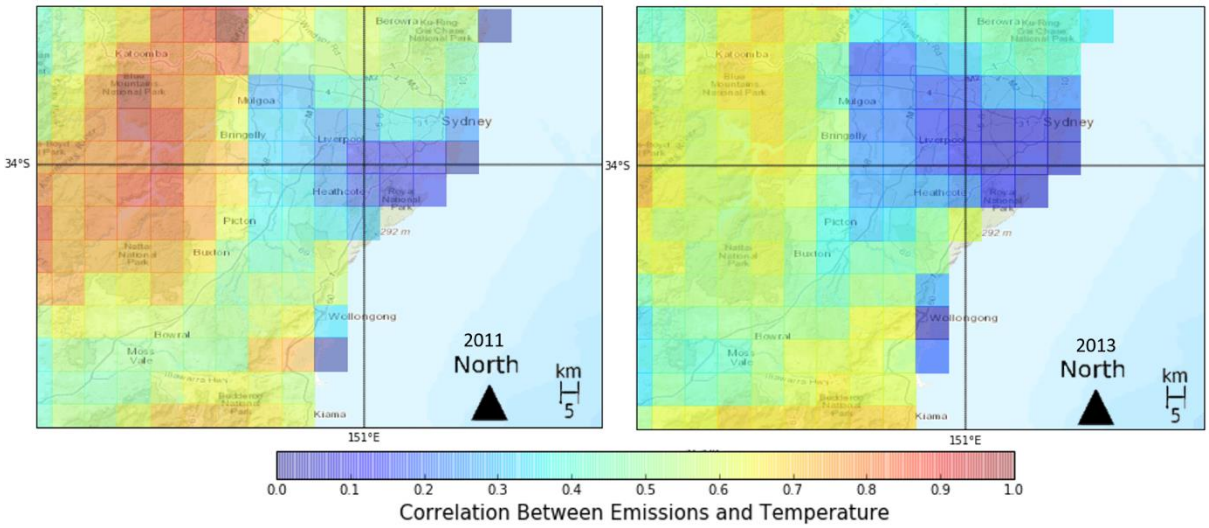


*Figure 47: Temporal correlation between Emissions and temperature: 2011 (left), 2013 (right) (9x9 km$^2$ resolution)*

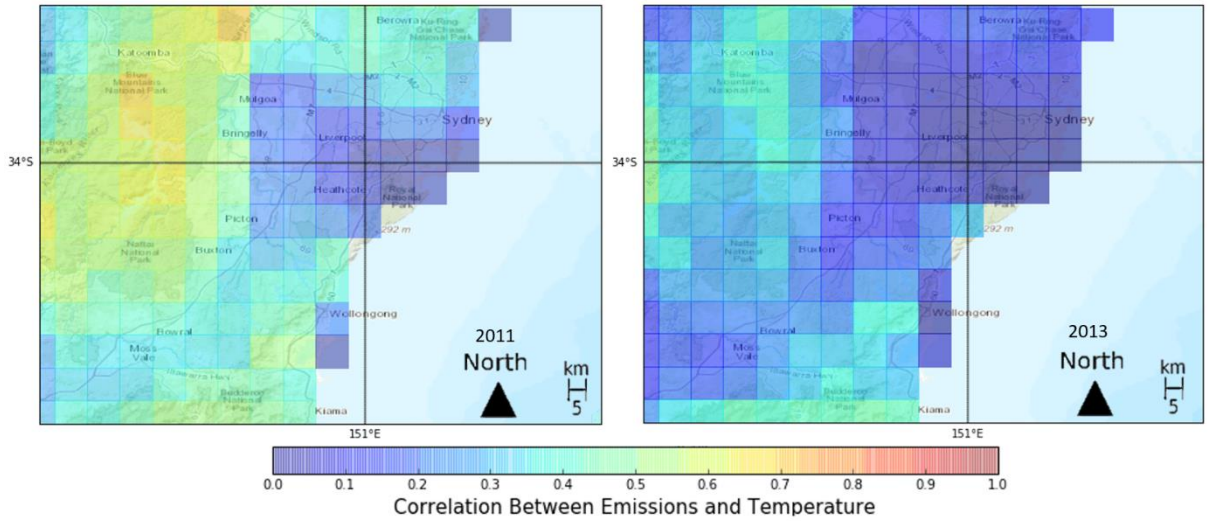


*Figure 46: Temporal correlation between Emissions and LAI: 2011 (left), 2013 (right) (9x9 km$^2$ resolution)*

## 7. Conclusion and recommendations

Predictions of BVOC emissions from multiple CTMs within the GMR were assessed within this study. This involved three distinct components - a model intercomparison between three different model implementations, an assessment of seasonal variability of predicted emissions using an annual 2013 dataset, and a comparison between the outputs of one model using February 2011 and 2013 data.

The model intercomparison has shown that each model predicts different spatial distributions of emissions, with the CSIRO-CTM-Original predicting significantly lower quantities of emissions over the entire domain. These predictions also show greater agreement with the measured values obtained during previous field studies although no speciated emission predictions were available. Conversely, CSIRO-CTM-MEGAN and MEGAN-Offline both over predicted isoprene emissions, and under predicted monoterpene emissions when compared to values obtained during previous field studies. According to the literature these discrepancies are mostly explained by issues with the emission factor prescribed to eucalyptus species which dominate the study region and issues with prescribed ground moisture levels. The CSIRO-CTM-Original model produced predictions that were relatively homogenous across the entire domain, with very little spatial variability being present. This is in contrast to both CSIRO-CTM-MEGAN and MEGAN-Offline which predict significantly higher levels of spatial variability. The reason for this is likely the inclusion of PFT data which introduces a greater level of spatial complexity and gradation to predicted emissions. If PFTs could somehow be integrated into the CSIRO-CTM-Original, it would most likely produce predictions of the appropriate magnitude with the spatial sensitivity of MEGAN predictions.

It was also shown that environmental factors and seasonal variability influence temporal and spatial variability of emissions in a number of different ways within each model used within the model intercomparison, and the assessment of seasonal variability. Temperature and PAR (where available) were the principle factors that determined the temporal variability of emissions predicted by each of the models. However, the spatial distribution of LAI and the PFT ‘broadleaf vegetation’ was found to be the major influence on the spatial variability of emissions predicted by each of the models. It is expected that the variables that influence temporal distribution will be relatively accurate as they are derived from meteorological models that are commonly used and well validated. The variables that influence the spatial variability of emissions are, however, not validated to the same standard and more difficult to

accurately measure. For example, the CSIRO-CTM-Original model run used in this study employs the same LAI dataset for different years and the PFT datasets used within both MEGAN implementations are dated. This is expected to introduce some degree of error to the spatial distribution of predicted emissions as vegetation is not constant from year to year, owing to large scale climate drivers. Urban expansion, urban greening, and climate change in the future will also have a significant effect on the distribution of BVOC emitting vegetation which cannot be accounted for using the same dataset from year to year.

An assessment of the seasonal variability of predicted BVOC emissions revealed that a clear sinusoidal seasonal pattern exists, with the highest quantities occurring in summer and lowest in winter. Despite this cycle, the spatial distribution remains almost constant year round. This pattern of variability is likely due to the fact that LAI, a variable that does not show much temporal variability, influences the spatial distribution of emissions. Temperature, and PAR, which are highly temporally variable, both influence the temporal distribution of emissions. To capture the seasonal changes in the spatial distribution of BVOC emissions it is important that appropriate LAI datasets are employed.

Each model predicted numerous emission hot spots with the majority occurring over national parks. In contrast, negligible emissions were predicted over urban areas despite higher temperatures. Because the Sydney region is bounded by 4 national parks, it is likely that under certain meteorological conditions once emitted from these areas, BVOCs are transported over urban areas where they react with anthropogenic compounds producing ozone and SOA, which both have the capacity to impact on human activates and the environment.

This study also highlights the high degree of uncertainty of emissions within the GMR that has been found in other studies undertaken in the region. To remove some of this uncertainty, flux measurements of BVOCs, such as those acquired by Emmerson et al. (2016), are important as they allow for modelled emissions to be validated which in turn would remove some uncertainty. Such measurements are expected to be obtained during the COALA campaign that is expected to take place in 2019 (COALA stearing group (2016)).

Recommendations to allow for improvements in the OEH BVOC modelling capabilities and further studies include:

- Plant level measurements of eucalyptus species to determine if the emission rate prescribed within MEGAN is accurate and applicable to the region.
- Where possible, the employment of LAI datasets within their models that are specific to the time period being studied. If this is not possible it would be beneficial to use a LAI dataset that was obtained during a period where large scale climate influences are similar state to the year being simulated.
- The implementation of MEGAN PFTs into the CSIRO-CTM.
- The acquisition of updated PFT datasets if they are integrated into the CSIRO-CTM.
- Further investigation of the potential for BVOC induced ozone exceedance events and - if their findings are significant - to implement some form of early warning system so that those at risk can avoid exposure.
- Further in situ monoterpene and isoprene emission flux measurements such as those acquired by Emmerson et al. (2016) acquired using aircraft and towers in the region to allow for better modelling and validation of emission estimates into the future.

## 8. References

Abbot, D. S., Palmer, P. I., Martin, R. V., Chance, K. V., Jacob, D. J. & Guenther, A. (2003). Seasonal and interannual variability of North American isoprene emissions as determined by formaldehyde column measurements from space. *Geophysical Research Letters,* 30.

Acton, W., Schallhart, S., Langford, B., Valach, A., Rantala, P., Fares, S., Carriero, G., Tillmann, R., Tomlinson, S. & Dragosits, U. (2015). Canopy-scale flux measurements and bottom-up emission estimates of volatile organic compounds from a mixed oak and hornbeam forest in northern Italy. *Atmospheric Chemistry and Physics Discussions,* 15**,** 29213-29264.

Arneth, A., Monson, R. K., Schurgers, G., Niinemets, Ü. & Palmer, P. I. (2008). Why are estimates of global terrestrial isoprene emissions so similar (and why is this not so for monoterpenes)? *Atmospheric Chemistry & Physics,* 8**,** 4605-4620.

Arneth, A., Schurgers, G., Lathiere, J., Duhl, T., Beerling, D., Hewitt, C., Martin, M. & Guenther, A. (2011). Global terrestrial isoprene emission models: sensitivity to variability in climate and vegetation. *Atmospheric Chemistry and Physics,* 11**,** 8037-8052.

Atkinson, R. & Arey, J. (2003). Gas-phase tropospheric chemistry of biogenic volatile organic compounds: a review. *Atmospheric Environment,* 37**,** 197-219.

Australian Bureau of Meteorology (2012). Annual Climate Summary 2011. *http://www.bom.gov.au/climate/annual_sum/2011/AnClimSum2011_HR1.0.pdf*.

Australian Bureau of Meteorology (2014). Annual Climate Report 2013. *http://www.bom.gov.au/climate/annual_sum/2013/AnClimSum2013_LR1.0.pdf*.

Australian Bureau of Meteorology (2016). Australian climate variability & change - Average maps. *http://www.bom.gov.au/climate/change/#tabs=Tracker&tracker=average-maps&tQ=map%3Dtmean%26season%3D02*.

Azzi, M., Cope, M., Day, S., Huber, G., Galbally, I., Tibbett, A., Halliburton, B., Nelson, P. & Carras, J. (2005). A Biogenic volatile organic compounds emission inventory for the Metropolitan Air Quality Study (MAQS) region of NSW. *17th International Clean Air & Environment Conference*.

Baker, K. R., Woody, M. C., Tonnesen, G. S., Hutzell, W., Pye, H. O. T., Beaver, M. R., Pouliot, G. & Pierce, T. (2016). Contribution of regional-scale fire events to ozone and PM2.5 air quality estimated by photochemical modeling approaches. *Atmospheric Environment,* 140**,** 539-554.

Baudic, A., Gros, V., Sauvage, S., Locoge, N., Sanchez, O., Sarda-Estève, R., Kalogridis, C., Petit, J., Bonnaire, N. & Baisnée, D. (2016). Seasonal variability and source apportionment of volatile organic compounds (VOCs) in the Paris megacity (France). *Atmospheric Chemistry & Physics,* 185.

Broome, R. A., Fann, N., Cristina, T. J. N., Fulcher, C., Duc, H. & Morgan, G. G. (2015). The health benefits of reducing air pollution in Sydney, Australia. *Environmental research,* 143**,** 19-25.

Chatani, S., Matsunaga, S. N. & Nakatsuka, S. (2015). Estimate of biogenic VOC emissions in Japan and their effects on photochemical formation of ambient ozone and secondary organic aerosol. *Atmospheric Environment,* 120**,** 38-50.

Coala Stearing Group (2016). COALA Characterizing Organics and Aerosol Loading over Australia (White Paper). *https://www2.acom.ucar.edu/sites/default/files/accord/COALA_whitepaper_20160707.pdf*.

Cope, M., Hess, G., Lee, S., Tory, K., Azzi, M., Carras, J., Lilley, W., Manins, P., Nelson, P. & Ng, L. (2004). The Australian air quality forecasting system. Part I: Project description and early outcomes. *Journal of Applied Meteorology,* 43**,** 649-662.

Cope, M., Keywood, M., Emmerson, K., Galbally, I., Boast, K., Chambers, S., Cheng, M., Crumeyrolle, S., Dunne, E., Fedele, R., Gillett, R., Griffiths, A., Harnwell, J., Katzfey, J., Hess, D., Lawson, S., Miljevic, B., Molloy, S., Powell, J., Reisen, F., Ristovski, Z., Selleck, P., Ward, J., Zhang, C. & Zeng, J. (2014). Sydney particle study- Stage II. *http://www.environment.nsw.gov.au/resources/aqms/SydParticleStudy10-13.pdf*.

Cope, M., Lee, S., Noonan, J., Lilley, B., Hess, D. & Azzi, M. (2009). Chemical Transport Model-Technical Description. *Centre for Australian Weather and Climate Research*.

Emmerson, K. (2016). Personal Communication

Emmerson, K., Galbally, I., Guenther, A., Paton-Walsh, C., Guerette, E., Cope, M., Keywood, S., Molloy, S., Dunne, E. & Thatcher, M. (2016). Current estimates of biogenic emissions from Eucalypts uncertain for Southeast Australia. *Atmospheric Chemistry & Physics*, 16.

Fisher, J. A., Jacob, D. J., Travis, K. R., Kim, P. S., Marais, E. A., Chan Miller, C., Yu, K., Zhu, L., Yantosca, R. M. & Sulprizio, M. P. (2016). Organic nitrate chemistry and its implications for nitrogen budgets in an isoprene-and monoterpene-rich atmosphere: constraints from aircraft (SEAC 4 RS) and ground-based (SOAS) observations in the Southeast US. *Atmospheric Chemistry and Physics*, 16**,** 5969-5991.

Geron, C. D., Daly, R. W., Arnts, R. R., Guenther, A. B. & Mowry, F. L. (2016). Canopy level emissions of 2-methyl-3-buten-2-ol, monoterpenes, and sesquiterpenes from an experimental Pinus taeda plantation. *Science of The Total Environment*, 565**,** 730-741.

Ghirardo, A., Xie, J., Zheng, X., Wang, Y., Grote, R., Block, K., Wildt, J., Mentel, T., Kiendler-Scharr, A. & Hallquist, M. (2015). Urban stress-induced biogenic VOC emissions impact secondary aerosol formation in Beijing. *Atmospheric Chemistry & Physics Discussions*, 15.

Glasius, M. & Goldstein, A. H. (2016). Recent Discoveries and Future Challenges in Atmospheric Organic Chemistry. *Environmental science & technology*, 50**,** 2754-2764.

Grell, G. A., Knoche, R., Peckham, S. E. & Mckeen, S. A. (2004). Online versus offline air quality modeling on cloud-resolving scales. *Geophysical Research Letters,* 31.

Grell, G. A., Peckham, S. E., Schmitz, R., Mckeen, S. A., Frost, G., Skamarock, W. C. & Eder, B. (2005). Fully coupled "online" chemistry within the WRF model. *Atmospheric Environment,* 39**,** 6957-6975.

Guenther, A. (2013). Biological and chemical diversity of biogenic volatile organic emissions into the atmosphere. *ISRN Atmospheric Sciences,* 2013.

Guenther, A., Hewitt, C. N., Erickson, D., Fall, R., Geron, C., Graedel, T., Harley, P., Klinger, L., Lerdau, M. & Mckay, W. (1995). A global model of natural volatile organic compound emissions. *Journal of Geophysical Research: Atmospheres,* 100**,** 8873-8892.

Guenther, A., Jiang, X., Heald, C., Sakulyanontvittaya, T., Duhl, T., Emmons, L. & Wang, X. (2012). The Model of Emissions of Gases and Aerosols from Nature version 2.1 (MEGAN2. 1): an extended and updated framework for modeling biogenic emissions. *Geoscientific Model Development,* 5**,** 1471-1492.

Guenther, A., Karl, T., Harley, P., C.Wiedinmyer, Palmer, P. I. & Geron, C. (2006). Estimates of global terrestrial isoprene emissions using MEGAN (Model of Emissions of Gases and Aerosols from Nature). *Atmospheric Chemistry and Physics,* 6.

Guenther, A. B., Monson, R. K. & Fall, R. (1991). Isoprene and monoterpene emission rate variability: observations with eucalyptus and emission rate algorithm development. *Journal of Geophysical Research: Atmospheres,* 96**,** 10799-10808.

Guenther, R. (1993). Isoprene and monoterpene emission rate variability: model evaluations and sensitivity analyses. *Journal of Geophysical Research,* 98.

Hart, M., De Dear, R. & Hyde, R. (2006). A synoptic climatology of tropospheric ozone episodes in Sydney, Australia. *International journal of climatology,* 26**,** 1635-1649.

He, C., Murray, F. & Lyons, T. (2000). Monoterpene and isoprene emissions from 15 Eucalyptus species in Australia. *Atmospheric Environment,* 34**,** 645-655.

Hess, G., Tory, K., Cope, M., Lee, S., Puri, K., Manins, P. & Young, M. (2004). The Australian air quality forecasting system. Part II: case study of a Sydney 7-day photochemical smog event. *Journal of applied meteorology,* 43**,** 663-679.

Houweling, S., Dentener, F. & Lelieveld, J. (1998). The impact of nonmethane hydrocarbon compounds on tropospheric photochemistry. *Journal of Geophysical Research: Atmospheres,* 103**,** 10673-10696.

Hurley, P. (2008). TAPM V4. Part 1: technical description. *CSIRO Marine and Atmospheric Research* 25**,** 59.

Ito, A., Sillman, S. & Penner, J. E. (2009). Global chemical transport model study of ozone response to changes in chemical kinetics and biogenic volatile organic compounds emissions due to increasing temperatures: Sensitivities to isoprene nitrate chemistry and grid resolution. *Journal of Geophysical Research: Atmospheres,* 114.

Jacob, D. J. 1999. *Atmospheric Chemistry*, Princeton University Press.

Jiang, N., Riley, M., Scorgie, Y., Betts, A., Kirkwood, J., Duc, H., Trieu, T., Salter, D., Ji, F. & Chang, L. (2015). Enhancing air quality forecast in New South Wales. *Proceedings of 22nd International Clean Air and Environment Conference (CASANZ)***,** 20-23.

Jiang, N., Scorgie, Y., Hart, M., Riley, M. L., Crawford, J., Beggs, P. J., Edwards, G. C., Chang, L., Salter, D. & Virgilio, G. D. (2016). Visualising the relationships between synoptic circulation type and air quality in Sydney, a subtropical coastal-basin environment. *International Journal of Climatology*.

Jonckheere, I., Fleck, S., Nackaerts, K., Muys, B., Coppin, P., Weiss, M. & Baret, F. (2004). Review of methods for in situ leaf area index determination: Part I. Theories, sensors and hemispherical photography. *Agricultural and forest meteorology,* 121**,** 19-35.

Jones, R. (1968). The leaf area of an Australian heathland with reference to seasonal changes and the contribution of individual species. *Australian Journal of Botany,* 16**,** 579-588.

Katzfey, J. (2015). CSIRO modelling and weather prediction reserch: From global to street scales. *CSIRO Marine and Atmospheric Research*.

Kefauver, S. C., Filella, I. & Peñuelas, J. (2014). Remote sensing of atmospheric biogenic volatile organic compounds (BVOCs) via satellite-based formaldehyde vertical column assessments. *International Journal of Remote Sensing,* 35**,** 7519-7542.

Kesselmeier, J. & Staudt, M. (1999). Biogenic volatile organic compounds (VOC): an overview on emission, physiology and ecology. *Journal of atmospheric chemistry,* 33**,** 23-88.

Kirstine, W. & Galbally, I. (2004). A simple model for estimating emissions of volatile organic compounds from grass and cut grass in urban airsheds and its application to two Australian cities. *Journal of the Air & Waste Management Association,* 54**,** 1299-1311.

Kleindienst, T. E., Lewandowski, M., Offenberg, J. H., Edney, E. O., Jaoui, M., Zheng, M., Ding, X. & Edgerton, E. S. (2010). Contribution of primary and secondary sources to organic aerosol and PM2. 5 at SEARCH network sites. *Journal of the Air & Waste Management Association,* 60**,** 1388-1399.

Kowalczyk, E. A., Wang, Y., Law, R., Davies, H., Mcgregor, J. & Abramowitz, G. (2006). The CSIRO Atmosphere Biosphere Land Exchange (CABLE) model for use in climate models and as an offline model. *CSIRO Marine and Atmospheric Research*

Laothawornkitkul, J., Taylor, J. E., Paul, N. D. & Hewitt, C. N. (2009). Biogenic volatile organic compounds in the Earth system. *New Phytologist,* 183**,** 27-51.

Lathiere, J., Hauglustaine, D., Friend, A., Noblet-Ducoudré, N. D., Viovy, N. & Folberth, G. (2006). Impact of climate variability and land use changes on global biogenic volatile organic compound emissions. *Atmospheric Chemistry and Physics,* 6**,** 2129-2146.

Lin., G., Joyce E, P. & Zhou., C. (2016). How Will Secondary Organic Aerosols Change in the Future? *Geophysical Research Letters,* 43.

Mcgrath-Spangler, E., Molod, A., Ott, L. & Pawson, S. (2015). Impact of planetary boundary layer turbulence on model climate and tracer transport. *Atmospheric Chemistry and Physics,* 15**,** 7269-7286.

Mcgregor, J. L. & Dix, M. R. 2008. An updated description of the conformal-cubic atmospheric model. *High resolution numerical modelling of the atmosphere and ocean.* Springer.

Millet, D., Baasandorj, M., Hu, L., Mitroo, D., Turner, J. & Williams, B. (2016). Nighttime chemistry and morning isoprene can drive urban ozone downwind of a major deciduous forest. *Environmental Science & Technology*.

Müller, J. F., Stavrakou, T., Wallens, S., De Smedt, I., Van Roozendael, M., Potosnak, M. J., Rinne, J., Munger, B., Goldstein, A. & Guenther, A. B. (2008). Global isoprene emissions estimated using MEGAN, ECMWF analyses and a detailed canopy environment model. *Atmospheric Chemistry & Physics,* 8**,** 1329-1341.

Murphy, B. F. & Timbal, B. (2008). A review of recent climate variability and climate change in southeastern Australia. *International journal of Climatology,* 28**,** 859-879.

Nelson, P., Azzi, M., Carras, J., Cope, M., Day, S., Halliburton, B., Huber, G., Tibbett, A., Bentley, S. & Galbally, I. (2002). Biogenic emissions in the Greater Sydney Region. *CSIRO Investigation Report ET/IR*.

Nsw Environmnetal Protection Authority (2012). Air Emissions Inventory for the Greater Metropolitan Region in New South Wales Technical Report No. 2: Biogenic and Geogenic Emissions: Results. *www.epa.nsw.gov.au/resources/air/120046AEITR2Biogenic.pdf*.

Nsw Environmnetal Protection Authority (2015). Chapter 8 - Air Quality *New South Wales State of the Environmnet 2015*.

Nsw Office of Environment and Heritage (2010). State of Knowledge: Ozone. *www.environment.nsw.gov.au/resources/aqms/10577sokozone.pdf*.

Nsw Office of Environment and Heritage (2014). Advisory Committee on Tunnel Air Quality- TP02: Air Quality Trends in sydney. *http://www.chiefscientist.nsw.gov.au/__data/assets/pdf_file/0003/52986/Road-Tunnels_TP02_Air_Quality_Trends_in_Sydney.pdf*.

Oderbolz, D., Aksoyoglu, S., Keller, J., Barmpadimos, I., Steinbrecher, R., Skjøth, C. A., Plaß-Dülmer, C. & Prévôt, A. (2013). A comprehensive emission inventory of biogenic volatile organic compounds in Europe: improved seasonality and land-cover. *Atmospheric Chemistry and Physics,* 13**,** 1689-1712.

Pacifico, F., Harrison, S. P., Jones, C. D. & Sitch, S. (2009). Isoprene emissions and climate. *Atmospheric Environment,* 43**,** 6121-6135.

Palmer, P. I., Abbot, D. S., Fu, T. M., Jacob, D. J., Chance, K., Kurosu, T. P., Guenther, A., Wiedinmyer, C., Stanton, J. C. & Pilling, M. J. (2006). Quantifying the seasonal and interannual variability of North American isoprene emissions using satellite observations of the formaldehyde column. *Journal of Geophysical Research: Atmospheres*, 111.

Pugh, T., Ashworth, K., Wild, O. & Hewitt, C. (2013). Effects of the spatial resolution of climate data on estimates of biogenic isoprene emissions. *Atmospheric Environment,* 70**,** 1-6.

Pyle, J., Shepherd, T., Bodeker, G., Canziani, P., Dameris, M., Forster, P., Gruzdev, A., Müller, R., Muthama, N. J. & Pitari, G. (2005). Ozone and climate: a review of interconnections. *IPCC/TEAP Special Report: Safeguarding the Ozone Layer and the Global Climate System*.

Rattanavaraha, W., Chu, K., Budisulistiorini, S. H., Riva, M., Lin, Y.-H., Edgerton, E. S., Baumann, K., Shaw, S. L., Guo, H. & King, L. (2016). Assessing the impact of anthropogenic pollution on isoprene-derived secondary organic aerosol formation in PM 2.5 collected from the Birmingham, Alabama, ground site during the 2013 Southern Oxidant and Aerosol Study. *Atmospheric Chemistry and Physics,* 16**,** 4897-4914.

Sakulyanontvittaya, T., Duhl, T., Wiedinmyer, C., Helmig, D., Matsunaga, S., Potosnak, M., Milford, J. & Guenther, A. (2008). Monoterpene and sesquiterpene emission estimates for the United States. *Environmental science & technology,* 42**,** 1623-1629.

Sindelarova, K., Granier, C., Bouarar, I., Guenther, A., Tilmes, S., Stavrakou, T., Müller, J.-F., Kuhn, U., Stefani, P. & Knorr, W. (2014). Global data set of biogenic VOC emissions calculated by the MEGAN model over the last 30 years. *Atmospheric Chemistry and Physics,* 14**,** 9317-9341.

Smolander, S., He, Q., Mogensen, D., Zhou, L., Bäck, J., Ruuskanen, T., Noe, S., Guenther, A., Aaltonen, H. & Kulmala, M. (2014). Comparing three vegetation monoterpene emission models to measured gas concentrations with a model of meteorology, air chemistry and chemical transport. *Biogeosciences,* 11.

Steinbrecher, R., Smiatek, G., Köble, R., Seufert, G., Theloke, J., Hauff, K., Ciccioli, P., Vautard, R. & Curci, G. (2009). Intra-and inter-annual variability of VOC emissions from natural and semi-natural vegetation in Europe and neighbouring countries. *Atmospheric Environment,* 43**,** 1380-1391.

Street, R. A., Hewitt, C. N. & Mennicken, S. (1997). Isoprene and monoterpene emissions from a Eucalyptus plantation in Portugal. *Journal of Geophysical Research: Atmospheres,* 102**,** 15875-15887.

Tesemma, Z., Wei, Y., Peel, M. & Western, A. (2014). Effect of year-to-year variability of leaf area index on variable infiltration capacity model performance and simulation of streamflow during drought. *Hydrology and Earth System Sciences Discussions,* 11**,** 10515-10552.

Trieu, T., Duc, H. N. & Scorgie, Y. (2015). Performance of TAPM-CTM as an airshed modelling tool for the sydney region. *22nd International Clean Air & Environment Conference*.

Unger, N. (2013). Isoprene emission variability through the twentieth century. *Journal of Geophysical Research: Atmospheres,* 118.

Van Donkelaar, A., Martin, R. V., Park, R. J., Heald, C. L., Fu, T.-M., Liao, H. & Guenther, A. (2007). Model evidence for a significant source of secondary organic aerosol from isoprene. *Atmospheric Environment,* 41**,** 1267-1274.

Verdon, D. C., Wyatt, A. M., Kiem, A. S. & Franks, S. W. (2004). Multidecadal variability of rainfall and streamflow: Eastern Australia. *Water Resources Research,* 40.

Wahner, A. (2015). Atmospheric Chemistry in Europe and Asia presentation *The Second Sino-Europeam School on Atmopsheric Chemistry*

Watterson, I., Mcgregor, J. & Nguyen, K. (2008). Changes in extreme temperatures of Australasian summer simulated by CCAM under global warming, and the roles of winds and land-sea contrasts. *Australian Meteorological Magazine,* 57**,** 195-212.

White, D. A., Turner, N. C. & Galbraith, J. H. (2000). Leaf water relations and stomatal behavior of four allopatric Eucalyptus species planted in Mediterranean southwestern Australia. *Tree Physiology,* 20**,** 1157-1165.

Wiedinmyer, C., Tie, X., Guenther, A., Neilson, R. & Granier, C. (2006). Future changes in biogenic isoprene emissions: how might they affect regional and global atmospheric chemistry? *Earth Interactions,* 10**,** 1-19.

Winters, A. J., Adams, M. A., Bleby, T. M., Rennenberg, H., Steigner, D., Steinbrecher, R. & Kreuzwieser, J. (2009). Emissions of isoprene, monoterpene and short-chained carbonyl compounds from Eucalyptus spp. in southern Australia. *Atmospheric Environment,* 43**,** 3035-3043.

Zare, A., Christensen, J. H., Gross, A., Irannejad, P., Glasius, M. & Brandt, J. (2014). Quantifying the contributions of natural emissions to ozone and total fine PM concentrations in the Northern Hemisphere. *Atmospheric Chemistry & Physics,* 14**,** 2735-2756.

Zeng, G., Williams, J. E., Fisher, J. A., Emmons, L., Jones, N. B., Morgenstern, O., Robinson, J., Smale, D., Paton-Walsh, C. & Griffith, D. W. (2015). Multi-model simulation of CO and HCHO in the Southern Hemisphere: comparison with observations and impact of biogenic emissions.

## Appendix 1 – Unix commands used

Note: As a system running UNIX was not available for the majority of the study Ubuntu v16.04 LTS was run within an Oracle Virtual Box environment on a pc running windows 10. However, it is expected that this will not influence the execution of the following scripts

### 1.1 ncdump

| | |
|---|---|
| sudo apt-get install netcdf-bin | Installs current version of ncdump |
| ncdump -h in.nc | prints all headers of ‘in.nc’ to terminal |

### 1.2 NCO (NETCDF Operators)

| | |
|---|---|
| sudo apt-get install nco | Installs current version of NCO |
| ncecat -O -u date in.nc* out.nc | Appends and concatenates ‘in.nc’ files along record dimension ‘date’ and outputs ‘out.nc’ |

### 1.3 Ncview

| | |
|---|---|
| sudo apt-get install ncview | Installs current version of ncview |
| ncview in.nc | Opens a visual interface that displays the data contained in ‘in.nc’ |

## Appendix 2 – Modules used within Python 2.7

| | |
|---|---|
| matplotlib.pyplot | Create temporal linear plots |
| mpl_toolkits.basemap – Basemap | Create maps with or without overlays |
| mpl_toolkits.basemap – maskoceans | Mask all grid boxes over water |
| netCDF4 | Import netcdf formatted data into Python |
| numpy | Perform operations over arrays |
| scipy.interpolate | Regrid data to smaller resolution |
| scipy.stats.mstats – pearsonr | Calculate Pearson R statistic between two values |

## Appendix 3 – Sample Python 2.7 scripts

```
# -*- coding: utf-8 -*-
"""
Create spatial average CSIRO-CTM-Original February 2011 Domain 3
Python v2.7.11
@author: Jordan Capnerhurst 2016
"""

# import required modules
from mpl_toolkits.basemap import Basemap
import matplotlib.pyplot as plt
import numpy as np
import netCDF4
from mpl_toolkits.basemap import maskoceans

# Set colour map for output map
# Others at: 'http://matplotlib.org/examples/color/colormaps_reference.html'
cool = cm = plt.get_cmap('jet')

# Import Netcdf4 dataset "FebCTM.nc" from location '.'
f = netCDF4.Dataset('./FebCTM.nc', 'r')

# Create arrays containing Netcdf4 data
#                   [variable]   [date, hour, lon, lat ] Note: data in UTC time
v = f.variables['store_Bio'][:, 14:23, 0, :, :]
v2 = f.variables['store_Bio'][:, 0:14, 0, :, :]

# concatenate to local time
vcon = np.concatenate((v, v2), axis=1)

# average over date and hour average to create spatial average
vmean = vcon.mean(axis=(0, 1))

# convert from kg/grid/hour to kg/km^2/hour
vmean2 = vmean/9
```

```
# import spatial information from Netcdf4 dataset
datalats = f.variables['lat'][:] #  latitudinal data
datalons = f.variables['lon'][:] #  longitudinal data

# Mesh longitudinal and latitudinal data to create 2d mesh
mlons, mlats = np.meshgrid(datalons, datalats)

# Define map parameters (llcrnlon= lower left corner longitude etc.)
map = Basemap(llcrnrlon=150.1, llcrnrlat=-34.7177,
            urcrnrlon=151.651, urcrnrlat=-33.5651, epsg=4269)

# Define type of map to be used from ESRI online services and output resolution
# Others at 'http://server.arcgisonline.com/arcgis/rest/services'
map.arcgisimage(service='World_Topo_Map', xpixels=820, verbose=True)

# Change size of outputted figure
plt.figure(figsize=(10, 10))

# set transparency of map and max/min of colour bar
trans = 0.2
max = 100
min = 0

# Mask oceans and dams as BVOCs emitted in these areas in negligible quantities
mocedata = maskoceans(mlons, mlats, vmean2,  inlands=True, resolution='h',
                    grid=1.25)

# Create colourmesh to overlay basemap
map.pcolormesh(mlons, mlats, mocedata, latlon=True, zorder=1,
            cmap=cool, alpha=trans, vmax=max, vmin=min)

# Draw Meridians and labels
map.drawmeridians(np.arange(0, 360, 1), labels=[0, 0, 0, 1], fontsize=10,
                color='black', linewidth=2)
map.drawparallels(np.arange(-90, 90, 1), labels=[1, 0, 0, 0], fontsize=10,
                color='black', linewidth=2)
```

```
# Add colour bar
col = map.pcolormesh(mlons, mlats, mocedata, latlon=True, zorder=0.45,
                     cmap=cool, alpha=trans, vmax=max, vmin=min)

# Define colourbar parameters
cb = map.colorbar(col, "right", size="5%", pad="2%")
cb.set_label('Average Total Biogenic Emissions (kg/$km^2$/hr)', fontsize=15)

# Output map to Python 2.7 interface
plt.show()

# Save map as .png to current working directory
plt.savefig('./bmap_syd.png')

# -*- coding: utf-8 -*-
"""
Create Timeseries of Isoprene and Monoterpenes MEGAN-offline
Python 2.7.11
@author: Jordan Capnerhurst 2016
"""

# import required modules
import matplotlib.pyplot as plt
import numpy as np
import netCDF4

# Import Netcdf4 dataset "FebOMEGAN.nc" from location '.'
f = netCDF4.Dataset('./FebOMEGAN.nc', 'r')

# Create arrays containing Netcdf4 data
#             [variable(spp.)][date, hour, lon, lat ] Note: data  in UTC time
#              1 hour difference due to daylight savings
v = (f.variables['ISOP'][1:29, 15:24, 0, :, 10:125]*68.12)
v2 = (f.variables['ISOP'][1:29, 0:15, 0, :, 10:125]*68.12)
ter = (f.variables['TERP'][1:29, 15:24, 0, :, 10:125]*136.298)
ter2 = (f.variables['TERP'][1:29, 0:15, 0, :, 10:125]*136.298)
```

```
# concatenate back to local time
vcon = np.concatenate((v, v2), axis=1)
tercon = np.concatenate((ter, ter2), axis=1)

# Reshape array for month
rv1 = vcon.reshape(672, 128, 115)
rter1 = tercon.reshape(672,  128, 115 )

# Calculate standardss devitations
# and convert from moles spp./grid/sec to kg/km^2/hour
stdevjmeg1 = np.std(rv1, axis=(1, 2))*3.6
stdevjmeg2 = np.std(rter1, axis=(1, 2))*3.6

# average over land and lon to create spatial average
# and convert from moles spp./grid/sec to kg/km^2/hour
v1 = rv1.mean(axis=(1, 2))*3.6
ter1 = rter1.mean(axis=(1, 2))*3.6

# Add monoterpenes and isoprene to same array for plotting
tot2 = [sum(x) for x in zip(v1, ter1)]
totarr2 = np.array(tot2)  # milimoles to kilograms

# Add monoterpenes and isoprene to same array for std. deviations
tot2 = [sum(x) for x in zip(stdevjmeg1, stdevjmeg2)]
totstdjmeg = np.array(tot2)

# use dates as x axis
date = np.arange(v1.shape[0])  # assume that delta time between data is 1
date21 = (date/24.)  # use days instead of hours

# Change size of outputted figure
plt.figure(figsize=(15, 5))

# plot averages
plt.plot(date21, ter1, linestyle='-', linewidth=1.2, c='k',
        label=' MEGAN-Offline Monoterpene Emissions')
```

```
plt.plot(date21, v1, linestyle='--', linewidth=2.0, c='c',
        label=' MEGAN-Offline Isoprene Emissions')

# Create standard devation fill
plt.fill_between(date21, ter1-stdevjmeg2, ter1+stdevjmeg2, alpha=0.3,
                edgecolor='black', facecolor='black', linewidth=0.3 )

plt.fill_between(date21, v1-stdevjmeg1, v1+stdevjmeg1, alpha=0.3,
                edgecolor='black', facecolor='cyan', linewidth=0.3 )

# define plot asthetics
plt.xlabel('Day')
plt.ylabel('Average Emissions (kg/$km^2$/hr)')
plt.title('Speciated Emissions February 2011')
plt.ylim(0, 25)
plt.xlim(0, 27)

# change ticks
plt.xticks(range(1, 28, 1), [str(i) for i in range(1, 28, 1)])
plt.yticks(np.arange(0, 48, 2))

# Display legend
plt.legend(loc='upper right')

# Output map to Python 2.7 interface
plt.show()

# Save map as .png to current working directory
plt.savefig('./bmap_syd.png')
```

## Appendix 4 – Topography of Sydney basin from ESRI API

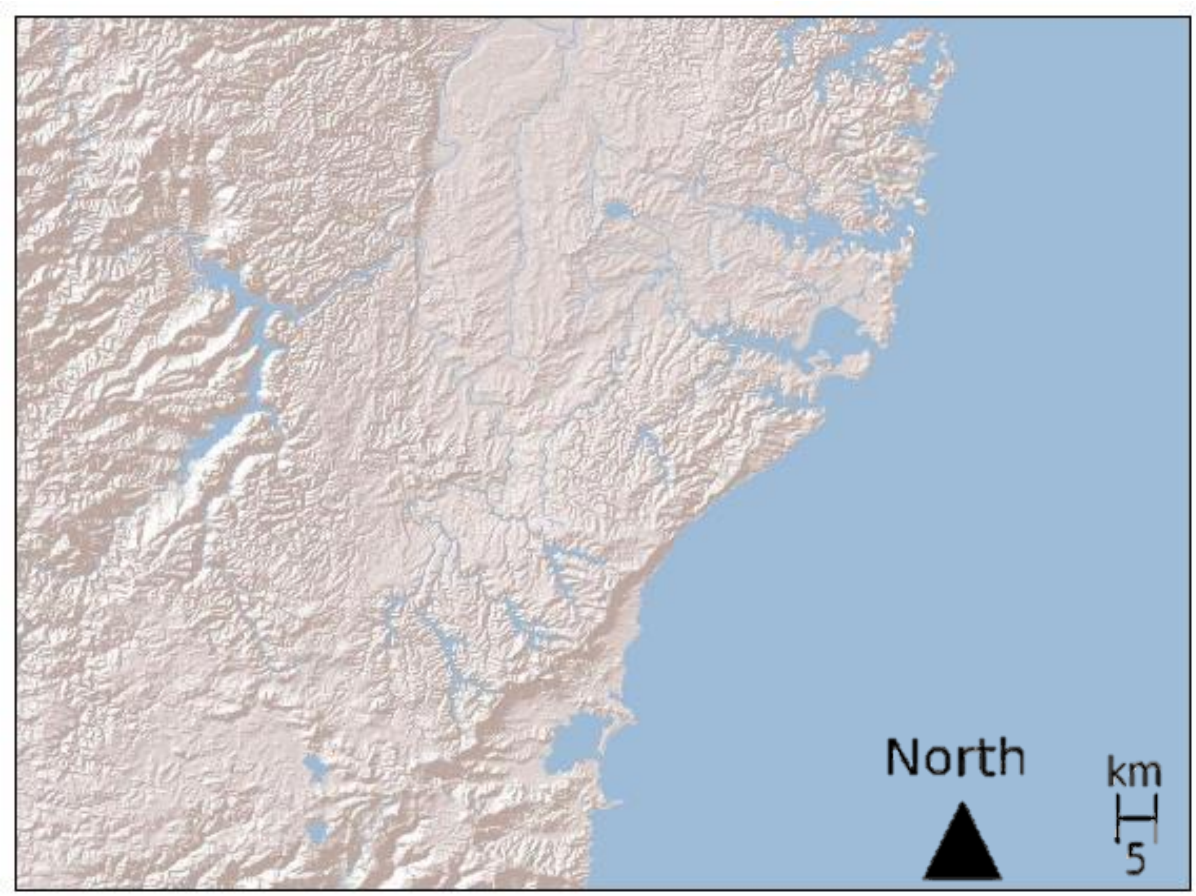


## Appendix 5 – High temperature event case study

Day 0 – CSIRO-CTM-MEGAN Higher than MEGAN-Offline (All in kg/km$^2$/hour)

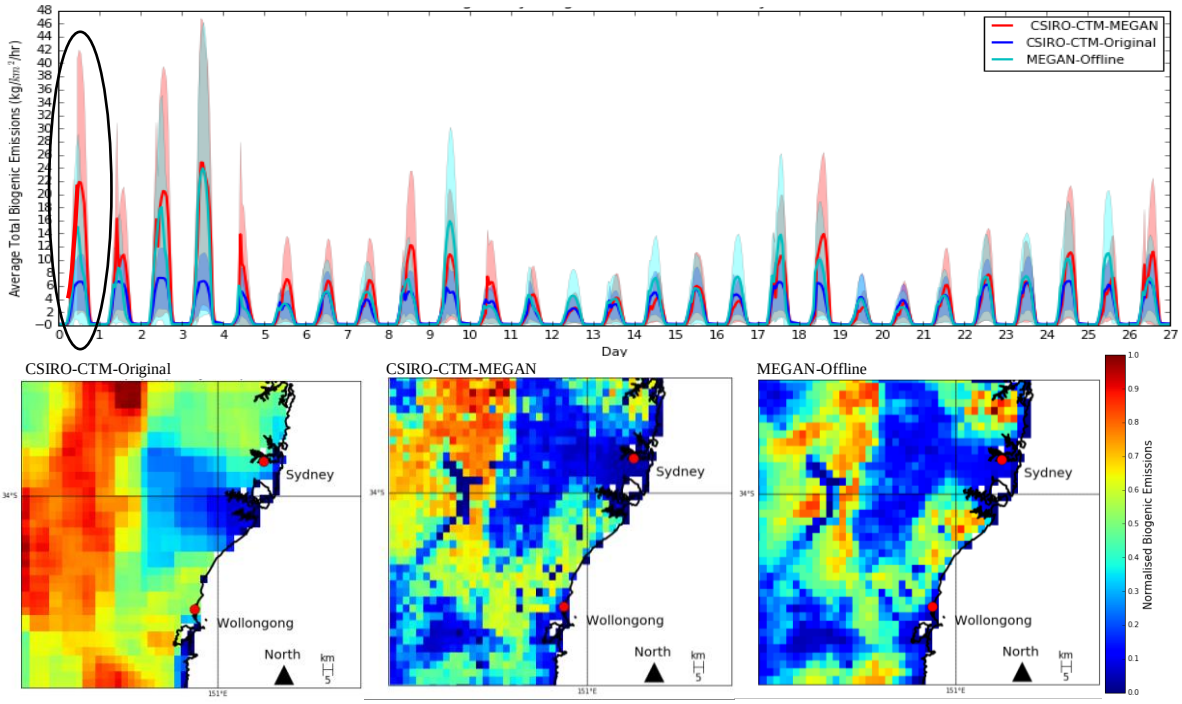

Day 3 – CSIRO-CTM-MEGAN roughly the same as MEGAN-Offline (All in kg/km$^2$/hour)

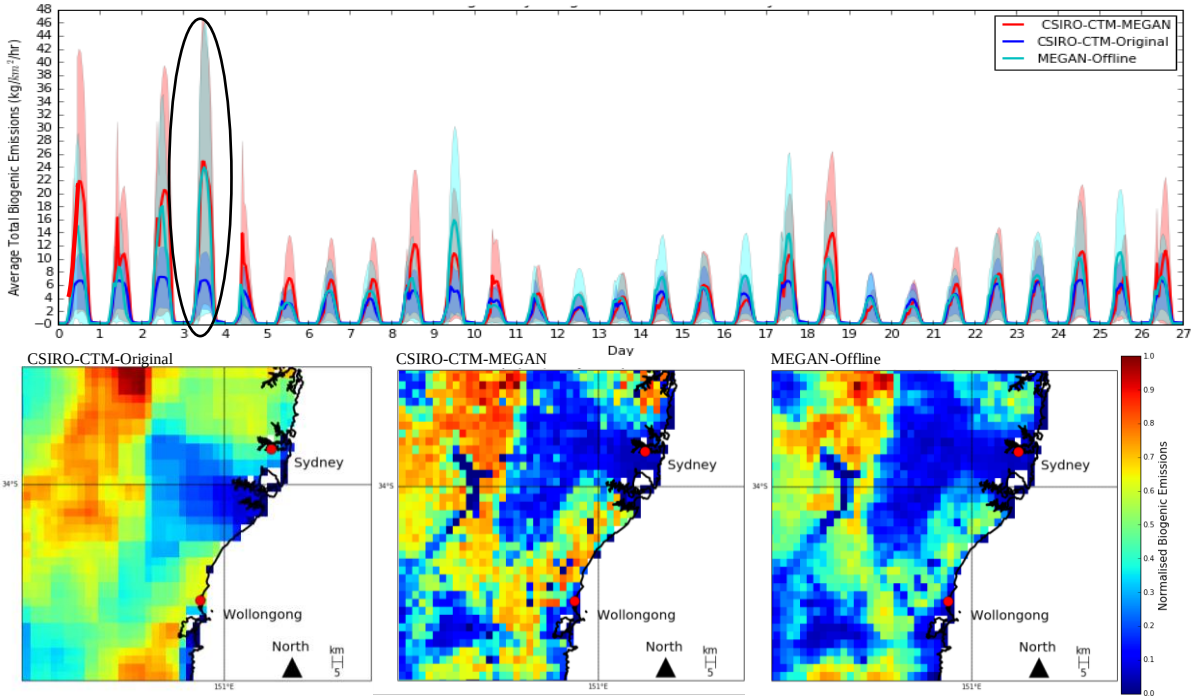


Day 9 – MEGAN-Offline higher than CSIRO-CTM-MEGAN (All in kg/km$^2$/hour)

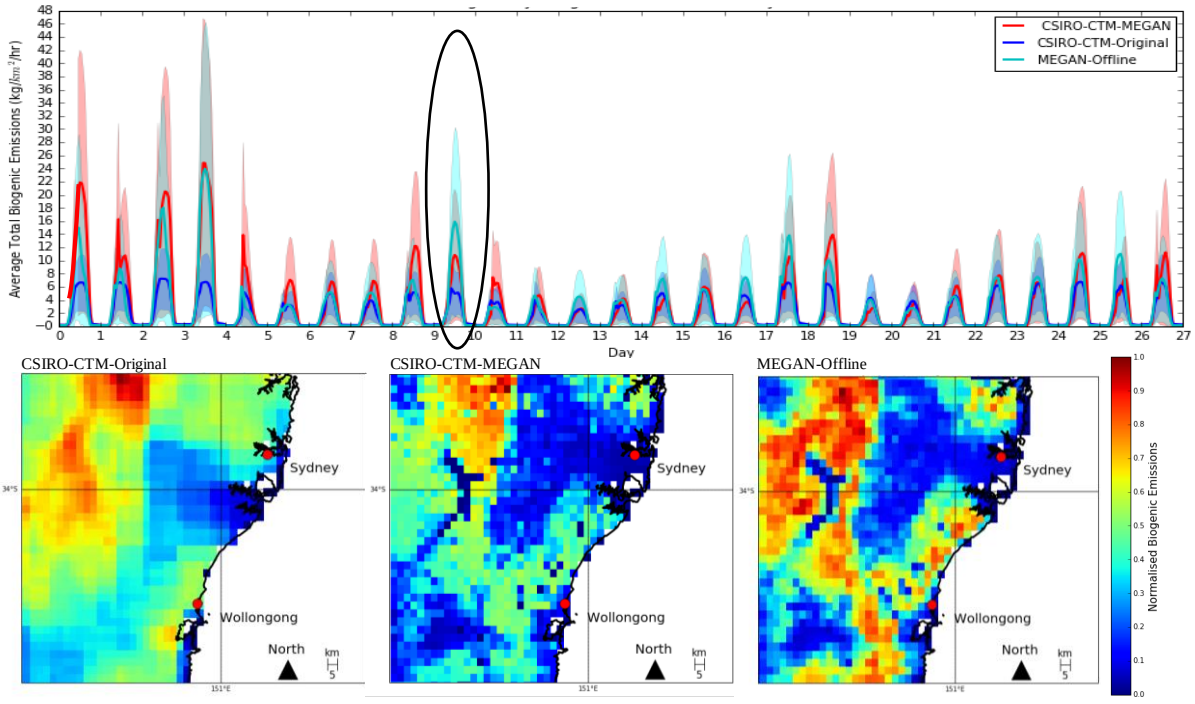

Day 20 – All very similar (All in kg/km^2/hour)

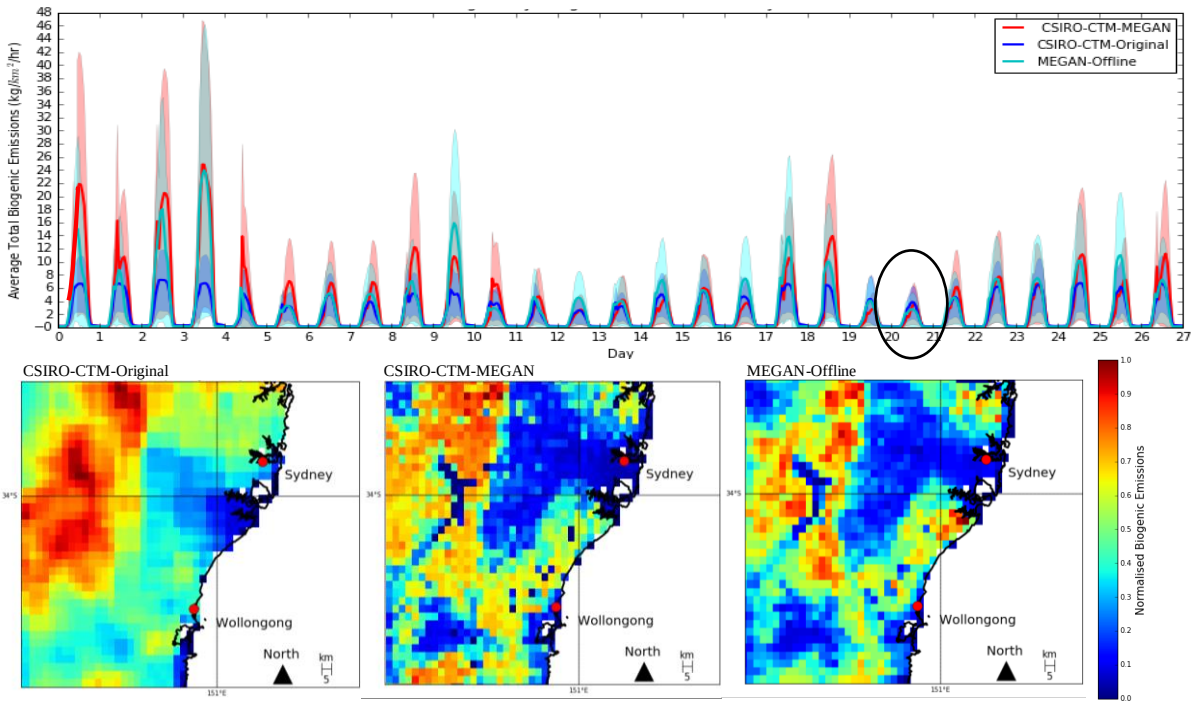


## Appendix 6 – Original 1x1 km$^2$ MEGAN-Offline Maps

Total Average Biogenic Emissions MEGAN-Offline Domain 3 February 2011 1x1km$^2$

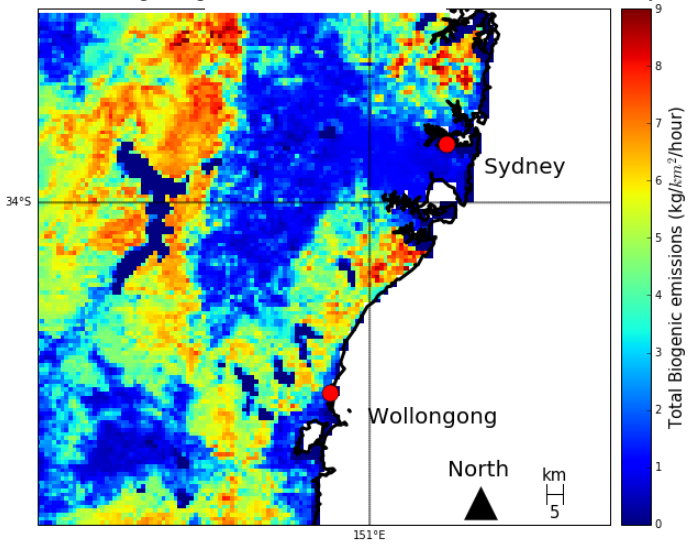

Leaf area Index MEGAN-Offline Domain 3 February 2011 1x1km$^2$

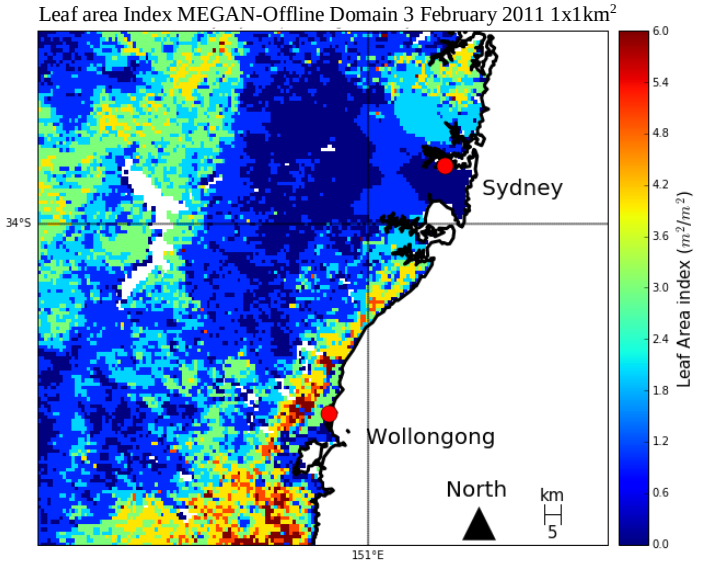


Average monthly Temperature MEGAN-Offline Domain 3 February 2011 1x1km$^2$

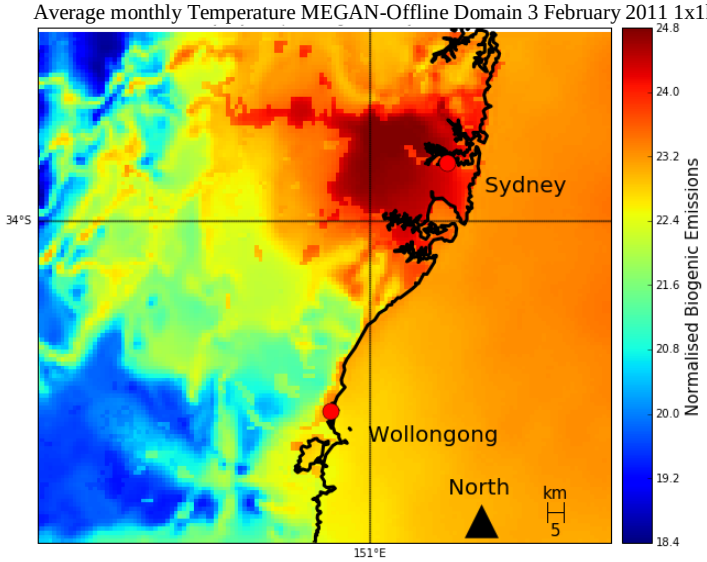

PFT Broadleaf vegetation

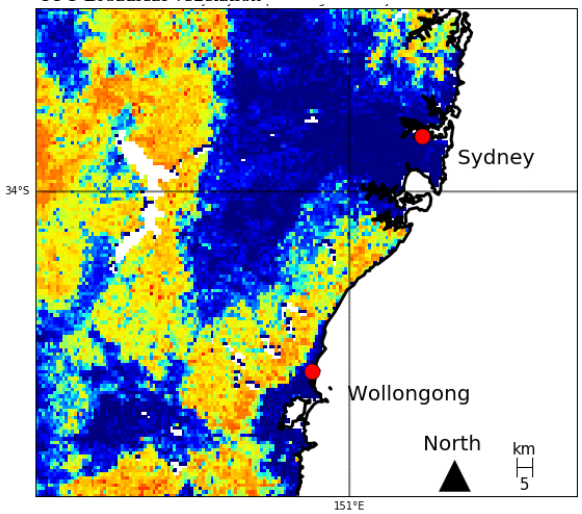


PFT Herbaceous vegetation

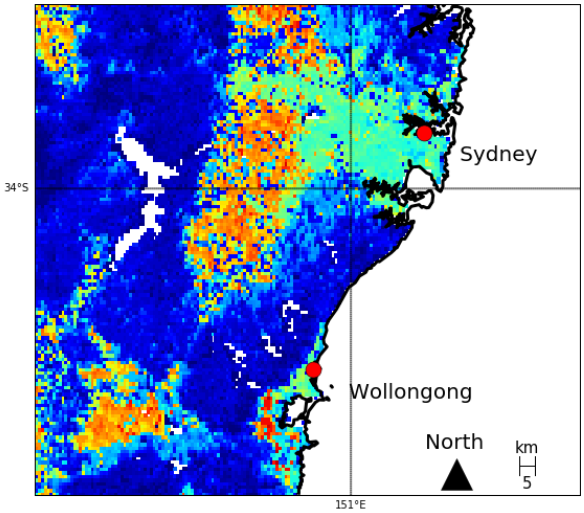


PFT Needle leaf vegetation

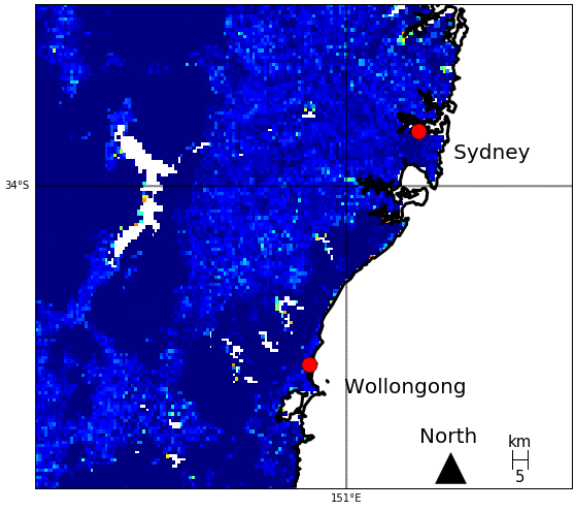


PFT Shrub

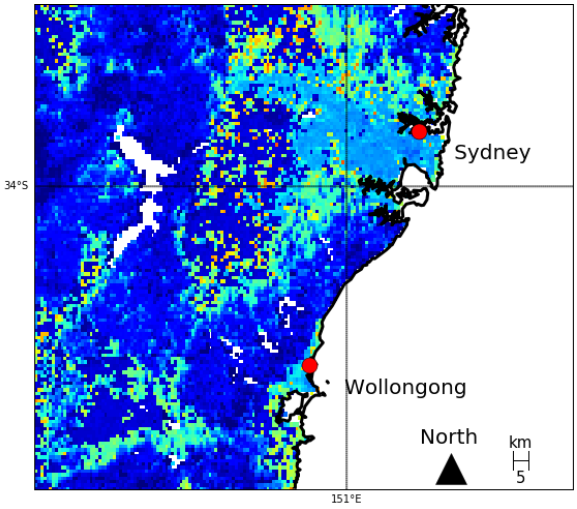


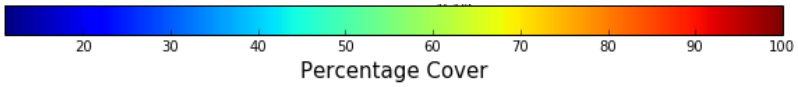

# Appendix 7 – Night and day emissions Comparison February 2011

CSIRO-CTM-Original Daytime Emissions

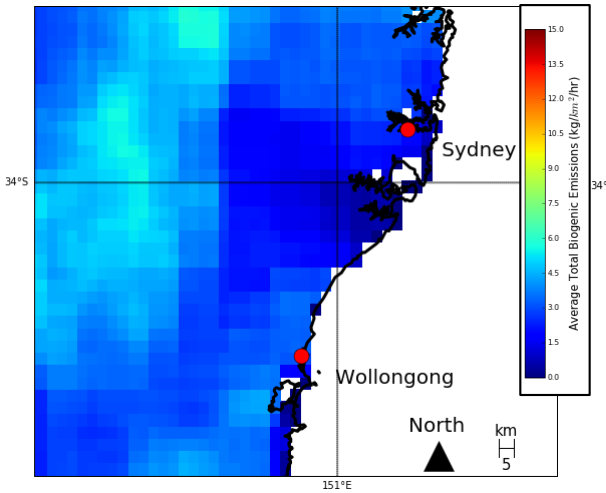


CSIRO-CTM-Original Night time emissions

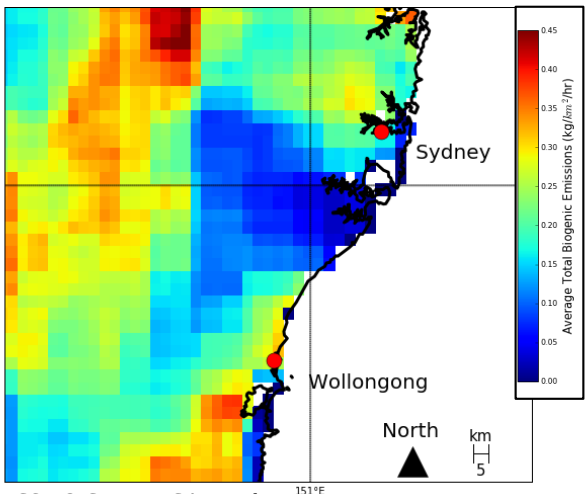


CSIRO-CTM-MEGAN Daytime Emissions

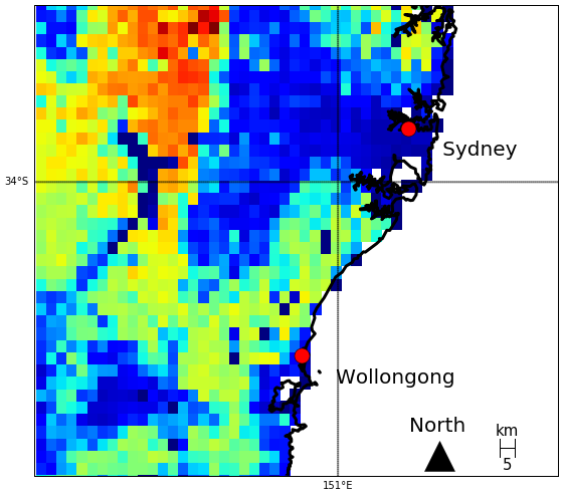


CSIRO-CTM-MEGAN Night time emissions

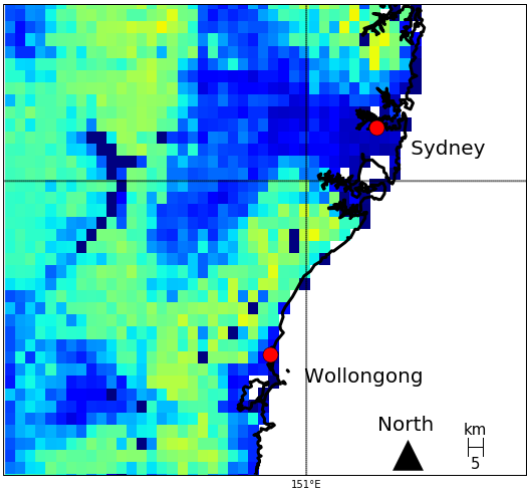

## Appendix 8 – CSIRO-CTM-Original February 2011 LGA Map

CSIRO-CTM-Original D2 Average monthly BVOC emissions overlayed using transparency onto NSW Local government area map.

NSW Department of Primary Industries 2012

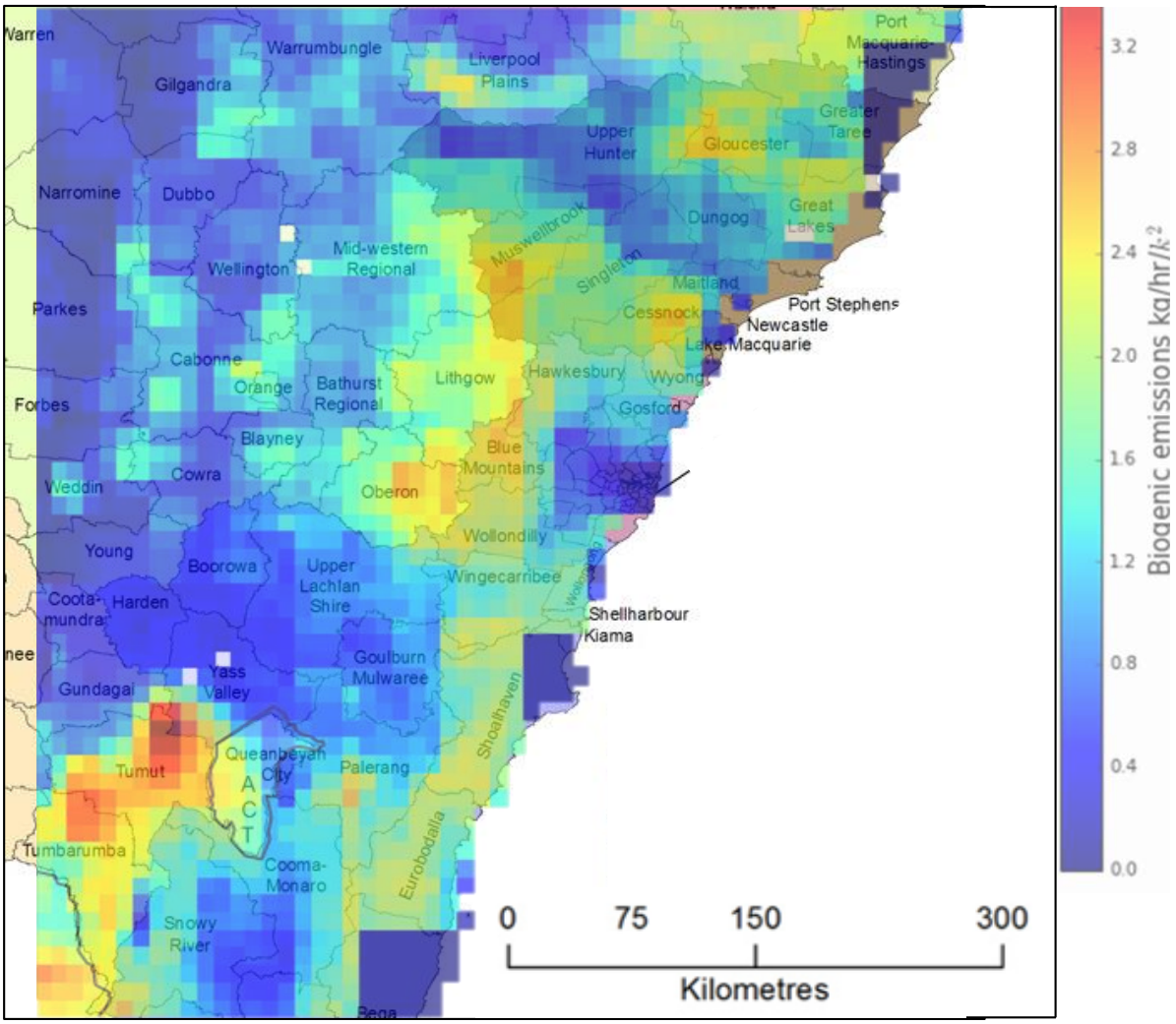

## Appendix 8 – Monthly Biogenic Emissions from EPA 2008 inventory D3 and D2

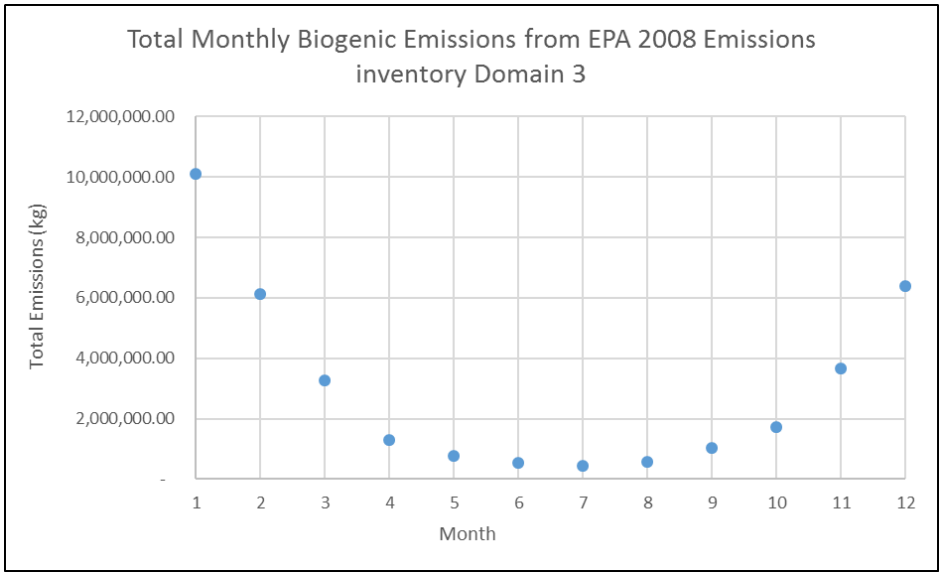


**February Monthly totals (Summed over Domain 3)**

CSIRO-CTM-Original: 16,461,814 kg (2011)

MEGAN-Offline: 24,791,219 kg (2011)

CSIRO-CTM-MEGAN: 25,485,820 kg (2011)

CSIRO-CTM-EPA: 6,141,839.65 kg (2008)

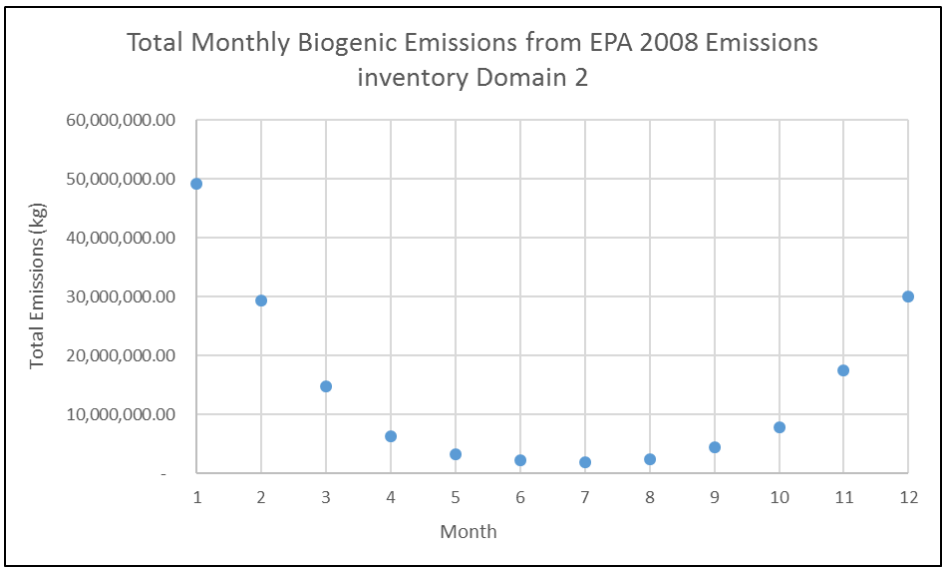


**February Monthly totals (Summed over Domain 2)**

CSIRO-CTM-Original: 45,949,853 kg (2011)

MEGAN- Offline: 48,064,311 kg (2011)

MEGAN CTM: 49,371,724 kg (2011)

CSIRO-CTM-EPA: 29,293,338 kg (2008)

**Appendix 9 – Annual Biogenic Emissions from EPA 2008 inventory D2**

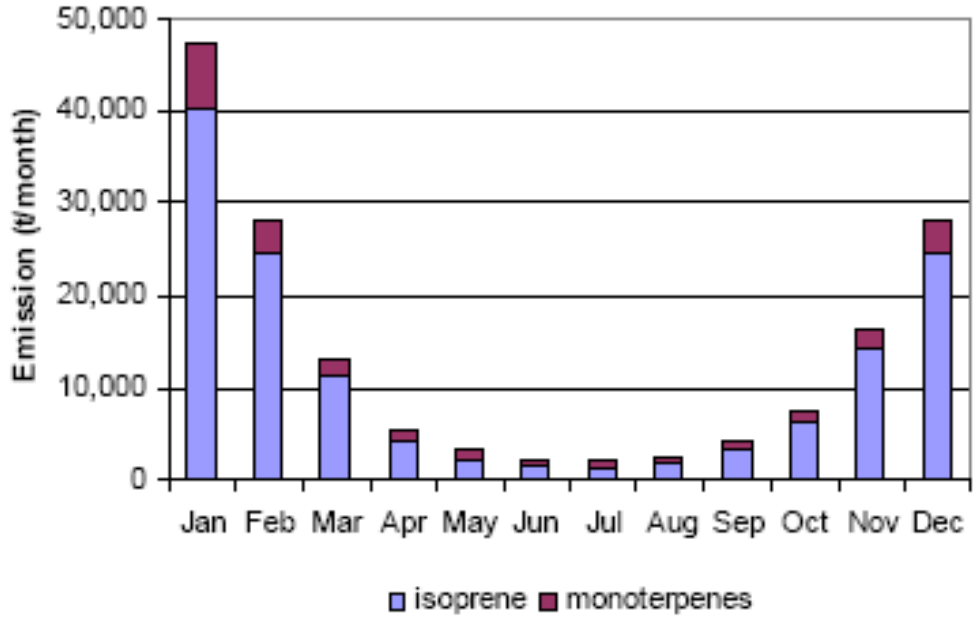


**Appendix 10 – Hourly emissions of total BVOCs 2008 Domain 2**

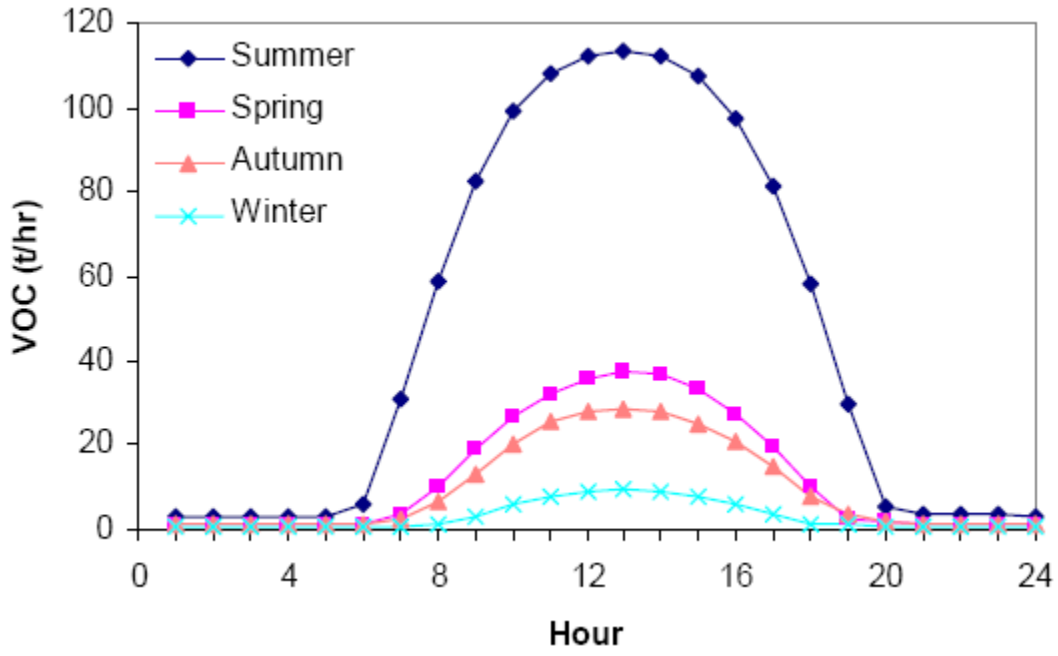

**Appendix 11 – Comparison between 1. NSW EPA 2008 emission inventory and 2. OEH 2013 CSIRO-CTM-Original predictions**

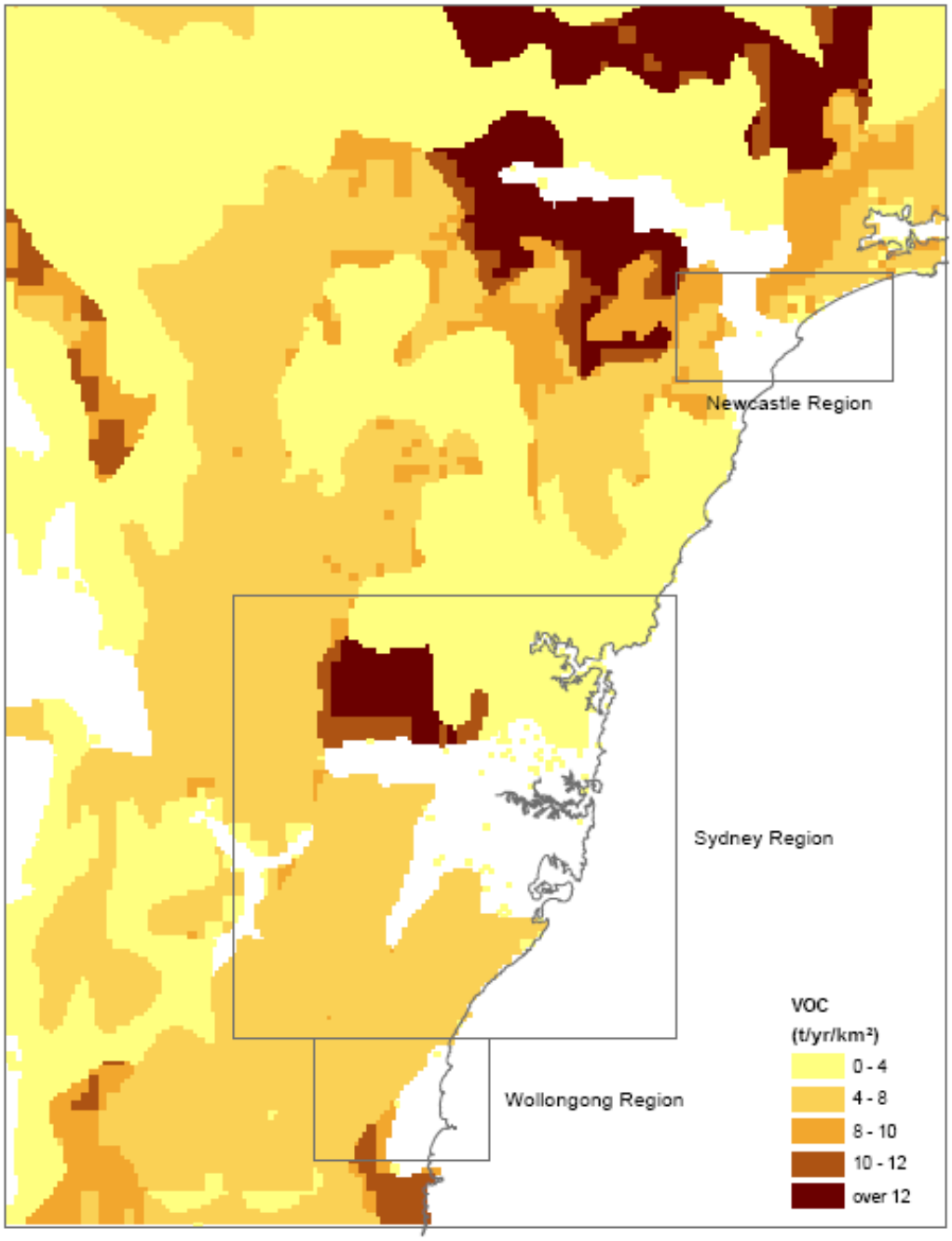

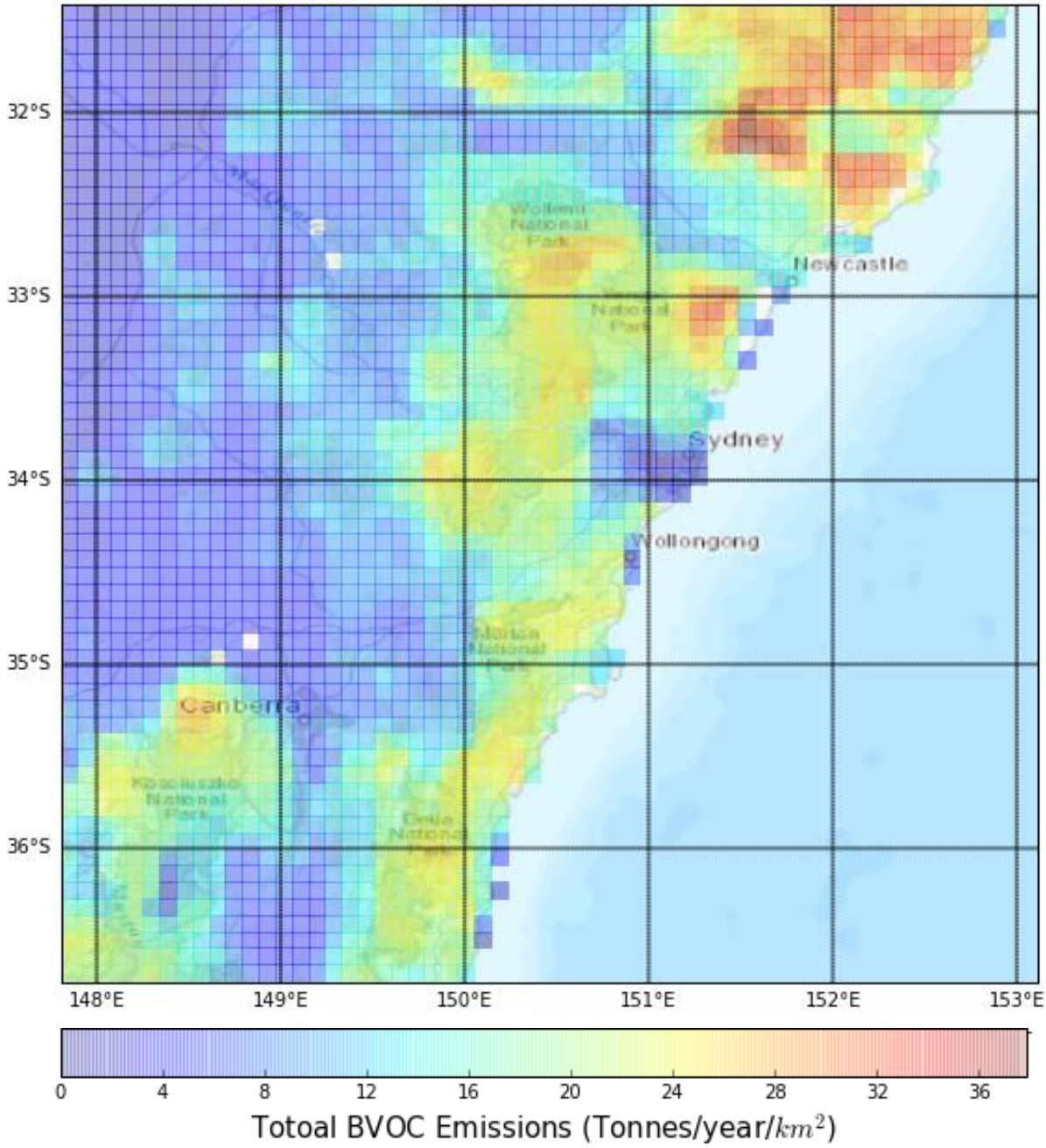
32°S
33°S
34°S
35°S
36°S
148°E
149°E
150°E
151°E
152°E
153°E
Newcastle
Sydney
Wollongong
Canberra
0
4
8
12
16
20
24
28
32
36
Totoal BVOC Emissions (Tonnes/year/$km^2$)

**Appendix 12 – NSW Average temperature maps from BOM**

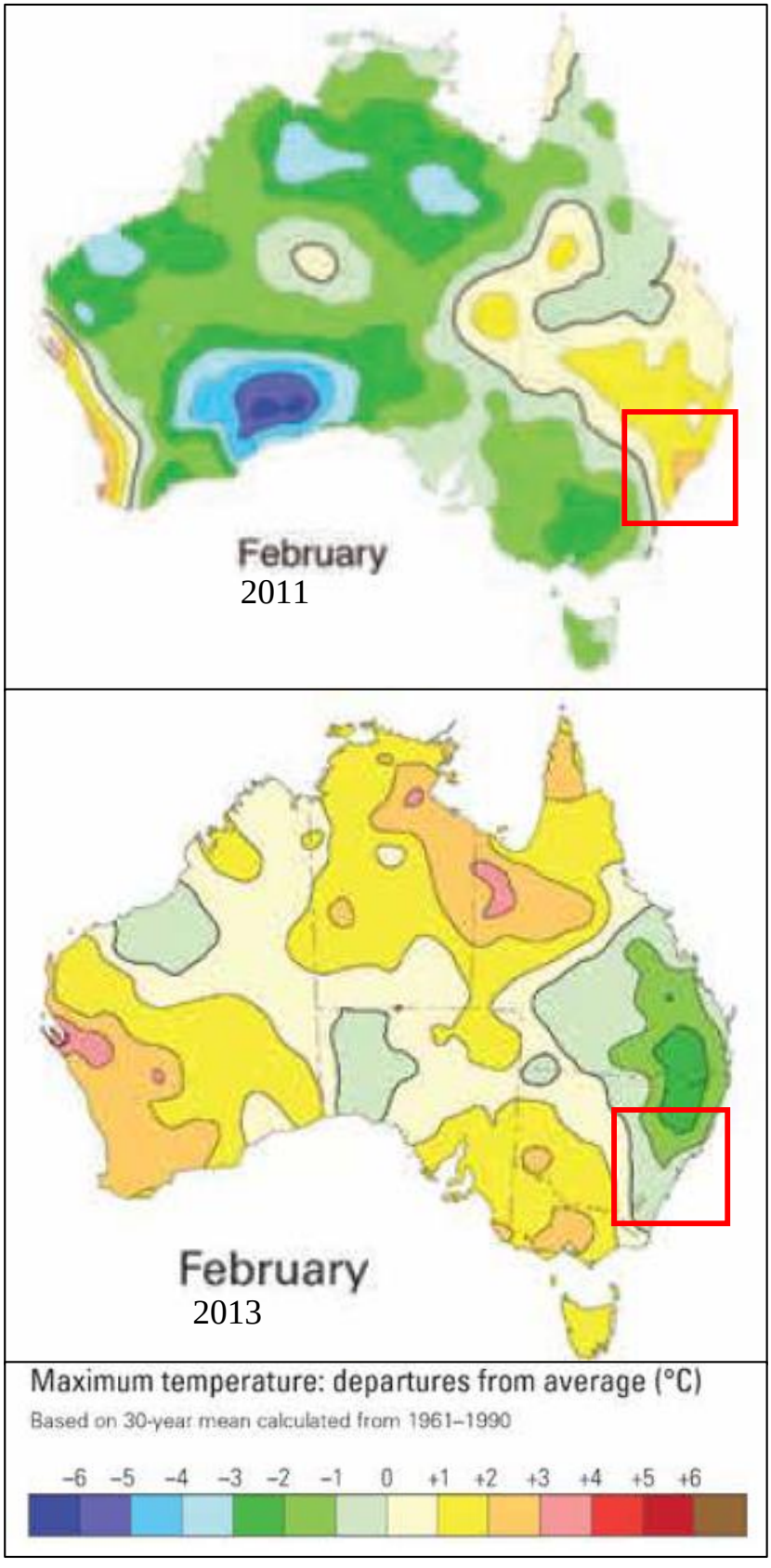

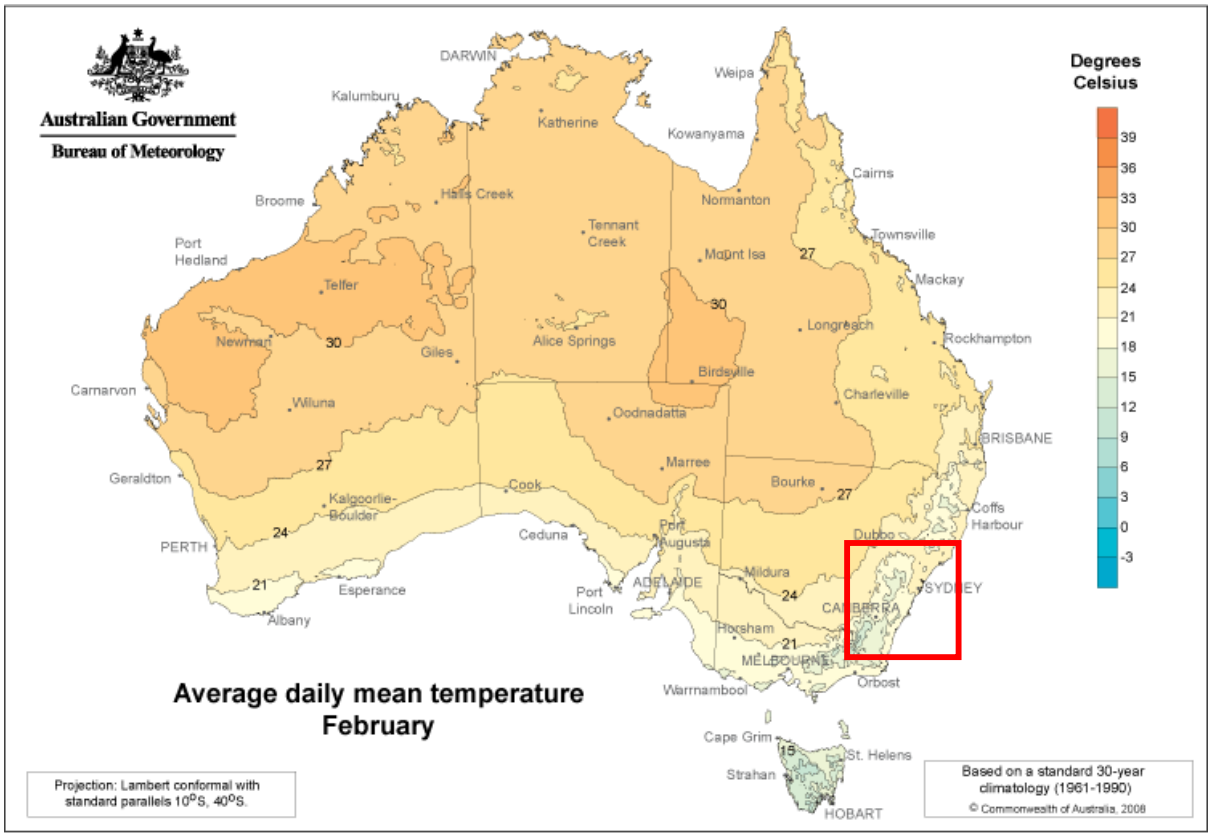
Australian Government
Bureau of Meteorology
Degrees Celsius
39
36
33
30
27
24
21
18
15
12
9
6
3
0
-3
DARWIN
Kalumburu
Katherine
Weipa
Kowanyama
Cairns
Broome
Halls Creek
Normanton
Tennant Creek
Townsville
Port Hedland
Mount Isa
Mackay
Telfer
Longreach
Newman
Alice Springs
Rockhampton
Giles
Birdsville
Carnarvon
Charleville
Wiluna
Oodnadatta
BRISBANE
Marree
Geraldton
Bourke
Cook
Coffs Harbour
Kalgoorlie-Boulder
Dubbo
Ceduna
Port Augusta
PERTH
Mildura
ADELAIDE
SYDNEY
Esperance
Port Lincoln
CANBERRA
Albany
Hocsham
MELBOURNE
Orbost
Warrnambool
Cape Grim
St. Helens
Strahan
HOBART
Average daily mean temperature
February
Projection: Lambert conformal with standard parallels 10°S, 40°S.
Based on a standard 30-year climatology (1961-1990)
© Commonwealth of Australia, 2008

## Appendix 13 – Vegetation maps used within Nelson et al. (2002) CSIRO-CTM modelling study obtained from Geoscience Australia

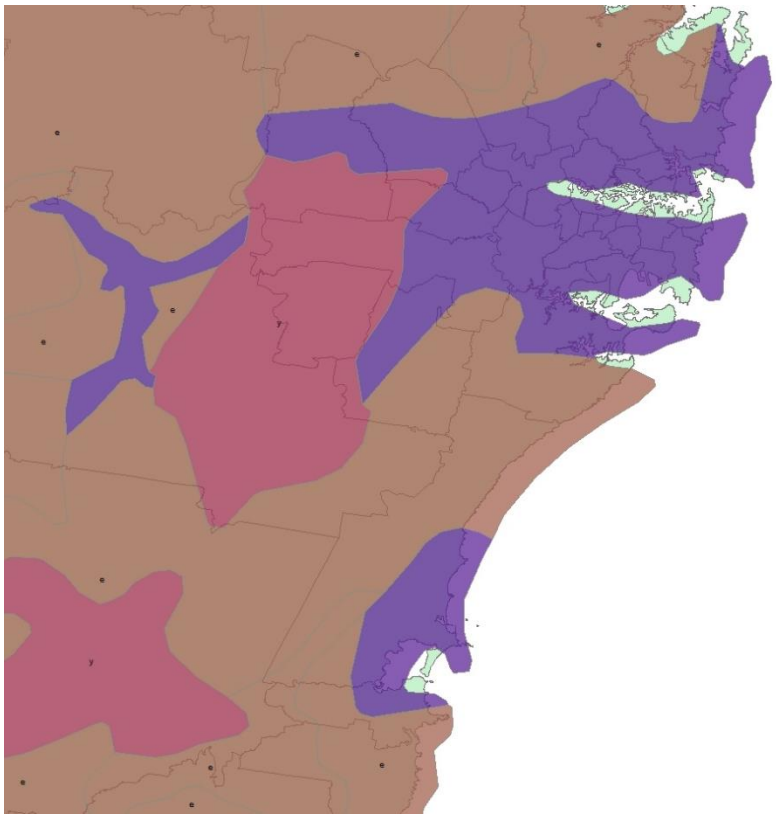

TALLEST STRATUM - SPECIES DOMINANT

| Attribute value | Description |
|---|---|
| a | Astrebla (mitchell grass) |
| b | Banksia |
| c | Casuarina including Allocasuarina |
| d | Dichanthium (bluegrass) |
| e | Eucalyptus |
| f | Fabaceae (includes clovers and medics) |
| g | Graminoids |
| h | Hakea |
| k | Chenopodiaceae (eg. saltbush and bluebush) |
| m | Melaleuca |
| n | Northofagus |
| o | Owenia (desert walnut) |
| p | Conifers |
| q | Myoporum (sugarwood) |
| r | Heterodendrum (rosewood) |
| s | Stipa (corckscrew grass) |
| t | Triodia and/or Plectrachne |
| u | Cereals |
| v | Saccharum (Sugar cane) |
| w | Acacia including Racosperma |
| x | Mixed or other |
| y | Other Grasses |
| z | Asteracaea (daisies) |

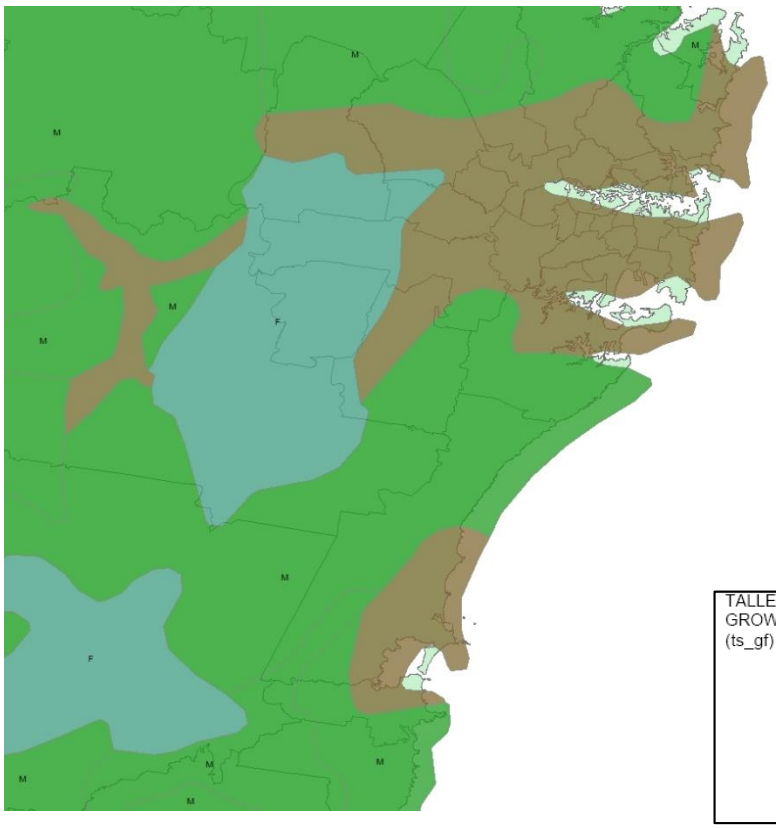

| | |
|---|---|
| TALLEST STRATUM - GROWTH FORM (ts_gf) | F = *Other herbaceous plants*<br>G = *Tussocky or tufted grasses*<br>H = *Hummock Grasses*<br>L = *Low trees <10 metres*<br>M = *Medium trees 10-30 metres*<br>S = *Tall Shrubs >2 metres*<br>T = *Tall trees >30 metres*<br>Z = *Low shrubs <2 metres* |

## Appendix 14 – Yearly temporal distribution of emissions split in half

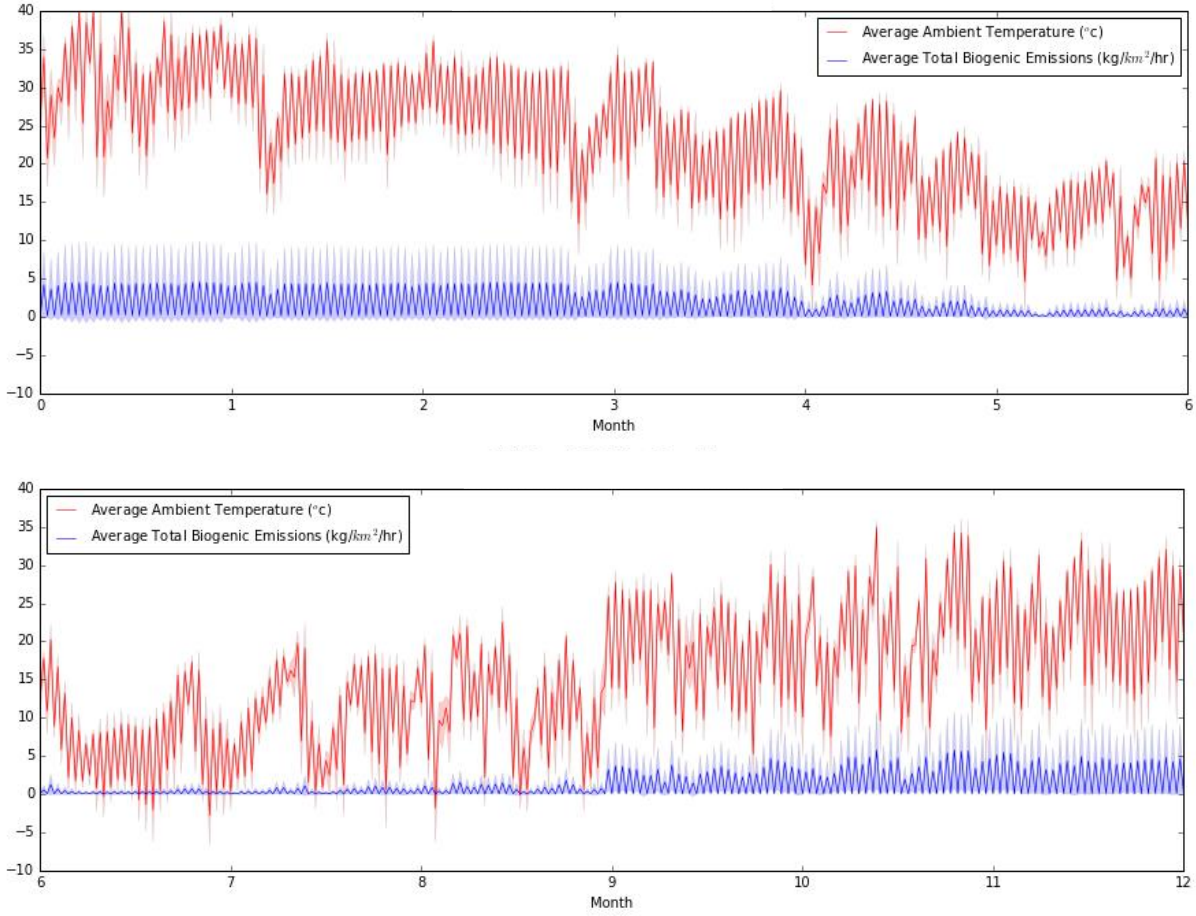


## Appendix 15 – Monthly spatial correlation between emissions and environmental Variables 2016

| | Jan | Feb | Mar | Apr | May | Jun | Jul | Aug | Sep | Oct | Nov | Dec |
|---|---|---|---|---|---|---|---|---|---|---|---|---|
| Temp | 0.51 | 0.82 | 0.75 | 0.75 | 0.61 | 0.44 | 0.58 | 0.49 | 0.56 | 0.67 | 0.69 | 0.73 |
| LAI | 0.98 | 0.98 | 0.98 | 0.96 | 0.95 | 0.92 | 0.91 | 0.90 | 0.90 | 0.93 | 0.95 | 0.98 |

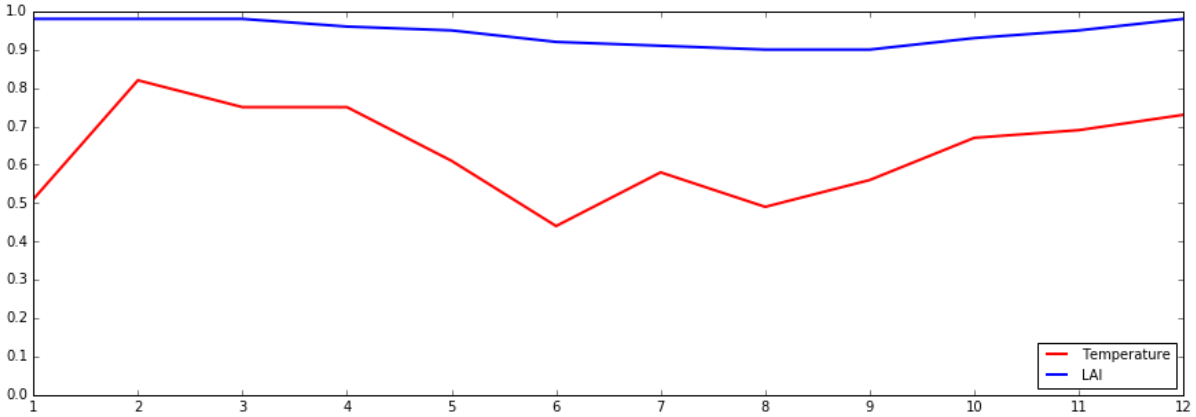

**Appendix 16 – In depth diagram of SOA and Ozone production from BVOCs**

**Wahner (2015)**

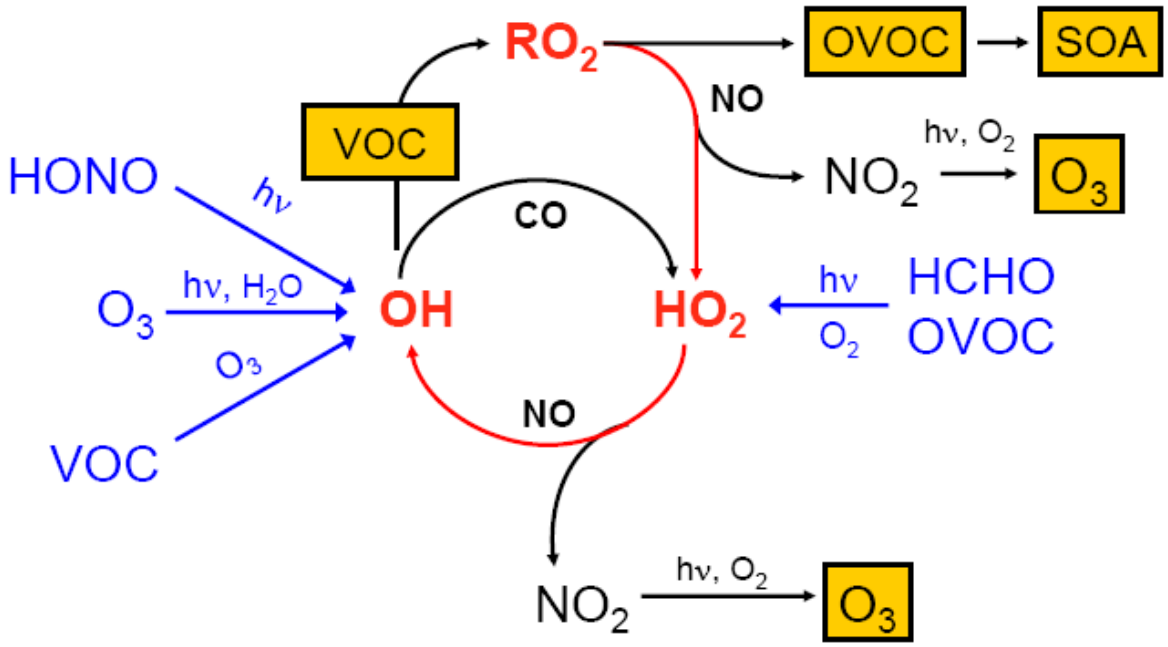


**Appendix 17 – Array data format visual explanation**

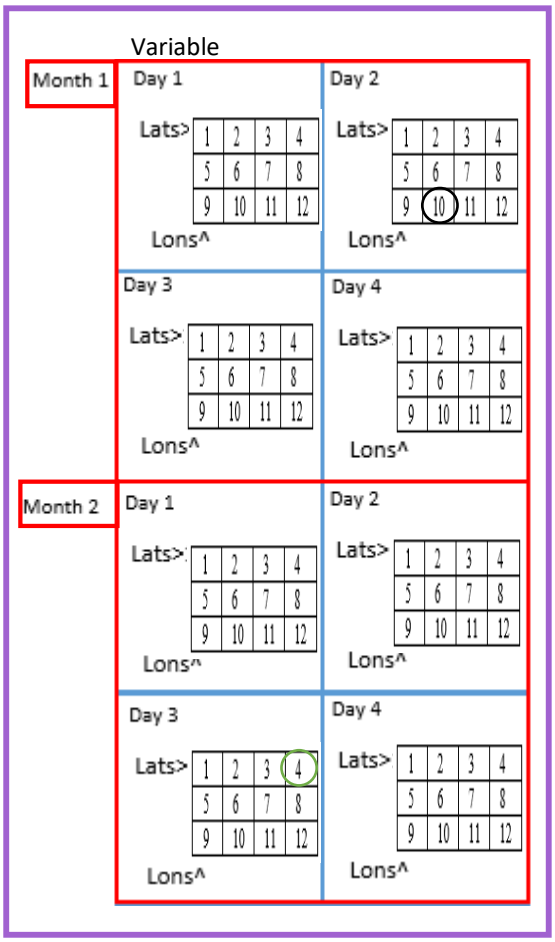


To the left is a visual representation of the data structure that the modelled data was obtained as.

Example 1: the value in month 1, day 2, latitude 2, longitude 3.

Expressed in python as ([variable][1, 2, 2, 3])

Is 10 (black circle)

Example 2: the value in month 2, day 3, latitude 4, longitude 1.

Expressed in python as ([variable][2, 3, 4, 1])

Is 4 (green circle)

## Appendix 18 – GMR LGA population map